Advances in Colloid and Interface Science 345 (2025) 103624

Contents lists available at ScienceDirect

Advances in Colloid and Interface Science

journal homepage: www.elsevier.com/locate/cis

Active drops driven by surface and polymorphic phase transitions: Current understanding and emerging perspectives

Diana Cholakova *

Department of Chemical and Pharmaceutical Engineering, Faculty of Chemistry and Pharmacy, Sofia University, 1 James Bourchier Avenue, 1164 Sofia, Bulgaria

ARTICLE INFO

Keywords:
Emulsion
Surfactant
Lipid
Rotator phase
Swimmer
Non-spherical particles
Rheology

ABSTRACT

Small emulsion droplets typically adopt spherical shapes under positive interfacial tension, minimizing unfavorable oil-water contact. This shape, along with the initial drop size, are generally preserved upon drop freezing or melting. However, in a series of studies, we demonstrated that simple temperature fluctuations near the melting point of the dispersed oil phase can spontaneously induce a wide range of dynamic behaviors in droplets. These activities include morphogenesis into various non-spherical shapes such as hexagonal, triangular, and tetragonal platelets, rods and fibers; the formation of complex composite micrometer-sized structures in the presence of adsorbed latex particles on initially spherical droplets; spontaneous desorption of the initially adsorbed particles; the generation of synthetic microswimmers capable of self-propulsion through the continuous phase, driven by the rapidly growing elastic filaments; spontaneous drop fragmentation and bursting into smaller particles (with sizes down to 20 nm) without any mechanical energy input; and the engulfment of the surrounding media spontaneously producing double water-in-oil-in-water droplets. All these phenomena were found to be intricately related to surface and polymorphic phase transitions proceeding within the droplets. The underlying mechanisms and control parameters were systematically investigated and published in a series of papers. The present review aims to summarize the key discoveries, present them within a unified conceptual framework, and compare them with other processes reported in the literature to lead to similar outcomes. Furthermore, the practical implications of these phenomena are discussed, and potential future research directions in this emerging area at the intersection of emulsion science and phase transition phenomena are outlined.

1. Introduction

The active soft matter is a rapidly expanding interdisciplinary field connecting soft condensed matter physics, material science, chemistry, biology, nanotechnology, and engineering. By definition, active systems are inherently out-of-equilibrium, continuously consuming energy to produce motion, mechanical work or other non-equilibrium behaviors driven by dynamic changes in their molecular organization, phase state, or microstructural rearrangements [1–5]. These materials offer advanced functionalities beyond those of traditional passive materials, making them widely studied for applications in material design, targeted cargo delivery, microrobotics, soft actuators, sensors, and as model systems for the development of next-generation bioinspired and autonomous materials [6–9].

Emulsions, thermodynamically unstable mixtures of two immiscible liquids, typically have spherical droplets due to the minimization of the interfacial energy at positive interfacial tension. Recently, the generation and stabilization of non-spherical emulsion droplets has gained significant attention because of their potential applications in active soft matter field [10–14]. Several approaches have been developed to create and stabilize such anisotropic droplet shapes, typically by introducing interfacial constraints that prevent drops from relaxing into a spherical shape. One widely used approach involves the formation of rigid interfacial layers composed of proteins or saponins, which are capable of withstanding capillary forces and thereby can stabilize non-spherical morphologies [15,16]. However, these non-spherical shapes typically arise during mechanical agitation and lack precise shape control.

Another effective strategy relies on the usage of particle-coated (Pickering) emulsion droplets to form supracolloidal structures with anisotropic geometries [14,17,18]. In a series of studies, Weitz et al. demonstrated that when droplets are partially covered with colloidal particles (surface coverage of around 70–90 %) and are brought into

* Corresponding author.
E-mail address: dc@dce.uni-sofia.bg.

https://doi.org/10.1016/j.cis.2025.103624
Received in revised form 23 July 2025;
Available online 5 August 2025

close contact, complete coalescence is inhibited, as the surface area of the resulting spherical droplet would be insufficient to accommodate all adsorbed particles. As a result, coalescence is arrested, and the partially fused droplets maintain stable, non-spherical shapes stabilized by a jammed particle layer [14,18].

An alternative approach to stabilizing non-spherical droplets involves the presence of crystalline phases within the droplets [19–22]. In these studies, micromanipulation techniques have been used to induce partial fusion between partially crystalline droplets [19,20], while microfluidic methods have enabled extrusion of mixed oily phase into an aqueous solution at temperatures where its partial freezing occurs [21,22]. This partial solidification forms an internal crystalline endoskeleton, stabilizing the elongated cylindrical shape formed during the extrusion.

In another studies, Spicer et al. demonstrated that crystallization-induced dewetting in tristearin droplets stabilized by sodium dodecyl sulfate and decanol can produce elongated non-spherical crystalline particles from initially spherical oily droplets [23–25]. This deformation arises when the crystal growth rate matches the dewetting rate of the still-liquid oil fraction from the just frozen one, thus generating interfacial tension gradients that elongate the freezing droplet under rapid cooling conditions ($\geq$ 5 °C/min).

More recently, a novel line of research has emerged within this domain, focusing on the unusual behavior of emulsion droplets undergoing phase transitions. The conventional emulsion drops retain their spherical geometry during phase transitions such as freezing and melting. However, nearly simultaneous and independent investigations by the research groups of Denkov et al. [26] and Deutsch et al. [27] discovered unexpected phenomena in alkane droplets during cooling: instead of freezing directly into spherical shapes, in part of the cases, alkane emulsion drops exhibited a series of spontaneous shape transformations prior to crystallization at lower temperatures. Performing independent research on similar emulsion systems, Shinohara and co-authors revealed additional complexity in these systems [28,29]. These authors observed the formation of surface-ordered layers of plastic rotator phase emerging prior to the crystallization of droplets into their thermodynamically stable crystalline phase [28,29]. Although these authors did not observe formation of non-spherical shapes due to the relatively high cooling rates employed, their finding proved to be critical for elucidating the mechanism underlying drop self-shaping process.

The initial observations of the non-spherical liquid droplets formation upon cooling date back nearly two decades ago [26,27], however, in-depth and systematic investigation began only within the past ten years [30]. Since then, several research groups started to work in this area, uncovering a range of unexpected and interconnected phenomena. This has led to the emergence of a new research direction at the crossroad of active matter, soft condensed matter, interface science and physical chemistry of phase transitions [30–48].

Among the newly discovered behaviors are the spontaneous and controllable formation of anisotropic fluid, frozen and polymeric micrometer- and submicrometer-sized particles [30–33], the generation of synthetic microswimmers [34], the transformation of initial coarse emulsion into nanoemulsions with drops as small as 20 nm [35,36], and the spontaneous formation of double water-in-oil-in-water droplets [37]. Remarkably, these phenomena are driven by simple temperature variations and have been demonstrated in systems of very simple chemical composition (oil, water and surfactant). This provides a versatile platform for investigating fundamental processes such as morphogenesis, swimming, solid-solid phase transitions and nanoporosity formation. Beyond their fundamental aspect, these findings also have substantial applied significance. They offer new approaches for the fabrication of nanoparticles, nanodroplets, and regularly shaped colloidal particles [35,36,46], as well as the creation of complex hierarchical structures [30,31,49–53]. Moreover, these studies suggest alternative methods for drop size reduction [35,36,54], double emulsions formation [35,37], and modification of the rheological properties of emulsions [26,55].

The present review aims to summarize the main findings and underlying mechanisms related to the non-trivial processes observed with emulsion droplets undergoing phase transitions, and to outline the emerging lines of research and open questions in the field. The review is structured as follows: Section 2 introduces the self-shaping process, its mechanism and factors which can be used to control it. A comparison with the other existing methods able to produce non-spherical particles from initially spherical emulsion droplets is made at the end of Section 2. Section 3 presents the peculiarities seen when the self-shaping drops become (partially) covered with adsorbed solid particles. In the following Section 4, the special case observed in the final stages of the drop shape evolutionary sequence, when the drops acquire thin elastic tails and start to self-propel through the solution is presented and discussed. Section 5 presents the related studies about spontaneous emulsification, bursting and double emulsion formation observed with emulsion drops undergoing phase transitions. Section 6 describes the industrial relevance of the described processes and suggests potential applications. The final Section 7 presents an outlook and suggests possible direction for future research in the field.

2. Drop self-shaping

The spontaneous symmetry breaking and formation of various non-spherical fluid shapes in emulsion droplets subjected to cooling were first described in detail in Ref. [30] and termed drop self-shaping or drop shape-shifting. This section provides a comprehensive overview of the key trends observed to date.

We begin by outlining the general deformation sequence followed by all drops upon cooling. Next, we discuss the experimental conditions required to induce drop deformation. Section 2.3 discuss the underlying mechanisms driving the self-shaping, while the factors that can be used to control the process are reviewed in the following Section 2.4. Section 2.5 described the stability of the generated non-spherical particles, and the theoretical models developed to describe this phenomenon are reviewed in Section 2.6. Section 2.7 highlights the unique aspects observed in multicomponent droplet systems. Finally, Section 2.8 provides a brief overview of alternative methods reported in the literature that also lead to formation of non-spherical droplets, comparing them with the spontaneous self-shaping process.

2.1. General drop shape evolutionary sequence

According to the energy-minimization law, the small emulsion drops typically adopt a spherical shape at temperatures well above the bulk melting temperature of the dispersed oil, as this geometry minimizes the droplet surface area at a given volume. Usually, when emulsion droplets are cooled to temperatures where the dispersed oil phase freezes, the resulting solid particles obtain spherical or nearly-spherical shape.

Surprisingly, our research has uncovered an alternative process that leads to the spontaneous creation of non-spherical particles while cooling initially spherical emulsion droplets, see Fig. 1a [30,31]. Under controlled conditions, oily drops dispersed in an aqueous surfactant solution undergo shape transformations when a critical temperature is reached. The transformations begin with the emergence of multiple vertices, visible under reflected light, see Fig. 1b. Slow cooling ($\lesssim$ 1 °C/min) leads to regular deformations, forming icosahedral shapes with 12 distinct vertices and convex faces, see **Figs. 1**b and **2**a, whereas faster cooling results in irregular initial deformations with surface wrinkles, see Fig. 1**c** [30]. These wrinkles may gradually disappear in the later stages of shape evolution.

Further cooling flattens the icosahedra into octahedral shape, which appear hexagonal in two-dimensional projection, see **Figs. 1**b,d and **2**b. These “hexagonal prisms” or “platelets” have a three-dimensional shape consisting of a hexagonal base with a cylindrical frame and a thinner

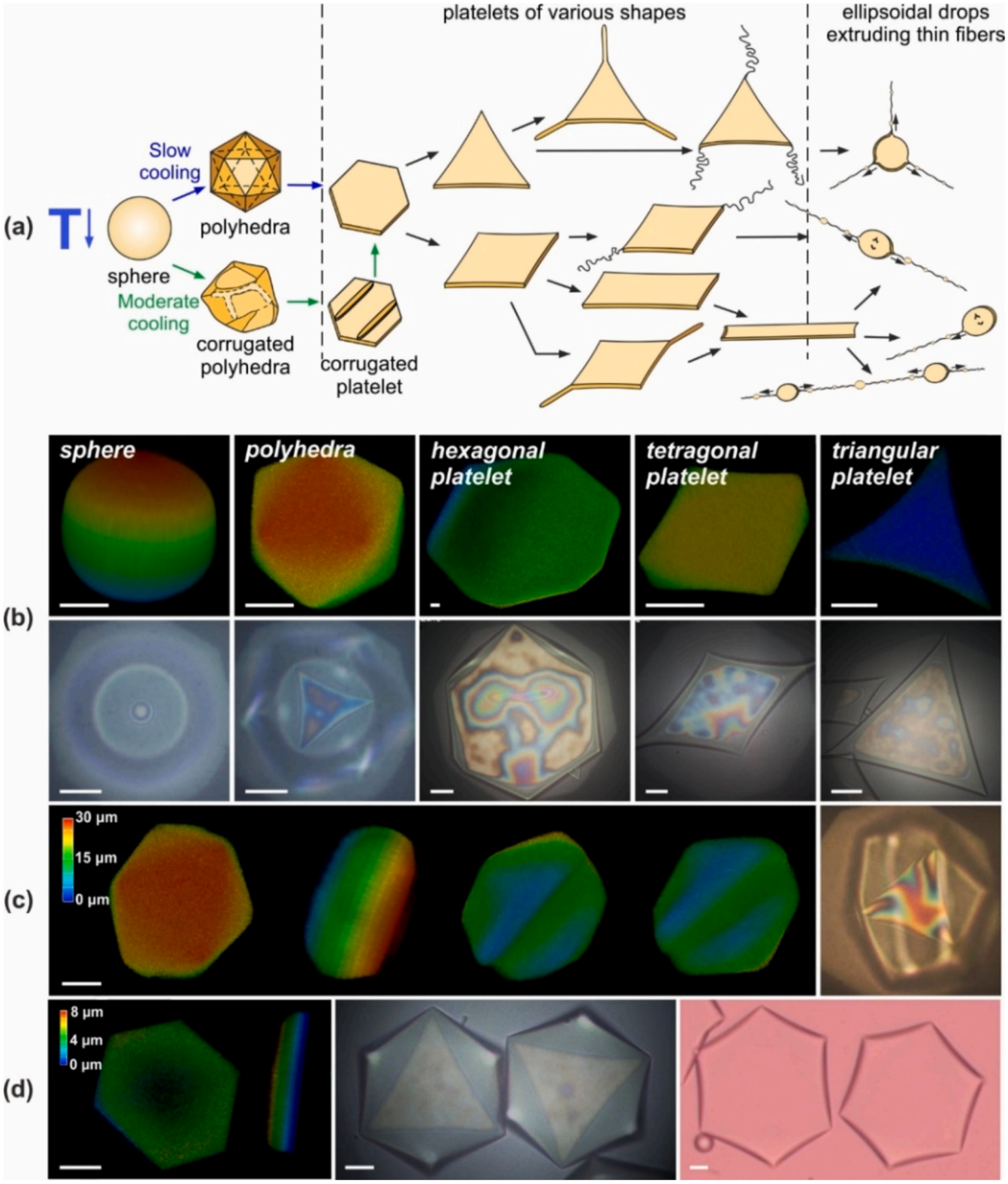

Fig. 1. Drop self-shaping evolutionary sequence. (a) Schematic representation of the main shapes observed during drop cooling [31]. (b) Confocal (upper row) and reflected light microscopy (lower row) images of droplets in various shapes, as indicated by the text on the figure. The colorful films observed in reflected light represent the thin liquid films formed between the capillary glass wall and the upper surface of the deforming droplet. Note that real flat platelets are shown in the confocal images; however, as explained in the text, the platelets typically have thinner central region and cylindrical frame as depicted in (d). (c) Images of a corrugated platelet. The wrinkles are clearly visible in the confocal microscopy images, appearing thicker and colored in blue. In reflected light, the wrinkles appear as lighter lines, see the last image. (d) Typical shape of a hexagonal platelet particle, with a thicker frame and a very thin central part, as seen in the confocal microscopy images. Reflected and polarized light images of similarly shaped particles are also shown. White scale bars = 10 μm. (For interpretation of the references to colour in this figure legend, the reader is referred to the web version of this article.)

central region, see Fig. 1d [38]. Depending on the specific oil-surfactant system and the applied cooling protocol, these hexagonal structures can have relatively uniform thickness. However, when this shape is maintained for an extended period, the central part becomes progressively thinner and may rupture, see Fig. 2c.

Next, droplets follow one of two possible evolutionary paths: the majority lose two sides to form tetragonal prisms (lower branch in the evolutionary sequence, Fig. 1a and Supplementary Movie 1), while others lose three sides leading to the formation of triangular prisms. Both type of particles feature a tetragon or triangle with a cylindrical

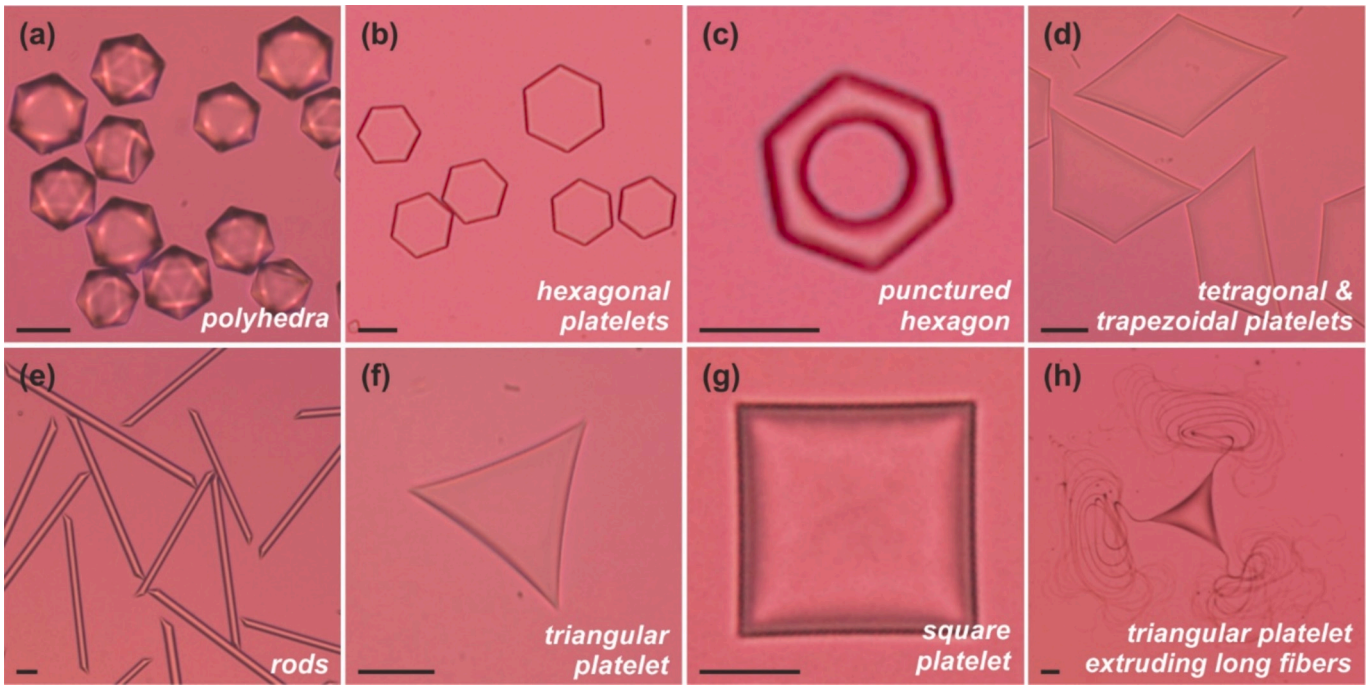

Fig. 2. Fluid non-spherical droplets with various shapes (as indicated with text on the pictures). These pictures were captured from optical microscopy experiments performed upon cooling using the following oil-surfactant solution emulsion systems: (a,d,e,f) hexadecane, C_{16}, in Tween 60; (b,c) C_{16} + 1 wt% Brij 52 in water; (g) hexadecane + nonadecane, C_{16} + C_{19}, (1:1, *v*/v) in Tween 60; (h) pentadecane, C_{15}, in Brij 58. Scale bars = 20 μm.

frame and a thinner central region, Fig. 1b, although we will refer to them as "prisms" or "platelets". These particles may also rupture in the center, resulting in the formation of doughnut-like particles.

The transformation from hexagonal prisms to tetragonal or triangular prisms is the most difficult stage in the drop deformation process [31,39], especially for larger droplets (diameter > 30–40 μm) stabilized by non-ionic surfactants with a sorbitan ring in the hydrophilic head (e.g., Tweens). For Tween-stabilized systems, the triangular prisms represent the final stage in the evolution for part of the droplets, Fig. 2f. In contrast, systems stabilized by non-ionic alcohol ethoxylate surfactants with linearly connected ethylene oxide units (e.g. Brijs or Lutensols), develop cylindrical protrusions at triangle tips, classified as fibers (d < 1.5 μm, Fig. 2h), or rods ($d \approx$ 2–5 μm, Fig. 3). These protrusions continue to grow until the non-spherical droplet solidifies into a non-spherical frozen lipid particle. In this review, the terms lipid and oil are used interchangeably to refer to hydrophobic phases within emulsion droplets.

The lower branch in the evolutionary scheme, Fig. 1a, presents a greater number of possible shape transformations. Since hexagons have six sides, two can disappear in two distinct ways: either parallel to each other, forming rhomboidal fluid particles (see Supplementary Movie 1), or adjacent to two other sides, producing trapezoidal shapes, see Fig. 2d [31]. Neighboring sides cannot vanish simultaneously, as the remaining structure cannot easily reconnect. Single-component droplets typically show 60° and 120° angles. In contrast, for multi-component droplets (prepared from two or more hydrophobic substances mixed prior to emulsification), often particles with square shape and 90° angles are observed, see Fig. 2g [56]. The square particles do not undergo further transformations upon cooling.

After forming rhomboidal and trapezoidal platelets, the particles elongate into long, rod-like structures, Fig. 2e. Upon further cooling and after reaching a certain aspect ratio (e.g. length/initial drop diameter ≥

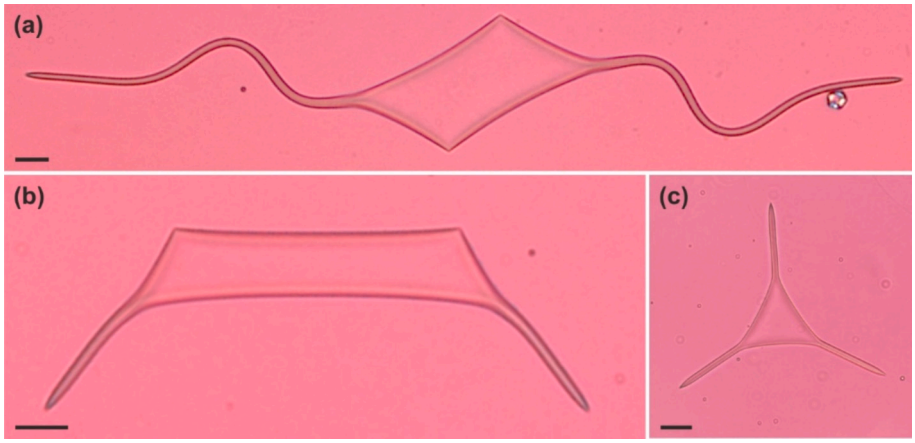

Fig. 3. Microscopy images of platelets extruding long rod-like threads. (a) A tetragonal platelet with thick rod-like asperities extruded from its acute angles. (b) A trapezoidal platelet extruding rod-like threads from its acute angles. (c) A triangular platelet extruding rod-like threads. In all images, hexadecane droplet dispersed in Brij 58 solution are shown. Scale bars = 20 μm.

22 ± 5 for hexadecane drops dispersed in Brij 58 ($C_{16}EO_{20}$) surfactant [31]), the rods undergo a capillary instability, see Supplementary Movie 2. This leads to the compaction of the main part of the oil volume into one or several droplets connected by thin fibers, with numerous smaller droplets often forming along these fibers. At this stage, the process is partially reversible; no real drop splitting occurs and gradual heating restores the initial droplet, see Supplementary videos 6–8 in Ref. [34]. This is only possible due to the elasto-plastic properties of the thin ordered layers of rotator phase present on the surface of the fibers (see Section 2.3 below), which wrap the inner liquid center of the fiber. If such layers were not present together with the liquid fraction, then no such transition would be possible and the extruded rods/fibers would not be flexible. For example, if the fibers become frozen, then upon heating they spontaneously disintegrate into numerous small droplets, as shown in Section 5.1 below.

After the capillary instability process, the evolution continues with the extrusion of thin fibers until final freezing occurs. As an intermediate step, before the capillary instability proceeds, thick or thin asperities may grow from the acute angles of the rhomboidal and trapezoidal particles as shown in Fig. 3.

The described evolutionary sequence presents the main shapes and their transformations observed upon cooling across all studied systems [30,31]. In addition to the main shapes described, various irregular intermediate shapes, such as pentagons or different 90° tetragons with multi-component drops, can also be observed during cooling. However, these shapes depend strongly on the specific experimental conditions and cannot be consistently reproduced in a controlled manner.

2.2. Necessary conditions for drop self-shaping

Experiments performed with various oil-surfactant combinations revealed four key conditions required for the spontaneous drop self-shaping process to occur, see Fig. 4 [30,31,40,57].

The first requirement is related to the chemical nature of the oil

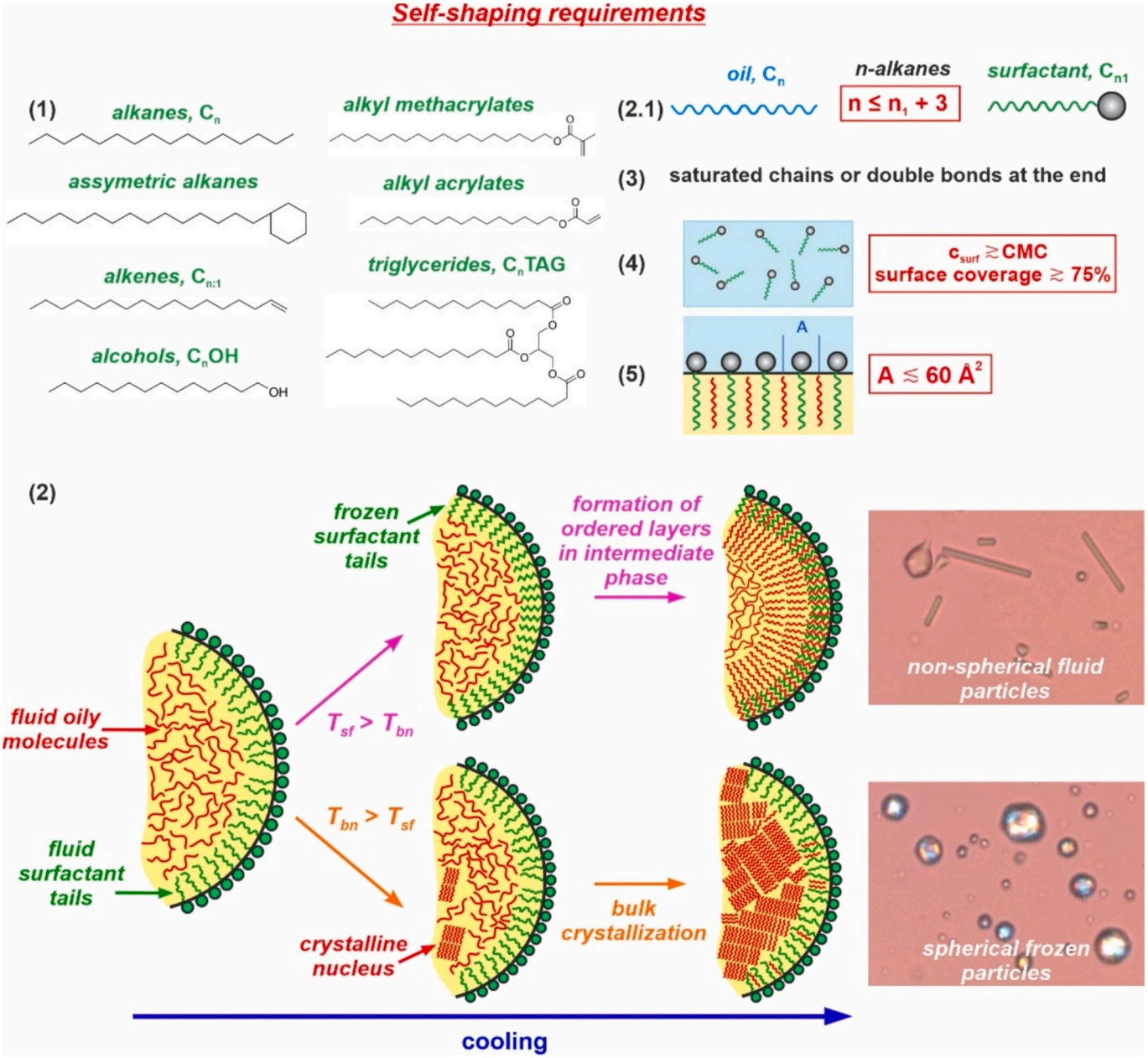

Fig. 4. Schematic representation of the necessary conditions for the occurrence of the self-shaping phenomenon. See the main text for detailed explanations. Part (2): Reproduced with permission from Ref. [40].

dispersed as emulsion droplets. To observe the formation of non-spherical particles upon cooling, the oil should be capable of forming phases of intermediate stability between the fully disordered liquid phase and the completely ordered crystalline phase, see Fig. 4 (1) [31,40]. Such intermediate phases are common in hydrophobic substances with linear molecular structures.

For instance, rotator phases in alkanes [58–62] are well-documented example, where molecules form layers with partial rotational freedom (the long-range order with respect to the rotational degree of freedom in the molecular ordering is missing). Such rotator phases have also been identified in linear alkenes [63], alcohols [64–67], aliphatic aldehydes [68], and more recently, in a novel family of materials based on (1,n'-divynyl)-oligocyclobutane (DVOCB) [69]. While not always referred to as rotator phases, but rather as polymorphic phases or 'gel phase', similar intermediate phases are also found in fatty acids [70], triglycerides [71–74], phospholipids [75–77], and other organic molecules with linear structures [59,71,78].

The broad range of hydrophobic substances capable of forming such intermediate phases makes the self-shaping process widely applicable. Moreover, experiments with oily mixtures combining oils that do not undergo spontaneous self-shaping on their own with those that do, revealed that the self-shaping process can be induced if at least 15 vol% of a "self-shaping substance" is incorporated into the non-self-shaping material [56]. This finding is particularly important from a practical perspective, as most industrially used chemical compounds are complex mixtures rather than pure substances.

The selection of a suitable hydrophobic phase is essential but not sufficient for droplet self-shaping. A second critical requirement involves the relation between the temperature at which crystal nucleation begins within the emulsion droplets and the temperature at which the surfactant's hydrophobic tails freeze [40]. Experiments show that the surfactant adsorption layer must crystallize *before* nucleation initiates inside the droplet volume to enable non-spherical shapes formation, see point (2) in Fig. 4. This typically happens when the surfactant tail is longer than the alkane chain. If internal nucleation occurs first within the droplet volume, deformations before crystallization are not possible [40].

The specific structural arrangement of oil molecules upon crystallization determines the maximal chain length differences (denoted as Δn) between the oil and surfactant tail allowing deformations to occur, see point (2.1) in Fig. 4. For linear alkanes, deformations are observed upon cooling when $\Delta n \leq$ 3C-atoms, where $\Delta n = z - x$, with z representing the number of C-atoms in the alkane and x in the surfactant tail [31]. For example, deformations will be observed for C_{19} (nonadecane) drops dispersed in surfactants with tails of 16 or more C-atoms.

However, for monoacid triglycerides (TAGs), the relationship is modified to $\Delta n = 2y - x$, where y is the number of C-atoms in a single fatty acid residue included in the TAG molecule [40]. This significant difference between alkanes and triglycerides arises because TAG molecules typically adopt a chair conformation upon cooling, with one of the fatty acid residues pointing in one direction, whereas the other two are oriented in the opposite direction [73]. As a result, the melting temperature of TAGs resembles that of an alkane with $2y$ C-atoms rather than that with y C-atoms. Therefore, drop shape deformations can occur even when $\Delta n = 6$, as in trilaurin droplets (C_{12}TAG) stabilized by C_{18}-tail surfactants [40].

The requirement for surfactant tails crystallization before bulk nucleation of linear oil molecules suggests that saturated tails are preferred [31]. If double bonds are present, they should be positioned near the chain end, as the presence of double bond in the middle of the alkyl chain increases molecular flexibility and significantly decreases the melting temperature [31].

The hydrophilic headgroup of the surfactant molecules also influences the deformations upon cooling. This is related to the possibility for formation of well-ordered adsorption layer with frozen surfactant tails. Typically, single-chained ionic surfactants, which have relatively small head groups, allow deformations to occur. For ethoxylated non-ionic surfactants, deformations were observed in molecules with up to ca. 30 ethylene oxide units (-CH_2-CH_2-O-) in the hydrophilic head, i.e. headgroup area $\approx$ 50 Å^2 [31,79]. However, deformations were inhibited in surfactants with larger hydrophilic moieties, see inset in Fig. 6b below.

Surfactant concentration is another key factor [57]. For hexadecane-in-water emulsions, the minimum surfactant concentration required for deformations was found to be approximately equal to the critical micelle concentration (CMC), or for ionic surfactants – to the solubility limit below the Krafft temperature. This holds for low oil volume fractions (e.g. about $\leq$1 vol%, as used in the model optical microscopy experiments). At higher oil contents, greater surfactant concentrations are needed. This can be estimated considering that at least 75 % of the drop surface should be covered with a surfactant able to induce the self-shaping process, as found from experiments with mixtures of surfactants, where one surfactant induces self-shaping and the other does not for the given hydrophobic phase [57].

When an appropriate oil-surfactant combination is selected, droplets undergo self-shaping upon cooling. The next section discusses the mechanism of the observed process.

2.3. Mechanism

At positive interfacial tension, the drops usually adopt a spherical shape to minimize the energetically unfavorable contact between oil molecules situated at the droplet surface and the surrounding aqueous medium. However, in the self-shaping process, droplets transform into various non-spherical shapes with significantly larger surface areas compared to their initial spherical state.

The mechanism explaining the observed drop shape-shifting was initially suggested by *Denkov* et al. on the basis of microscopy observations and data available in the literature [30]. In later studies, this mechanism was confirmed with interfacial tension measurements [80], differential scanning calorimetry (DSC) [38] and small angle X-ray scattering (SAXS) experiments [81]. The proposed mechanism includes formation of plastic (rotator) phases next to the drop surface which are templated by the freezing of surfactant adsorption layer, see Fig. 5.

Before explaining the proposed mechanism in details, we explain our reasoning for excluding other potential explanations. The simplest possible explanation for the observed deformations is that they proceed at nearly zero or ultra-low interfacial tension (IFT, σ), thereby eliminating any significant energetic penalty associated with the surface area increase. However, the interfacial tension measurements for most of the systems studied by us excluded this possibility as the interfacial tensions were found to remain relatively high (above 3–5 mN/m), see Fig. 6d [40,80]. Note that the surface freezing phenomenon is typically associated with a steep decrease in the IFT values against temperature due to the immobilization of the frozen surface molecules whose entropy (S_S) suddenly becomes significantly lower compared to the entropy of the molecules in the bulk phase (S_B), $d\sigma/dT \approx -(S_S - S_B) > 0$ for temperatures below the surface freezing temperature [83,84]. However, the absence of steep decrease in the IFT(T) curves for the polysorbate surfactants shown in Fig. 6d, is most probably related to the fact that these surfactants are technical mixtures of molecules with different hydrophilic moieties. Hence, the explained entropy effect interferes with the possibility for exchange of different molecules of the adsorption layer with the bulk solution, which is not completely suppressed after the surface freezing and no steep decrease in the IFT(T) is observed [80].

As the possibility for having ultralow interfacial tension was excluded for most of the systems studied by us, another mechanism involving the formation of multilayers of ordered phase adjacent to the drop surface was suggested and confirmed to be operative [30,38,40,80,81].

Notably, in a parallel series of studies, the ultra-low interfacial tension mechanism was invoked to explain similar observations seen in

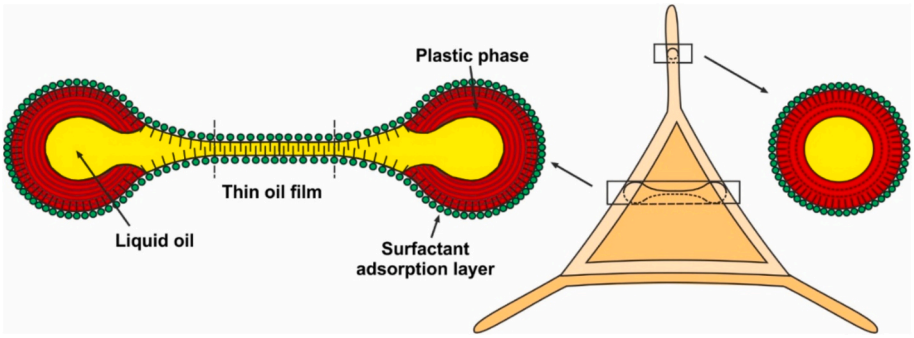

Fig. 5. Schematic representation of the drop self-shaping mechanism including formation of plastic phases near the drop surface. Cross-sections of the deformed triangular particle with cylindrical protrusions are shown. Upon cooling, the surfactant tails adsorbed on the particle surface freeze, inducing ordering of the adjacent oil molecules (shown in red). This structured phase counteracts the inner capillary pressure of the liquid oil within the particle, enabling the formation of various non-spherical fluid shapes during the cooling. Adapted from Ref. [82]. (For interpretation of the references to colour in this figure legend, the reader is referred to the web version of this article.)

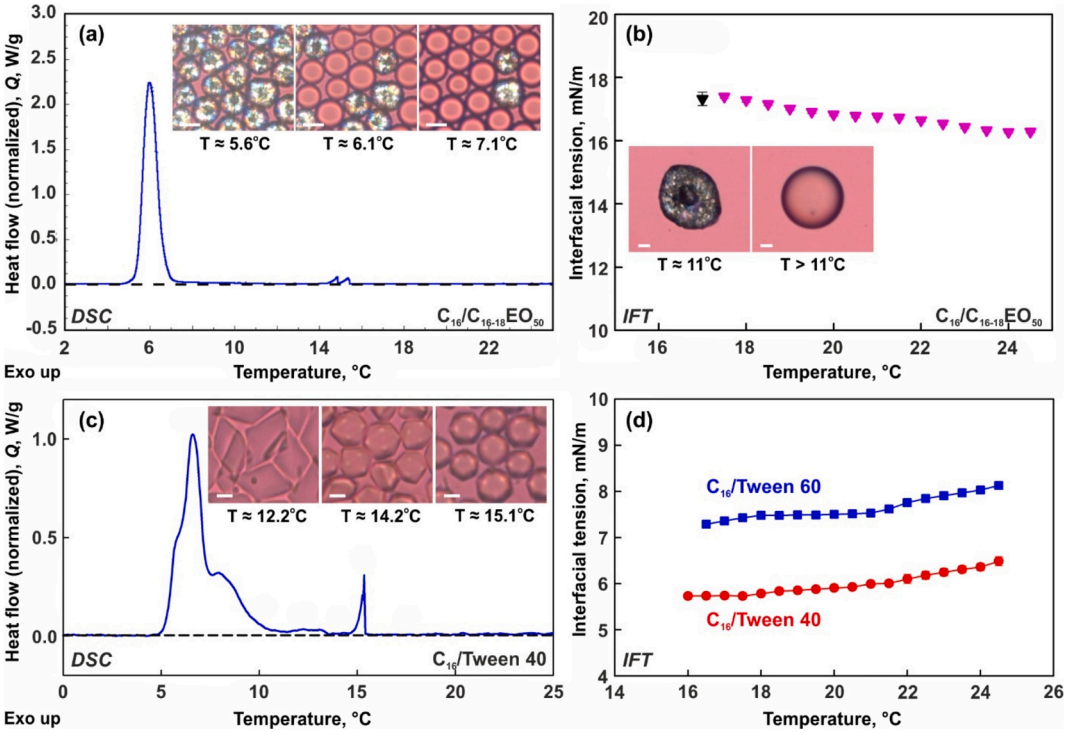

Fig. 6. Illustrative results of DSC and interfacial tension (IFT) measurements for emulsion systems in which deformations are not observed (a,b) and systems in which deformations are observed (c,d). (a) Differential scanning calorimetry thermogram obtained upon cooling of hexadecane drops dispersed in 1.5 wt% Lutensol AT50 ($C_{16\text{-}18}EO_{50}$) surfactant solution. Drops in this system do not deform upon cooling due to the relatively voluminous surfactant head group. Depending on their size, the freezing is observed after different supercooling. In this case, the sample contains drops with initial diameter ≈ 12 μm which freeze at T ≈ 6 °C. At this temperature the DSC peak is observed. (b) IFT vs T measurements for the system shown in (a). The measured IFT is ca. 16–18 mN/m. (c) DSC thermogram for hexadecane drops dispersed in Tween 40 solution. The drop shape deformations begin around 15.1 °C where the first peak in the thermogram is observed. No drop freezing is observed down to 12.2 °C in the microscopy experiments, i.e. the released enthalpy is entirely due to the plastic phase formation on the deforming particles surface. (d) Interfacial tensions measured at the C_{16} – Tween 40/Tween 60 interfaces. The measured values are much lower than those for the non-self-shaping systems, however they remain much higher than 1 mN/m. Scale bars in all pictures = 10 μm. The figures are adapted from Refs. [38, 80].

hexadecane drops dispersed in C_{18}TAB cationic surfactant (octadecyltrimethylammonium bromide), which has a Krafft point of ≈ 36 °C [85], whereas the hexadecane melts at 18 °C [33,41,42]. This system undergoes similar drop shape deformations upon cooling, although the observed shapes are more irregular. Furthermore, theoretical analysis suggests that both the ultra-low interfacial tension and the plastic phase formation hypotheses are theoretically feasible if one assumes that the energy density at the highly curved edges of the deformed droplets is lower than that of the flatter regions [30,32,86]. Therefore, it remains possible that these two distinct mechanisms operate in different experimental systems (e.g. for some of those classified in *Group A*, see Fig. 9e below, the ultra-low interfacial tension mechanism may be operative). However, since the rotator phase mechanism is more complex, next we present the arguments that validate its applicability to the systems we have studied in detail. For a more in-depth discussion on the ultra-low interfacial tension mechanism, readers are redirected to the original works by Sloutskin and co-authors, where this mechanism is thoroughly explained [33,41–43,46].

The rotator phases have properties closer to those of the crystalline phases rather than the liquid phase. For example, the shear storage

modulus of the rotator phases of alkanes was found to be ≈ 10^4–10^5 Pa depending on the chain length, which is about one order of magnitude lower compared to the shear storage modulus of the crystalline phases [87]. In comparison, the shear storage modulus of the liquid alkanes at low frequency is zero. Furthermore, the enthalpy for transition of the liquid to rotator phase accounts for ca. 65–80 % of the total enthalpy of the liquid to crystalline phase transition [58]. Rotator phases have been previously observed not only in bulk materials, but also as surface layers [58,83,84,88,89], as well as in micro- and nanoconfinements [81,90–93]. It has been also established that the stability of the rotator phases increases significantly in confinements, as well as when mixtures of molecules are present [58].

Therefore, their formation was invoked to explain the observed emulsion drop deformations. The simplest possible mechanism would be that the entire particle volume structures in a plastic rotator phase upon cooling. However, this hypothesis is contradicted by the continuous shape evolution and the elastic properties of the deforming particles. Additionally, when the whole particle volume transitions into a rotator phase, faint colors appear in polarized light microscopy images, see Fig. 7c, whereas the deforming fluid droplets remain colorless.

Therefore, another more complex mechanism was suggested. This mechanism highlights the critical role of the surfactant adsorption layer crystallization, which must occur before bulk nucleation begins, Fig. 4 (2) [40]. Upon cooling, a mixed surfactant-oil monolayer forms at the

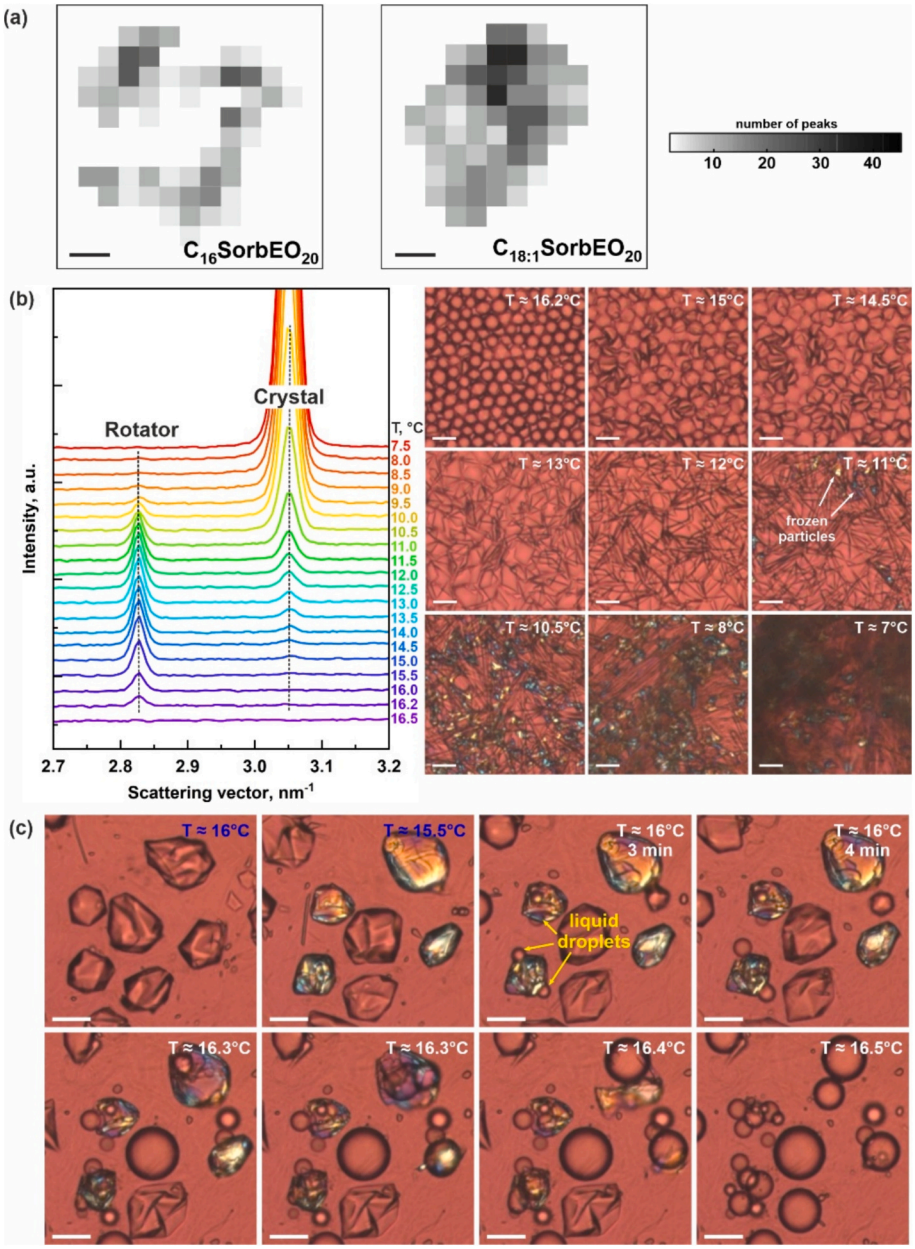

Fig. 7. (a) Microbeam SAXD analysis of hexadecane drops stabilized by $C_{16}SorbEO_{20}$ surfactant, which is able to induce self-shaping (left picture) and $C_{18:1}SorbEO_{20}$ surfactant (right picture) which does not induce self-shaping. Formation of ordered multilayers is detected in the left picture, whereas the whole drop freezes in the right picture. Adapted from Ref. [29]. Scale bars = 10 μm. (b) SAXS spectra and corresponding optical microscopy observations performed with hexadecane drops stabilized by $C_{16}SorbEO_{20}$ surfactant. Rotator phase peak is observed at temperatures where the drop deformations begin before the crystalline peak emerges at lower temperatures. (c) Optical microscopy images of hexadecane drops, stabilized by $C_{16}EO_{10}$ surfactant. The following temperature protocol has been applied to the sample: cooling from 23 °C to 15.3 °C at 0.5 °C/min rate; temperature increase to 16 °C and isothermal storage for 5 min; heating to 16.5 °C. Melting of the bulk rotator phase formed is observed at $T \approx 16.5$ °C and the drops restore their spherical shape. (b,c) Adapted from Ref. [81]. Scale bars = 20 μm.

drop surface which serves as a template for the inner ordering of the oily molecules next to the drop surface. These molecules organize into multilayers of a plastic rotator phase (or another intermediate in stability phase). This surface-ordered phase possesses a sufficient mechanical strength to counteract the inner capillary pressure of the liquid oil, enabling the formation of various non-spherical fluid shapes. A schematic representation of the proposed mechanism in shown in Fig. 5 [30,31]. Note that the thickness of the platelet center varies over time and also, it may be covered with thin layers of plastic rotator phase.

Non-spherical shapes can only exist at a finite interfacial tension if the capillary pressure of the liquid oil inside the droplet is mechanically overcome. Otherwise, the drops will remain spherical due to the surface energy minimization principle. The mechanical balance between the interfacial tension and the bending moment created by the plastic rotator phase can be expressed as: $K_B \geq \sigma r^2$, where K_B is the bending elasticity constant of the interface (including the multilayers of the rotator phase), σ is the interfacial tension, and r is the radius of curvature [30]. Typical values of the parameters are $r \approx 0.5$–1 μm and $\sigma \approx 2$–10 mN/m. Therefore, the bending elasticity constant should be at least 10^{-15} to 10^{-14} J to counteract the inner capillary pressure. However, these values are several orders of magnitude higher than those reported in the literature for frozen lipid bilayers and adsorption monolayers, where $K_B \approx 10^{-18}$ to 10^{-17} J [30,94,95]. Therefore, the drop deformation can only be explained by the formation of multilayers of plastic rotator phases (or other type of intermediate in stability phases) adjacent to the drop surface.

This mechanism is supported by the results from various experimental techniques used in the drop self-shaping studies, as well as by numerous other experimental observations. In particular, the interfacial tension measurements described in details in Ref. [80] demonstrate that the IFT remained $\gtrsim 2$ mN/m for all of the studied systems [31]. Furthermore, significant decrease of the IFT upon decrease of the temperature was observed only for the systems in *Group A* (see Fig. 9e below), which were also found to have the smallest thickness of the rotator phase via the DSC analysis performed in Ref. [38]. For the systems in *Groups B* and *C*, the IFT remained even higher than 5 mN/m until the freezing of the millimeter droplet used for measurements by the pendant drop method proceeded, see Fig. 6d. For all of the studied systems, the interfacial tension measured at temperatures at which the drop shape deformations begin was ≥4 mN/m [80].

Two experimental techniques have been used to detect the formation of plastic rotator phases. Indirect detection of the rotator phases in self-shaping drops allowing to estimate the rotator phase thickness, has been achieved through DSC experiments [38]. Furthermore, direct structural information evidence confirming the formation of rotator phases in alkane drops undergoing spontaneous shape changes upon cooling has been obtained via SAXS measurements [28,29,81,96,97]. In their studies *Shinohara* et al. used microbeam SAXD to show the formation of a plastic rotator phase adjacent to the drop surface in a system of 30–50 μm hexadecane drops dispersed in a $C_{16}SorbEO_{20}$ (Tween 40) surfactant solution [29]. In contrast, when the surfactant was replaced with one containing a double bond in the middle of its hydrophobic tail ($C_{18:1}SorbEO_{20}$), the entire drop froze without forming the rotator phase [29]. Fig. 7a presents maps of the internal structures obtained with the two different surfactants. The intensity of each pixel in these maps represents the scattering intensity measured from the respective region of the droplet, as probed by a micrometer-sized X-ray beam. Note that these studies were performed several years before the discovery of the self-shaping process and were conducted with relatively high cooling rates, which did not allow sufficient time for the formation of regular non-spherical shapes upon cooling.

In more recent studies, our group investigated similar systems using experimental conditions that are known to facilitate shape deformations during cooling [81,97]. Notably, rotator phase formation was detected only for hexadecane drops stabilized by surfactants allowing the spontaneous deformations upon cooling, see Fig. 7b. For the hexadecane drops, stabilized by $C_{12}SorbEO_{20}$ (having too short hydrophobic tail) no such peak was detected [81]. Furthermore, the detailed investigations demonstrated that under appropriate conditions, the entire drop volume may structure in a rotator phase before the final crystallization and the formation of the triclinic phase proceeds. This rotator phase remained stable in a narrow temperature interval upon cooling. If heated, it melted up to ca. 16.5 °C, transforming the drops back to the characteristic spherical shapes, see Fig. 7c [81].

The SAXS/WAXS experiments confirmed the formation of the rotator phase in drops undergoing self-shaping upon cooling. However, these studies do not provide direct information regarding the thickness of the rotator phase. An estimate of this thickness was made using data from DSC experiments performed with emulsion samples [38]. In these experiments, the heat released during the cooling of the samples was detected. The results show that for all studied systems in which drop deformations occur upon cooling, peaks appear in the thermograms at temperatures higher than the freezing temperature, see Fig. 6c. These peaks can only be explained by the formation of an ordered phase, which causes the observed heat release. In contrast, for systems where no drop shape deformations are not observed, a single Gaussian-shaped peak is seen at the temperatures corresponding to the drop freezing process, see Fig. 6a.

The results from DSC measurements provide quantitative information on the percentage of molecules which undergo liquid-to-rotator phase transition before drop freezing. By combining this information with optical microscopy images and a geometrical model of the three-dimensional particle shape, we were able to estimate the thickness of the plastic rotator phase formed on the surface of various non-spherical droplets [38]. In these estimates, it was assumed that the ordered phase formed is adjacent to the particle surface, as suggested by the experimental observations. The analysis revealed that the number of ordered layers on the surface of tetragonal platelets is around 22 ± 6 layers (i.e. 45 ± 12 nm), whereas for thin, fiber-like particles, the number of layers is around 3–4 (6–10 nm). A detailed description of the models used for these estimates is available in Ref. [38]. Note that although the same oil-surfactant combination was used in these experiments (hexadecane drops stabilized by $C_{16}SorbEO_{20}$ surfactant), the rotator phase thickness in the tetragonal particles was estimated from experiments with 9.5 μm droplets, whereas for the formation of fiber-like particles, drops with initial diameter of 3 μm were used. Therefore, a direct comparison between the number of ordered layers in the two different systems may not be entirely correct due to the significantly different drop volumes.

These estimates facilitated a theoretical analysis of the bending elasticity constant dependence on the multilayer thickness, h_{PL}. Two different models relating K_B to h_{PL} for thin elastic shells are available in the literature. The model of Evans and Skalak [94,98] neglects the contribution of the non-zero shear modulus to the bending and finds that under this assumption, $K_B \sim h_{PL}^2$. The model of Kirchoff and Love [99], on the other hand, considers the opposite extrema – the bending of a fully solid isotropic layer in which the shear resistance between the separate molecular layers in the multilayer is accounted for. Under this assumption, the dependence becomes $K_B \sim h_{PL}^3$, and the balance between the IFT and bending moment created by the multilayers of the plastic phase is given by:

$$h_{PL} \geq h_{mono}\left(\sigma r^2 / K_{B,mono}\right)^{1/3}, \quad (1)$$

where $K_{B,mono}$ is the bending elasticity modulus for a monolayer incorporated in a multilayer stack. Using a high estimate for $K_{B,mono} \approx 10^{-17}$ J, $h_{mono} \approx 2$ nm, and $r \approx 1$ μm, we estimate that $h_{PL} \geq 16$ nm for $\sigma \approx 5$ mN/m and $h_{PL} \geq 7$ nm for $\sigma \approx 0.5$ mN/m [38]. These estimated values double if $K_{B,mono} \approx 10^{-18}$ J instead of 10^{-17} J. When the same calculations are performed under the Evans and Skalak assumption, thicknesses between 15 and 300 nm are calculated [30].

A comparison between the theoretical analysis and the results obtained from the calorimetry experiments [38] shows that the Kirchoff-

Love model better describes the multilayer thickness in self-shaping drops. This suggests that the rotator layers are strongly interlocked and exhibit high shear resistance, similar to that found in solid crystals. Note that this result is in good agreement with the shear storage and loss rheological moduli measured directly for the rotator phases in long chain alkanes [87].

Furthermore, several experimental observations also support the conclusion that the interfacial tension in the systems studied by us is not ultra-low, but positive. These observations include, but are not limited to: the circular shape of the holes formed in the deforming particles, see Fig. 2c; the immediate formation of spherical droplets upon drop breakage and disruption of the rotator phase, see **Section 5** below; the formation of cylindrical asperities demonstrating that the system exhibits a spontaneous curvature with a radius ranging from several tens of nanometers up to a micrometer (a possible origin for this spontaneous curvature is interfacial tension difference appearing on both surfaces of the thin rotator phase, e.g. between the liquid oil/rotator phase and rotator phase (adsorption layer)/surfactant solution); the fact that interactions between the individual fluid particles do not lead to particles bending, but rather – the particles preserve their individual shapes, indicating that they are relatively stiff. Based on SAXS, DSC, IFT measurements, and direct optical microscopy observations, we concluded that our findings cannot be explained with the ultra-low interfacial tension mechanism suggested previously by Sloutskin et al. [33,41–43,45,46]. Instead, they are explained with the formation of multilayers of plastic phase adjacent to the drop surface.

2.4. Control factors

The drop shape deformations upon cooling were found to be influenced by two primary factors, besides the appropriate oil-surfactant combination: the cooling rate and the initial drop size. As a general rule, smaller drops that are cooled at a slower rate and stabilized by surfactants with longer tails undergo shape transformations more easily and reach the final stages of the evolutionary sequence [31]. Illustrative results demonstrating the effect of the initial drop size are presented in Fig. 8. Therefore, when working with an unknown substance and seeking to assess its ability to form non-spherical particles during cooling, small emulsion droplets ($d < 10$ μm) should be prepared in a surfactant solution with sufficiently long hydrophobic tail (e.g., C_{18}). These drops should then be cooled from a temperature above the bulk melting temperature of the dispersed oil to the freezing temperature, at a low cooling rate (< 0.5 °C/min) to determine whether their spherical shape changes before freezing.

The cooling rate dependence can be easily explained, as lower cooling rates provide more time for molecular reorganization and ordering, allowing the formation of structures with minimal energy. This is particularly important for larger molecules, such as triglycerides, which are much less mobile than alkane molecules even in liquid state [40].

The fact that smaller droplets deform more easily is not trivial, because these droplets have higher capillary pressure, $p_c = 4\sigma d^{-1}$, where σ is the oil-water interfacial tension and d is the drop diameter. This experimental observation, however, can be attributed to the difference in the radius of curvature between smaller and larger droplets [31]. The curvature in smaller droplets is likely closer to the preferred curvature for the formation of the rotator phase, which facilitates the easier formation of this phase and respectively the easier drop shape deformations. Further dedicated investigations and molecular modeling is needed to fully understand this peculiarity.

The role of the specific surfactant-oil combination in the observed shape changes follows from the general rule for drop deformations upon cooling. For the same surfactant, which allows drop deformation (i.e. with not too voluminous head group and sufficiently long hydrophobic tail), drops from hydrophobic phases with shorter chain lengths will deform more easily than those composed of hydrophobic phase with longer chains. For example, under otherwise equivalent experimental conditions (initial drop size, cooling rate), when stabilized by the $C_{16}EO_{20}$ surfactant, C_{20} drops do not deform before freezing, while C_{19} and C_{18} drops reach the initial stages of the evolutionary sequence. In contrast, C_{16} and C_{17} drops are able to reach the final stages of the evolutionary sequence if sufficiently small drops are used or under slow cooling, whereas C_{15} and C_{14} drops easily deform to the final stages of the evolutionary sequence even cooled at higher rates (e.g., up to 2 °C/min) [31]. A reverse scenario also holds true: for the same hydrophobic substance, drops are more likely to deform when stabilized by surfactants with longer hydrophobic tails.

These observations can be explained by the fact that the length of the surfactant tail determines the temperature at which the adsorption layer freezes, see the schematics in Fig. 4. When surfactant molecules have longer tails than the dispersed oil, they freeze at a higher temperature compared to the oil, thereby allowing more time for the reordering of dispersed oil molecules and the formation of a surface-ordered phase.

A classification into four distinct groups was made depending on the temperature at which the drop deformations begin, T_d, and its comparison with the bulk melting temperature of the dispersed oil, T_m, see Fig. 9 [31]. In *Group A* are systems for which the drop deformations begin at $T_d > T_m$. For these systems, easy deformations and characteristic formation of thin fibers is observed. In *Group B* are systems for which $T_d \approx T_m$, and in *Group C* those for which $T_d < T_m$. In the fourth group, *Group D*, are systems in which drop shape deformations are not observed.

2.5. Stability of the non-spherical fluid and frozen particles

The described deformations proceed while the drops are in fluid state. Once the oil freezing temperature is reached, the entire particle undergoes a liquid-to-solid phase transition, allowing the formation of non-spherical particles in both micrometer and submicrometer size ranges. These frozen particles can maintain their non-spherical shape indefinitely if stored at temperatures below the bulk melting point of the frozen oil [30,31,55]. It should be noted that for binary alkane mixtures with a chain length difference greater than 4C-atoms, the preservation of

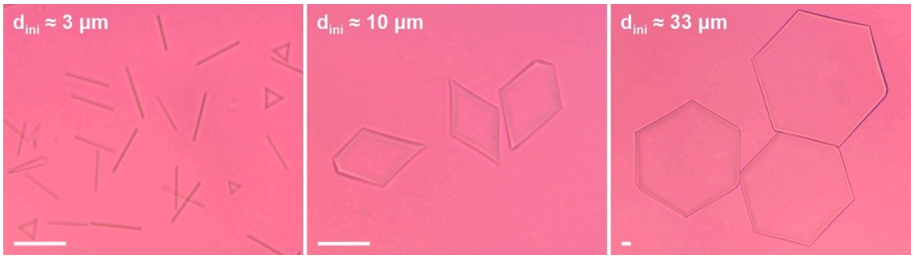

Fig. 8. Effect of initial drop size for the shape deformations upon cooling. The shape which can be observed with the same oil-surfactant emulsion system depends on the initial drop size. As a rule, the smallest drops deform easier compared to the bigger drops. This trend is illustrated for C_{16} drops in Tween 40 solution, cooled at 0.5 °C/min. The 3 μm drops elongate further transforming into thin long fibers before freezing. In contrast, the 10 μm drops will freeze into the tetragonal platelet shapes, whereas the bigger 33 μm drops reach only the hexagonal platelets stage. Scale bars = 20 μm.

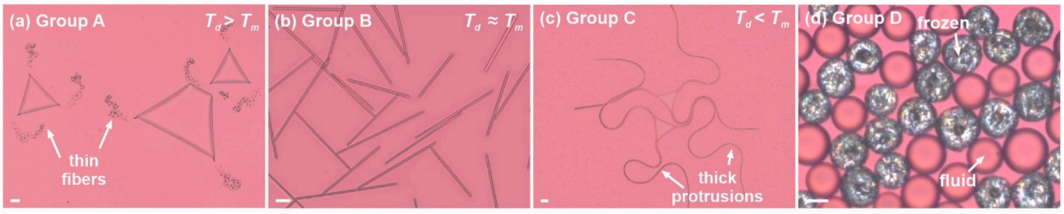

(e)	Main structural characteristic of surfactants	T_d vs T_m	Preferred shapes	Layers' strength (thickness)
Group A	Long tail and/or shorter EO chain Long tail anionic	$T_d > T_m$	Fibers with diameters ≈ 1.5 and ≤ 0.5 μm Different platelets and ellipsoidal drops extruding such fibers	Thin flexible layers
Group B	Sorbitan ring Short EO chain	$T_d \approx T_m$	Hexagonal platelets Rods with diameter ≈ 5 μm The platelets do not extrude asperities from their corners	Very strong (thick) layers
Group C	Larger EO head and/or shorter tail Long tail cationic	$T_d < T_m$	All shapes are observed with a transition from rods with diameter ≈ 5 μm into fibers with diameter < 1 μm	Intermediate (soft rods)
Group D	Short tail Very large head-group Double bond in the tail	T_d not observed	Spherical	Not detected

Fig. 9. Classification of the emulsion systems into four separate groups. (a-d) Microscopy pictures showing typical shapes formed with hexadecane drops dispersed in different surfactant solutions: (a) Brij S20, $C_{18}EO_{20}$; (b) Tween 60, $C_{16}SorbEO_{20}$; (c) Brij 58, $C_{16}EO_{20}$ and (d) Tween 20, $C_{12}SorbEO_{20}$. (e) Table with description of the main features of each group. Preferred shapes are determined from experiments with a continuous cooling and hexadecane drops. T_d and T_m denote the drop shape deformation temperature and melting temperature for the oil, respectively. Table shown in (e) is adapted from Ref. [15]. Note that for part of the systems classified in *Group A*, the ultra-low interfacial tension mechanism could not be completely excluded.

the non-spherical shape upon cooling is only possible if a third component with an intermediate chain length is added to the mixture [56]. Otherwise, the two alkanes partially phase separates upon cooling and the multi-component drops do not preserve their non-spherical shape upon freezing, see Section 2.7 and Fig. 12 below.

The stability of the non-spherical fluid particles, however, turn out to be somewhat more complex [39]. Careful experiments performed with various alkane-surfactant systems, cooled to a specific temperature and then maintained under isothermal condition for an extended period, showed that polyhedras, hexagonal, and tetragonal prisms are always unstable [39]. Particles evolved into these shapes continued to slowly evolve into subsequent stages of the drop shape evolutionary scheme even when the temperature was held constant [39]. In contrast, once triangular platelets are formed, they remain stable for several hours, showing no signs of shape change, see Fig. 10.

The stability of rod-like fluid particles was found to be governed by the structure of the surfactant adsorption layer. It is well known that commercial non-ionic alcohol ethoxylate surfactants consist of mixtures of molecules with varying structures, primarily differing in the number of ethylene oxide units present in the hydrophilic head [100,101]. As a result, dynamic exchange occurs between the molecules adsorbed on the non-spherical particle surface and those within the micelles in the aqueous phase, as the different molecular species will have different adsorption energies and kinetics. This exchange leads to continuous shape-shifting and capillary instability of the rods, stabilized by such surfactants (e.g. Tween 60). In contrast, rod-like particles stabilized by surfactants with narrower compositional variations (e.g. Brij 52, $C_{16}EO_2$) maintain their length once a constant temperature is established during the experiment, Fig. 10 [39].

Further experiments with varying degrees of subcooling showed that the rate of shape transformations under isothermal conditions increases non-linearly with the decrease of temperature. Additionally, the formation of fluid shapes extruding rods and fibers from their acute angles was observed in these experiments, not only for systems where this process was seen under constant cooling conditions, but also for the other systems [39]. This result indicates that the formation of all different shapes from the drop shape evolutionary sequence is generally possible for systems able to break symmetry upon cooling. However, the specific timescale at which these shapes are observed depends strongly on the specific oil-surfactant combination.

2.6. Theoretical modeling

The main stages of the drop shape evolution observed experimentally upon cooling were successfully predicted by a theoretical model [18]. In this model the fine balance between the rotator phase formation and surface tension is considered and the observed geometrical shapes are understood as local energy minima. The model considers only the chemical potential for the oily molecules, as it governs the relevant phase transitions. The total energy of the oily droplet is expressed as:

$$E = \mu_l V_l + \mu_r V_r + \sigma A, \tag{2}$$

where μ is the chemical potential per unit volume, V is the volume, A is the curved surface area, σ is the oil-water interfacial tension, and l and r subscripts refer to liquid and to the rotator phases, respectively. The rotator phase formation is energetically favorable only if $\Delta\mu = \mu_l - \mu_r > 0$.

The chemical potential difference for the oily molecules at a temperature 1 K below the rotator phase formation temperature, T_r, can be approximated as: $\Delta\mu \approx \Delta S_{lr}(T_r - T)$, where ΔS_{lr} is the entropy change per unit volume for the liquid-to-rotator phase transition, estimated as $\Delta S_{lr} \approx 6 \times 10^5$ N/m^{2}K [32]. Alternatively, using the thermodynamic relation for the Gibbs free energy at the phase transition temperature T_r, $\Delta G = \Delta H - T\Delta S = 0$, this becomes $\Delta\mu \approx \Delta H_{lr}(T_r - T)T_r^{-1}$, relating the potential

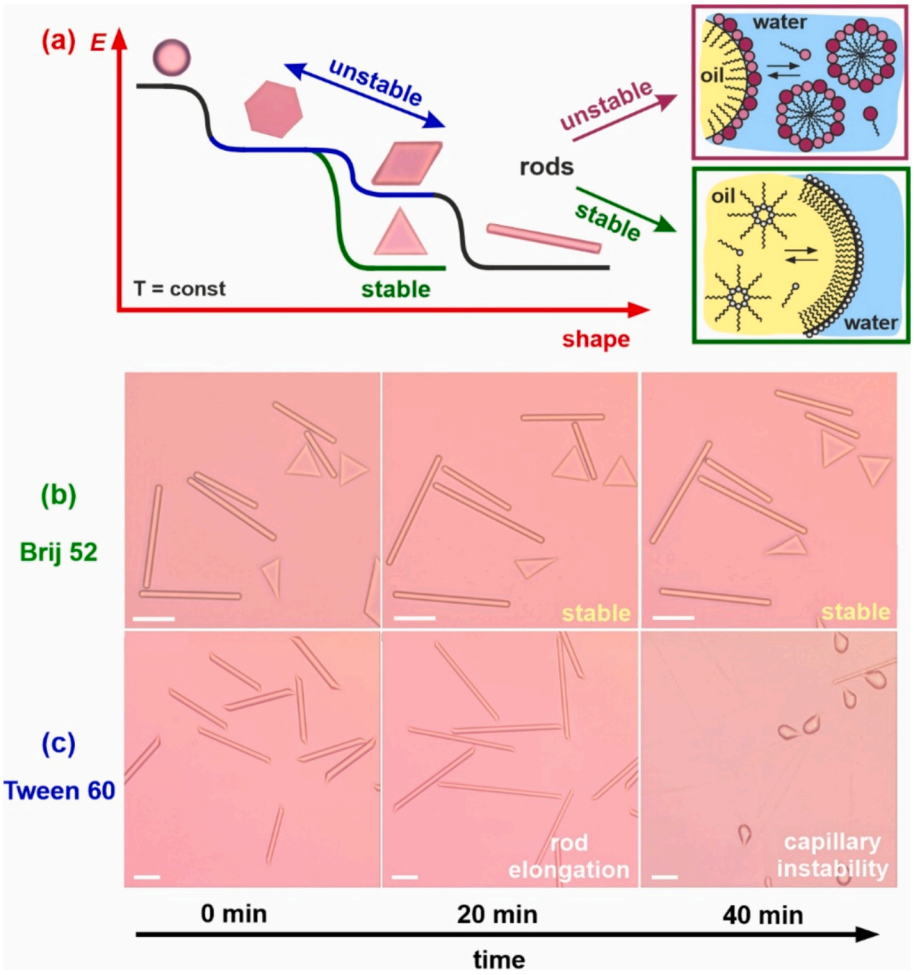

Fig. 10. Stability of fluid non-spherical particles under isothermal conditions. (a) A schematic energetic landscape illustrating that non-spherical fluid particles remain stable under isothermal conditions only when triangular platelets are formed or when rod-like particles are present, with the surfactant adsorption layer composition remaining relatively constant over time. (b,c) Optical microscopy images showing stable non-spherical hexadecane fluid particles in the presence of Brij 52 (b) and continuous shape evolution when the drops are stabilized by Tween 60 (c). Scale bars = 20 μm. Adapted and partially reproduced with permission from Ref. [39].

difference to the phase transition enthalpy (ΔH_{lr}).

To estimate the volume of the rotator phase, the model assumes that it scales with the perimeter of the polygonal frame, P: $V_r = PA_r$, where $A_r \approx 0.3\ \mu m^2$ is the cross-sectional area of the rotator phase formed at the platelet periphery. It is approximated as a spherical ring of outer diameter ≈ 2 μm and thickness ~ 100 nm. Rescaling the energy expression using the initial spherical droplet perimeter $P_0 = (6\pi^2 V)^{1/3}$, and neglecting constant terms, yields a dimensionless energy [32]:

$$\mathscr{E} = E\Big/\left(\sigma {P_0}^2\right) = \mathscr{S} - \alpha\mathscr{P} = \mathscr{S} - (A_r\Delta\mu)\Big/\left(V^{1/3}\sigma\left(6\pi^2\right)^{1/3}\right)\mathscr{P} \quad (3)$$

In this equation α is a positive dimensionless parameter. This expression reflects the competition between surface tension (which tries to minimize the surface area $\mathscr{S}$) and the energetic gain from the rotator phase formation (which favors larger values for the perimeter $\mathscr{P}$) [32].

To model the temperature-dependent drop shape evolution, a linear stability analysis was performed using this equation and a regular hexagon as starting shape [32]. This analysis revealed three linearly independent growing modes: one triangular mode and two parallelogram modes. The model predicts that small perturbations (ε) favor triangle formation, while larger perturbations lead to parallelograms and trapezoids. This result is consistent with the experimental observations, as the perturbation magnitude ε is expected to increase with both the increase of the cooling rate and decrease of the droplet size. Both factors lead to a less regular arrangement of topological defects on the drop surface, thereby increasing ε. Furthermore, this analysis showed that if all other parameters are held constant, $\alpha \propto \varepsilon^{1/2}$. Therefore, the model predicts that smaller drops would be less likely to evolve into triangles and more likely to form parallelograms, in agreement with the experimental data [31,32].

The model also successfully explains other observed phenomena, such as droplet puncturing leading to toroidal fluid structures. Additionally, it shows the possibility for the development of protrusions from the acute angles of the polygonal shapes. This latter behavior is reproduced only when elastic bending of the polygonal edges is included in the model, allowing vertex defects to be energetically resolved via localized curvature [31].

Later, the theoretical model was expanded to consider not only the evolution sequence once the platelets are formed, but also the complete three-dimensional evolution from the spherical shape into a flattened platelet [86]. In this model, the rotator phase was assumed to form predominantly near the edges of the polyhedron. Furthermore, a function encoding the tendency for rotator phase formation depending on the dihedral angle between two facets was introduced. The performed linear stability analysis demonstrated that, a small perturbation of the parameters defining the initial symmetrical icosahedron, results in the formation of octahedron, which then flattens into a platelet shape. A result in complete agreement with the experimental observations.

The flattening model [86,102] was argued to be applicable to both

rotator phase mechanism suggested by our group [30,31,38,81] and the elastic buckling mechanism developed by Sloutskin et al. [41,103]. However, the calculations showed that in order for the flattening to occur in presence of a single ordered surface layer, an initial perturbation is needed and the interfacial tension should decrease by at least four orders of magnitude during the cooling. This would allow the flattening to be driven solely by the buoyancy and elasticity competition [86]. Note that, on Earth, the initial perturbation is defined physically by the buoyancy of the droplets. However, if this mechanism is responsible for the shaping observed in part of the oil-surfactant combinations, it remains unclear whether the same evolutionary sequence can occur in the absence of gravity. Further experiments are needed to answer this question.

2.7. Multicomponent drops

Most industrially applicable substances consist of mixtures of molecules. Therefore, the ability of mixed drops to self-shape is crucial for the practical applications of self-shaping process. From the perspective of droplet self-shaping, chemical substances can be broadly classified into two main categories – "self-shaping" and "non self-shaping" substances. The first includes those that, when dispersed as oil droplets in a given surfactant, are able to deform upon cooling. The second category consists of chemical compounds which do not exhibit self-shaping under similar conditions.

Experiments with various mixtures prepared with self-shaping compounds show that all mixed drops are able to deform upon

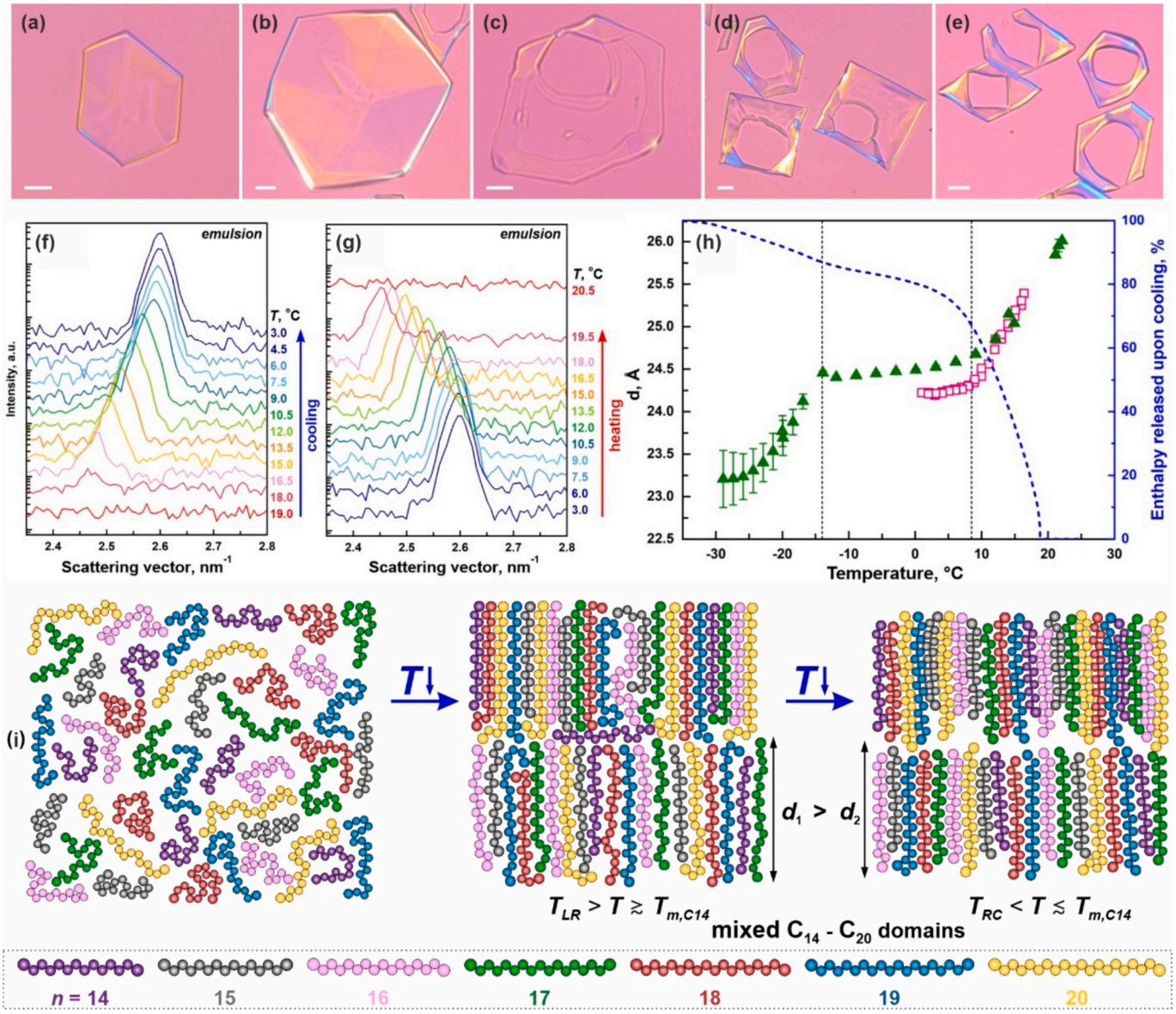

Fig. 11. Self-shaping process observed with multicomponent alkane drops. The chain-length difference between the two neighboring alkanes in the mixture is $\Delta n \leq$ 3C-atoms. (a-e) Collection of plastified particles with various non-spherical shapes. The plastified particles exhibit only faint colors on their periphery. The emulsion systems are: (a,b) $C_{16} + C_{19} = 1{:}1$ (*v*/v); (c) $C_{16} + C_{17} = 1{:}1$ and (d,e) $C_{16} + C_{18} = 1{:}1$. All emulsions are prepared in 1.5 wt% Tween 60 surfactant solution. Scale bars = 10 μm. (f,g) SAXS spectra obtained upon cooling (f) and heating (g) of 18 μm mixed emulsion droplets prepared with 1:..:1 mixture of all alkanes with chain lengths between C_{14} and C_{20} (a 7-component mixture) stabilized by $C_{18}EO_{20}$ surfactant. (h) Interlamellar spacing as a function of temperature for C_{14}-to-C_{20} mixture studied in bulk (filled green triangles) and in emulsion (empty pink squares). The dashed blue line shows the released enthalpy as a function of temperature measured using DSC. (i) Schematic representation of the mixing behavior within the rotator phase formed in C_{14}-to-C_{20} 7-component mixture. All molecules arrange together in a mixed rotator phase. (f-i) adapted from Ref. [81]. (For interpretation of the references to colour in this figure legend, the reader is referred to the web version of this article.)

cooling, following the evolutionary sequence as single-component drops, see Fig. 1a above [56]. The main difference is that, in mixed drops, alongside the typical 60° and 120° angles observed in platelets, many platelets with 90° angles are also present, see Fig. 11a-e. The mechanism driving drop self-shaping in mixed drops is similar to that observed for single-component drops.

A noteworthy difference arises during the solidification of deformed, non-spherical fluid particles [56]. Mixed drops, prepared with alkanes with chain length difference < 4C-atoms, preserve their anisotropic shape upon solidification, forming a single mixed rotator phase throughout the particle volime. Therefore, we refer to this liquid-to-solid phase transition as "plastification" to highlight the difference in the final solid phase obtained (as compared to the crystalline phase formed in single-component drops). This results from the significantly expanded area of rotator phase existence for alkane mixtures compared to the single alkanes [58]. The plastified particles display faint birefringence under polarized light due to partial molecular order in their rotational degrees of freedom, see Fig. 11a-e.

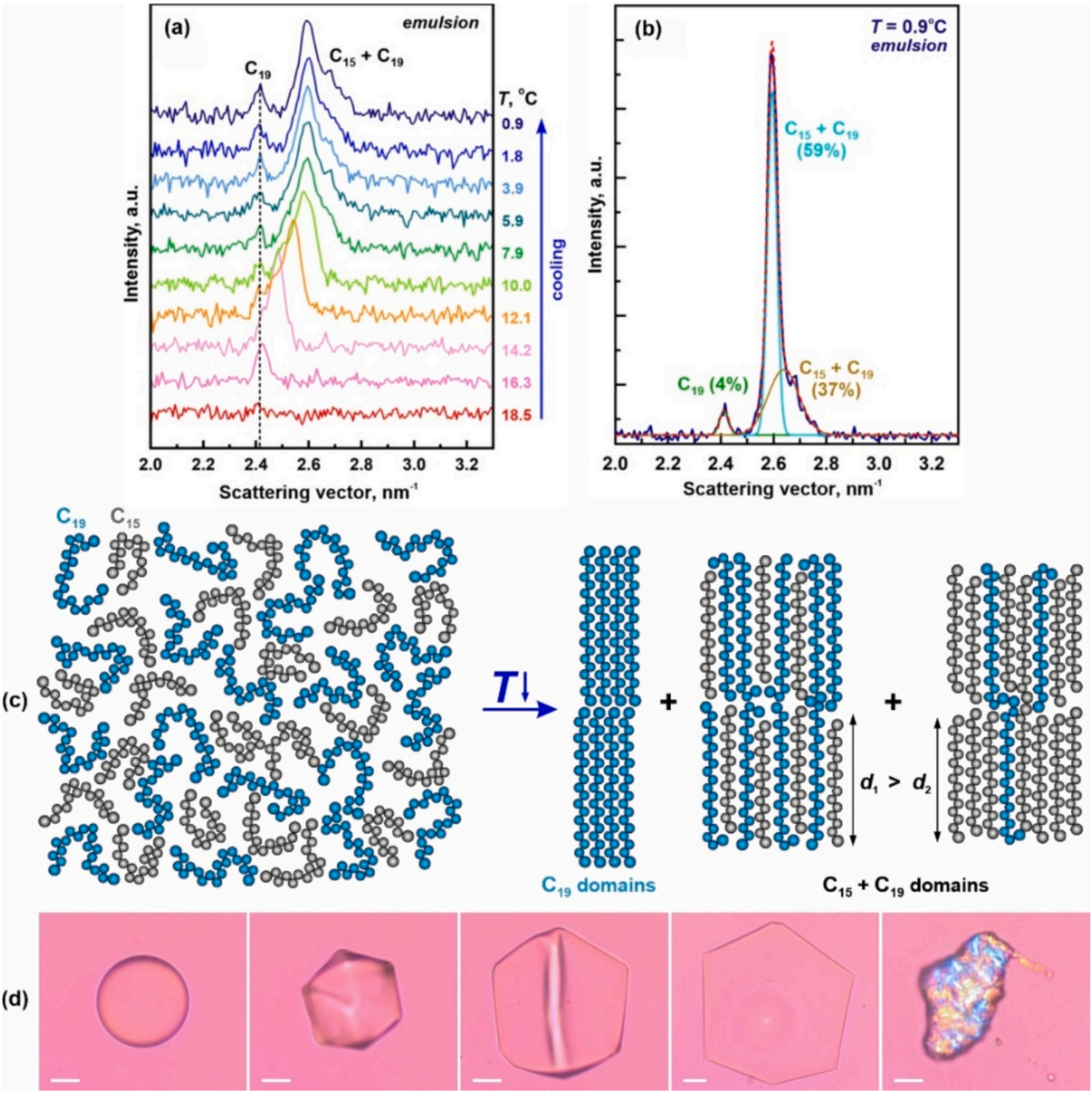

Fig. 12. Behavior of mixed alkane particles where $\Delta n \geq$ 4C-atoms. (a,b) SAXS spectra obtained upon cooling of $C_{15} + C_{19}$ (1:1) 18 μm drops stabilized by $C_{16}EO_8$ surfactant. (b) Peak deconvolution analysis of the spectra obtained at 0.9 °C. Three separate peaks are detected. (c) Schematic representation of the phases forming upon freezing of the $C_{15} + C_{19}$ mixture. (d) Drop shape evolution and partial freezing of $C_{14} + C_{20}$ (2:1 *v*/v) mixed drop dispersed in Tween 60 solution. Upon cooling, the usual drop shape evolutionary path is followed. However, when the freezing temperature of C_{20} is reached, part of the particle freezes, whereas the C_{14} molecules remain in a fluid state. The rotator phase stabilizing the non-spherical hexagon is broken and the particle does not preserve its non-spherical shape upon freezing. Scale bars = 10 μm. (a-c) Adapted from Ref. [104].

Structural analysis of mixed alkane drops [104] demonstrated a continuous structural rearrangement, leading to a decrease in the interlamellar rotator phase thickness across the entire temperature range from the onset of drops deformation to the melting point of the shortest alkane in the mixture, see Fig. 11f,i. Upon further cooling, a rotator-to-crystal phase transition occurs, leading to an additional reduction in interlamellar thickness, see Fig. 11h. The reversed trend is observed upon heating, Fig. 11g.

When the chain length difference between neighboring alkanes is ≥4C-atoms, their melting temperatures differ significantly. As a result, although completely miscible in the liquid state, such alkanes tend to partially phase separate upon freezing, see Fig. 12 [56]. Upon cooling from melt, once the freezing temperature of the longer chain alkane is reached, part of it crystallizes, disrupting the rotator phase structure that previously stabilized the non-spherical fluid shape. This disruption allows the positive interfacial tension to reshape the droplet back toward a nearly-spherical form, with the remaining liquid alkane confined inside and solid crystals decorating the surface, see Fig. 12d. Structural analysis of $C_{15} + C_{19}$ (1:1) drops revealed that about 8 % of C_{19} molecules separate into a distinct crystalline phase (4 % of all molecules), whereas the others are incorporated into two slightly different mixed phases with the shorter pentadecane molecules, as shown in Fig. 12a-c [104].

Experiments with many different alkane mixtures showed that the behavior of multicomponent systems is primarily determined by the greatest chain-length difference Δn between neighboring alkanes in the mixture [56]. When $\Delta n \leq$ 3C-atoms, the non-spherical fluid particles preserve their shapes after plastification, whereas larger differences lead to partial phase separation during freezing and formation of spherical frozen particles.

Another difference between the single- and multicomponent droplets is observed upon heating. In single-component drops, melting occurs rapidly within seconds once the bulk melting temperature of the dispersed lipid is reached. In contrast, multicomponent drops with $\Delta n \leq$ 3 exhibit melting over a wide temperature range. Initially, birefringence fades, indicating melting begins in the particle interior. The non-spherical shapes remain until the melting temperature of the longer-chain alkane is reached. This shows that the particle surface is enriched with the molecules of the longer component. The initial spherical shape restores once the melting temperature of the longer alkane in the mixture is surpassed [56].

Investigations of mixed drops revealed also that when a given non-self-shaping substance is mixed with a self-shaping one with a concentration of at least 15 vol%, drop shape deformations upon cooling become possible, see Fig. 13 [56]. This finding further broadens the applicability of the spontaneous self-shaping process.

2.8. Formation of non-spherical droplets using alternative methods

The described self-shaping process is very easy for experimental realization, requiring only a suitable combination of oil and surfactant. After emulsion droplets are formed, the system is slowly cooled from a temperature above the melting temperature of the oil until it freezes. Furthermore, as described, this process is widely applicable to a variety of chemical compounds containing linear chains in their structures.

To place the self-shaping process within the wider framework of methods that have been shown to generate non-spherical particles from initially spherical droplets, we present an overview of relevant techniques found in the literature. Our focus is limited to non-polymeric particles composed (mainly) of low-molecular weight compounds, as the currently reviewed process does not rely on the properties of the polymers. Reader interested in shape-changing polymeric particles are referred to a recent comprehensive review by Tanjeem et al., which discusses various mechanisms for achieving non-spherical polymeric structures [105]. Additionally, an interesting example of light-induced self-shaping is presented in Ref. [106], where polyelectrolyte droplets transform into hexagonal and multipodal structures driven by *cis-trans* isomerization under blue light irradiation. Information about non-spherical droplets formation using liquid crystal substances can be found in Refs. [107–113].

This review primarily considers studies involving micrometer-sized oil drops with diameter smaller than ca. 200–500 μm. However, larger droplets undergoing shape transitions have been also reported. Notable examples include the works of Čejková et al. [114] and Li et al. [115]. In Ref. [114], the evaporation of water has been shown to induce the growth of elongated spikes on initially spherical decanol droplet placed in an aqueous sodium dodecanoate solution containing sodium chloride. The decanol droplet eventually form branched structure resembling in shape the neuronal cells. Evaporation of the cyclohexane droplets placed on a water surface is shown to spontaneously shape the droplet into faceted polygonal shapes in Ref. [115]. This phenomenon is attributed to Marangoni-driven vortex flows in the underlying liquid subphase. These high-Reynolds-number flows generate asymmetric shear stresses that overcome the natural tendency of droplets to minimize surface energy, leading to the spontaneous formation of distinct edges and corners in the droplet shape.

2.8.1. Non-spherical drops stabilized by elastic interfacial film

The self-shaping process studied here is driven by the in-situ formation of multilayers of a plastic phase counteracting the inner capillary pressure. However, other types of elastic films present on the droplet surface can also stabilize non-spherical shapes, provided that they possess sufficiently high mechanical strength. Experimentally, this has been demonstrated in systems stabilized by surface-active proteins and natural surfactants such as saponins. For example, formation of irregularly shaped non-spherical droplets is demonstrated in Ref. [16] using 1 wt% saponins (*Sapindus Mukurossi* and *Quillaja* types). Such saponins form a rigid "solid" shell on the oil-water interface [116], thereby stabilizing the non-spherical morphology.

Non-spherical emulsion droplets have also been observed when stabilized by BsIA, a bacterial protein produced from *Bacillus subtilis*, see Fig. 14a [15]. This protein is known for its ability to form elastic interfaces at both oil-water and air-water boundaries [117,118]. Similar

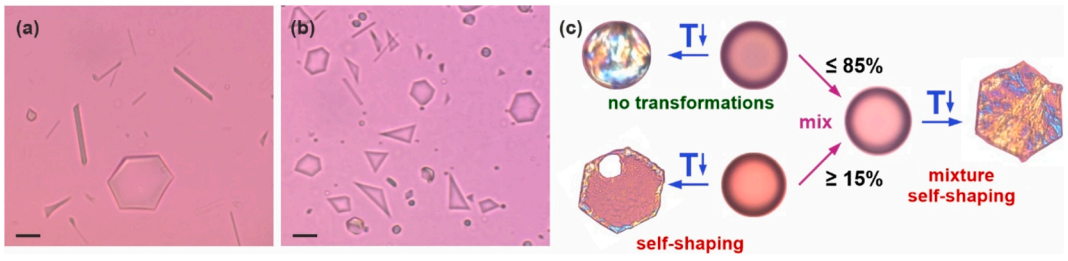

Fig. 13. Self-shaping of multicomponent drops containing self-shaping and non-self-shaping substances. (a,b) Deformed fluid particles prepared from: (a) coconut oil + hexadecane (1:1) mixture; (b) tetradecanol + hexadecane (1:1) mixture dispersed in Tween 60. Scale bars = 10 μm. (c) Schematics illustrating that at least 15 vol% of self-shaping substance are needed to be mixed with a non-self-shaping one to allow formation of non-spherical particles upon cooling. Adapted from Ref. [56].

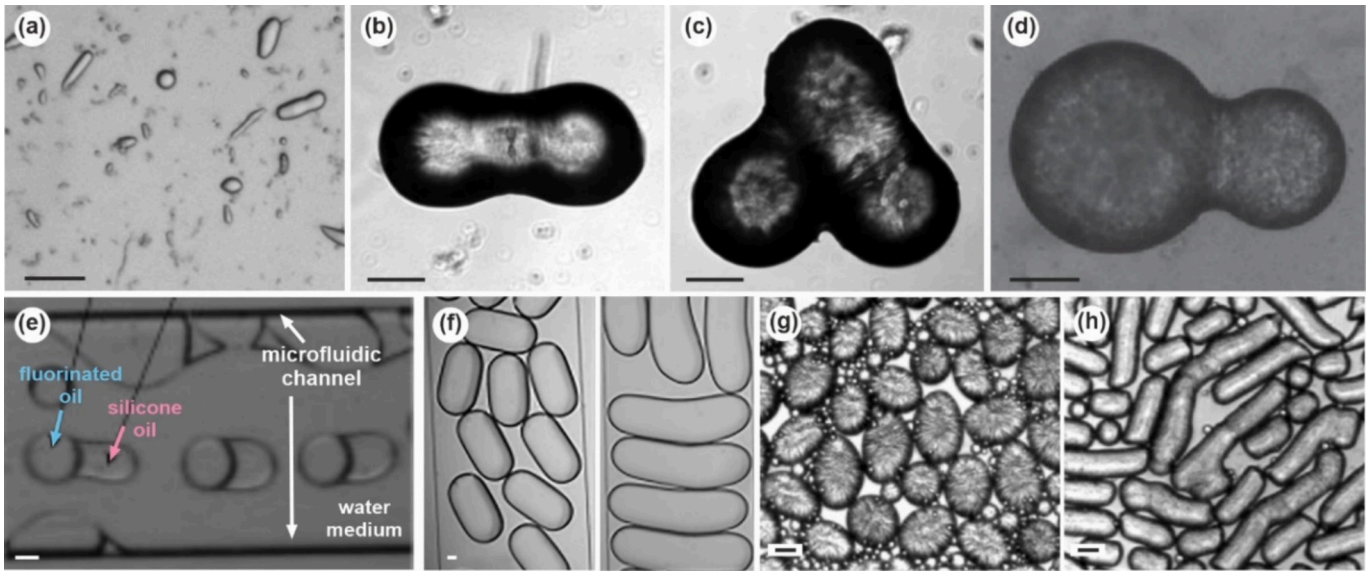

Fig. 14. Collection of non-spherical droplets generated using various methods. (a) Non-spherical drops trapped during vortex mixing of hexadecane into BsIA protein solution. Reprinted from Ref. [15]. (b,c) Non-spherical structures obtained upon arrested coalescence of Pickering droplets. The structures shown are obtained after polymerization. Adapted and reprinted with permission from Ref. [18]. Copyright © 2009 American Chemical Society. (d) Non-spherical drop obtained via arrested coalescence of 30 % wax-containing hexadecane drops dispersed in 0.5 wt% microfibrous cellulose and 10 mM sodium dodecylsulfate. Reprinted with permission from Ref. [19]. Copyright © 2016 The Royal Society Publishing. (e) Elongated double droplets generated at 0.55 μL/s flow rate in a hydrophilic chip. Adapted and reprinted with permission from Ref. [121]. Copyright © 2010 Elsevier B.V. (f) Non-spherical triglyceride droplets produced in a microfluidic chip. Drops with aspect ratios of 2.0 (left) and 3.4 (right) are shown. Adapted and reprinted with permission from Ref. [122]. Copyright © 2020 Elsevier Inc. (g,h) Anisotropic emulsion hexadecane-petrolatum mixed droplets produced by microfluidic techniques. The particles aspect ratio is governed by the exit temperature: (g) $T = 40$ °C; (h) $T = 30$ °C. Adapted and reprinted with permission from Ref. [21]. Copyright © 2018 Elsevier B.V. Scale bars for all images = 50 μm.

behavior has been reported with natural hydrophobins, small proteins containing 65–100 amino acid residues, produced by filamentous fungi [119,120].

It should be noted, however, that the non-spherical shapes formed in these studies cannot be precisely controlled. Instead, they result from the arrested deformation of liquid droplets during mechanical agitation (emulsification) or the application of external mechanical forces.

2.8.2. *Arrested coalescence*

Another approach for producing non-spherical micrometer-sized droplets, mechanistically governed by the presence of particles adsorbed on the droplet surface, was proposed in Ref. [14]. In this study, the authors induced coalescence between Pickering droplets that were incompletely coated with silica nanoparticles. When the coating of the resulted droplet exceeded approximately 90 %, the adsorbed particles underwent two-dimensional jamming, preventing the droplet from relaxing into a spherical shape. This resulted in the formation of partially fused non-spherical geometries, see Fig. 14b,c. Subsequent theoretical studies revealed that, for drops of equal initial size, arrested coalescence occurs only when the total surface coverage is between 143 and 181 % [17]. Lower coverages resulted in a complete coalescence and formation of spherical droplets, whereas at higher coverages, the individual drops were unable to merge.

Despite the fact that the coalescence occurs extremely rapidly, within tenths of microseconds, the authors of Ref. [14] managed to achieve partial control over the process. They observed that few seconds are required after the initial particle-particle contact for droplet rotation and rearrangement of the adsorbed particles to allow the bare drop surfaces to come into direct contact. This time window was used to position the droplets into target geometries before the coalescence occurred. Microfluidics techniques were used for these experiments, which allow precise control over droplet surface coverage. The formation of non-spherical supracolloidal structures composed of three or more drops arrested during their coalescence was also demonstrated [14]. However, the initial drop sizes were relatively large, around 100 μm, and the obtained geometries were limited to such in which the bonding angles between the partially coalesced droplets were either 60 or 120°.

In other studies, similar non-spherical shapes were obtained using arrested droplet coalescence [19,20]. Instead of relying on particle-armored droplets and particle jamming, the arrested shapes were achieved by precisely balancing interfacial and elastic droplet energy in drops comprising partially crystallized oil (liquid alkane mixed with high-melting wax), see Fig. 14d [19,20]. This process was realized using micromanipulation techniques, where one droplets was held at the tip of a capillary and manually brought into contact with another droplet. The extent of coalescence depended on the solid fat content in the two droplets, which determines their Young's modulus and the elastic energy stored within the microstructure. Depending on this, three distinct outcomes were observed – complete coalescence into a single spherical shape, arrested coalescence, or elastic stabilization in non-spherical shape. Furthermore, the arrested coalescence of three or more droplets was demonstrated as a viable method for preparation of complex anisotropic structures [20].

2.8.3. *Non-spherical Pickering droplets*

The initial model studies [14,17] demonstrating the formation of non-spherical, particle-stabilized emulsion droplets via arrested coalescence opened a new area for research in this field. Subsequent studies primarily aimed to increase the production rate of non-spherical particles (initially limited by the need for a manual droplet contact) and to expand the range of chemical compounds suitable for different technological applications, tailored to specific functional requirements.

Arrested droplet coalescence, induced by emulsion destabilization in bulk sample, has been used to prepare non-spherical droplets [123]. In this approach, hexadecane-in-water emulsions, stabilized by cetyltrimethylammonium bromide were prepared in the presence of dopamine hydrochloride. Coalescence was triggered by the addition of tris (hydroxymethyl)aminomethane hydrochloride, which initiated dopamine polymerization in the aqueous phase and caused accelerated

droplet coalescence while simultaneously generating surface-active dopamine particles. Under optimized particle coverage, non-spherical droplets were produced under arrested coalescence [123].

Non-spherical particles in bulk quantities were also produced in Ref. [124]. In this case, cyclodextrin particles were used to stabilize Pickering emulsions prepared with various oils. Depending on the particle and oil concentrations, as well as the chemical nature of the dispersed oil, particles with aspect ratios varying between ca. 1.15 and 1.70 were produced via a simple rotor-stator emulsification, without requiring specialized equipment. Additionally, an increase in emulsion viscosity was demonstrated with increasing aspect ratios of the Pickering droplets [124].

By combining particle-arrested coalescence with a system exhibiting low interfacial tension (IFT $<$ 0.7 mN/m), the authors of Ref. [125] successfully prepared non-spherical Pickering droplets. In this case, the non-spherical shapes emerged during ultrasound emulsification.

A different approach was used in Ref. [126], where buckling was induced in particle-stabilized "water-in-oil" (inverse) emulsion droplets. The droplets were composed mainly of ethylene glycol, while the continuous phase consisted of chlorobenzene. The ethylene glycol solubility ($\approx$ 1.5 μL/g) in the chlorobenzene was used to induce a controlled volume reduction of the dispersed droplets. This was achieved by placing the droplets into unsaturated chlorobenzene phase, thus inducing an ethylene glycol transfer from the droplets interior into the continuous phase until the solubility limit was reached. The controlled volume reduction led to buckling due to the fixed surface area of the particle shell covering the initial droplet. Easier buckling was observed for drops with larger initial sizes [126].

2.8.4. Microfluidic production of non-spherical droplets

Several methods employing microfluidics techniques have been also shown to be able to produce non-spherical droplets. For instance, microchips with finely tuned wettability have been used to create elongated double droplets when low flow rates are applied in the microchannels [121]. The double droplet consisted of two droplets composed of fluorinated and silicon oil which were placed in contact with one another, see Fig. 14e. An increase in the flow rate provided a partial control over the doublet droplet shape, transforming them into capped double droplets [121]. However, note that these non-spherical shapes are observed due to the non-zero interfacial tension between the two different oils from which the droplets are produced, combined with the viscous shear forces from the surrounding water flow.

In another study, a microfluidic-based approach was used to produce medium-chain triglyceride oil droplets with non-spherical shapes. These shapes were obtained during the breakup of the dispersed flow, governed by the flow rate and were preserved by adsorbing a surface active peptide in combination with a polyethylene glycol (PEG)-modified protein as a co-surfactant, see Fig. 14f [122]. This surfactant combination provided a strong interfacial network, allowing the droplets to retain their non-spherical shape for several hours. Control over the non-spherical droplet aspect ratio was demonstrated by varying the flow rate. However, highly deformed droplets tended to relax into shapes with smaller aspect ratios more quickly [122]. The non-spherical drops produced were relatively large, with diameters $\approx$ 250–300 μm.

Taking advantages of both microfluidics techniques and the presence of a crystalline fraction inside the droplets, endoskeleton ellipsoidal and spherocylindrical droplets were produced in Ref. [21]. The authors first created monodisperse droplets containing hexadecane mixed with a high melting wax at high temperatures, ensuring that the entire oily phase remained in a liquid state. Afterwards, a cooling step was applied in a narrow tube with a 100 μm diameter. This led to formation of elongated, partially frozen particles. Their aspect ratios were controlled by both flow rate and exit temperature, see Fig. 14g,h [21]. The smaller satellite droplets produced in the process remained spherical. However, a minimal solid fraction of ca. 25 % was required to maintain the non-spherical shape, and the outlet temperature needed to be lower than 45 °C [21]. This method is only applicable to drops with diameters larger than the narrow tube's diameter [21,22]. Similarly shaped non-spherical Pickering droplets can also be generated using a cone-cone shear cell [127].

2.8.5. Non-spherical Janus droplets

Another interesting examples for formation of micrometer-size non-spherical droplets have been demonstrated using Janus droplets composed of immiscible hydrophobic phases, such as hydrocarbon and fluorocarbon oils [128]. These biphasic oily droplets are initially produced at temperatures above the upper critical solution temperature, where the two oils are fully miscible. Subsequent cooling induces phase separation within the droplets, resulting in distinct internal morphologies, governed by the balance of surface tensions acting at the individual interfaces [128,129].

Changes in surfactant concentration, type, or configuration (e.g. UV-induced *cis-trans* isomerization in cationic azobenzene-based surfactants), have been shown to dynamically modulate the morphology of these Janus droplets by altering the interfacial tension between the two immiscible phases [129]. This has enabled a wide range of shape transformations, including switching from convex to concave shaped internal interfaces, transitions between encapsulated and inverted encapsulated states, and even the formation of snowman-like structures in which the two oily phases become nearly fully separated [129–132].

Due to their extreme sensitivity to subtle interfacial changes, such droplets have been proposed as effective transducers for visualizing minimal variations in oil-water interfacial tension [129], detecting surfactant gradients [131], and even serving as optical sensors for the early detection of foodborne pathogens, such as bacteria *Salmonella enterica* [133].

An overview of studies on non-spherical droplet formation highlights three main mechanisms proposed in the literature, aside from the self-shaping process observed upon cooling: (1) Arrested coalescence of Pickering droplets, achieved through appropriate surface coverage or during emulsification in bulk samples; (2) Formation of an elastic film on the droplet surface, which stabilizes corrugated shapes formed during emulsification; and (3) Microfluidics techniques, where elongated shapes are retained either during droplet formation or induced by forcing droplets through channels narrower than their diameter. However, these methods typically produce drops with diameters $\gtrsim$ 50–100 μm. Furthermore, the resulting shapes are either highly irregular, lacking precise control, or limited to ellipsoidal and spherocylidrical forms with relatively small aspect ratios. In contrast, the novel spontaneous self-shaping process offers unique advantages, enabling the controllable formation of highly regular, non-spherical fluid and frozen micrometer-size lipid particles, something which is not currently possible with the other existing methods.

3. Drop self-shaping in presence of adsorbed particles

Particle-stabilized emulsions, known as Pickering or Ramsden emulsions, are colloidal systems in which solid particles replace traditional surfactants to stabilize emulsion droplets against coalescence [134–137]. The adsorption of colloidal particles at the interface is considered to be nearly irreversible, as the desorption energy exceeds thousands k_BT (thermal energy) even for nanometer-size particles. Additionally, the solid particles adsorbed at the interface act as a physical barrier, further inhibiting direct contact between the droplets and enhancing their stability against coalescence. Pickering emulsions have found widespread applications in food science, pharmaceuticals, catalysis, electrochemistry and many other fields [138–140].

The unique molecular ordering at the drop surface observed upon cooling of micrometer-size droplets, stabilized by long chain surfactant molecules, presents a unique opportunity to study the competition between particle adsorption and surface order layer formation in Pickering emulsions prepared in the presence of (small amount of) surfactants.

These studies have revealed several unexpected phenomena, the key findings of which are summarized in this section.

3.1. Particle rearrangement upon surfactant adsorption layer freezing

Several unexpected phenomena were observed in self-shaping drops decorated with adsorbed latex particles, see Fig. 15 [53]. The samples were prepared by first emulsifying the oil phase into an aqueous phase containing latex particles and a small amount of electrolyte (NaCl or $CaCl_2$). Subsequently, the surfactant needed for the self-shaping process was introduced to the Pickering emulsion by dilution. Following this procedure, self-shaping oily droplets decorated with numerous latex particles were prepared.

At high temperatures the adsorbed latex particles were evenly distributed across the drop surface and remained mobile. Upon cooling, the alkyl chains of the surfactants able to induce self-shaping process freeze, see Section 2.3 above. This freezing led to the spontaneous ordering of adsorbed latex particles into a hexagonal lattice, see Fig. 16a. The freezing temperature observed in interfacial tension measurements closely matched the temperature at which the particles rearrangement occurred, demonstrating the relationship between the surface phase transition and the particle organization [53,80].

The observed ordering was explained with the formation of an interfacial tension gradient across the drop surface, see Fig. 16c. The freezing of the adsorption layer begins at a specific spot where a crystalline nucleus emerges. It does not occur instantaneously across the entire surface. Therefore, upon freezing, the interfacial tension in the frozen region decreases, while the fluid regions maintain a higher IFT. This difference creates an interfacial tension gradient, driving particles displacement from areas with higher IFT (frozen adsorption layer) toward areas with lower IFT (fluid adsorption layer) [53]. Note that, at this stage, the rotator phase formation has not begun yet, as the drops still retain their spherical shape.

Depending on the number of nucleus which emerge simultaneously, different types of particle arrangement are observed. In cases, where the nucleus formation is difficult and occurs at a single site, all adsorbed particles become pushed together toward one region of the drop surface, where they arrange into a close-packed hexagonal lattice. When few nuclei emerge simultaneously, they lead to regions devoid of particles, surrounded by areas with highly ordered latex particles, see **Figs. 16**a,b and **17**a.

In the limiting case, where only a few particles are initially adsorbed on the drop surface, no significant interruption of the regular shape deformations is observed due to their presence. In this scenario, the particles were pushed toward the areas of higher IFT, which then became the "defect" regions, i.e. the tips of the non-spherical shapes. The particles remained attached to the tips even after drop freezing, see Fig. 15a [53]. Similar observations were made for alkane droplets coated with nanometer- and micrometer-sized silica particles [49,50], where the particles were also observed to position themselves at the tips of the deformed droplets.

Furthermore, another intriguing method for creating patterns of nanoparticles adsorbed on the cholesteric liquid crystal emulsion droplets surface has been shown in Ref. [141]. In this study, the authors demonstrated that by adjusting the hydrophobicity of the particles, the surfactant concentration, and the pH of the continuous phase, it is possible to induce spontaneous particle assembly into fingerprint-resembling structures. The formation of these patterns was found to be related to the elasticity of the cholesteric liquid crystal matrix that constituted the droplets and which led to surface anchoring of the

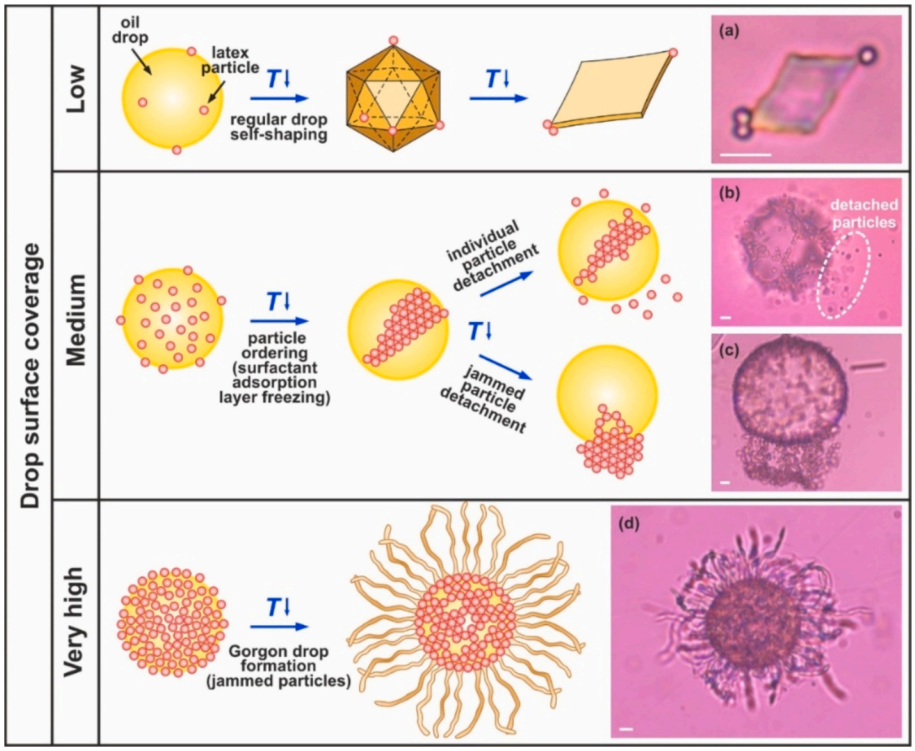

Fig. 15. Main processes observed upon self-shaping of alkane drops with adsorbed latex particles. (a) The drop shape deformations proceed via its usual course when there are only a few particles attached to the drop surface. The particles ultimately accumulate at high-energy defect sites, such as the tips of the deformed drops. (b) At intermediate to high surface coverage, latex particles disrupt the typical self-shaping process due to the inability of the rotator phase to fully cover the drop surface. In systems where particle detachment is possible (see section 3.2 for details), the particles first detach from the surface, allowing the droplet to follow its usual deformations sequence. (d) At very high surface coverage, when particles are densely packed and strongly interacting (jammed particles), numerous fluid fibers emerge between the adsorbed particles. The resulting droplet shapes resembles the head of the Gorgon Medusa form Greek mythology and are referred to as Gorgon drops. The schematics are adapted from Ref. [53]. Scale bars = 5 μm.

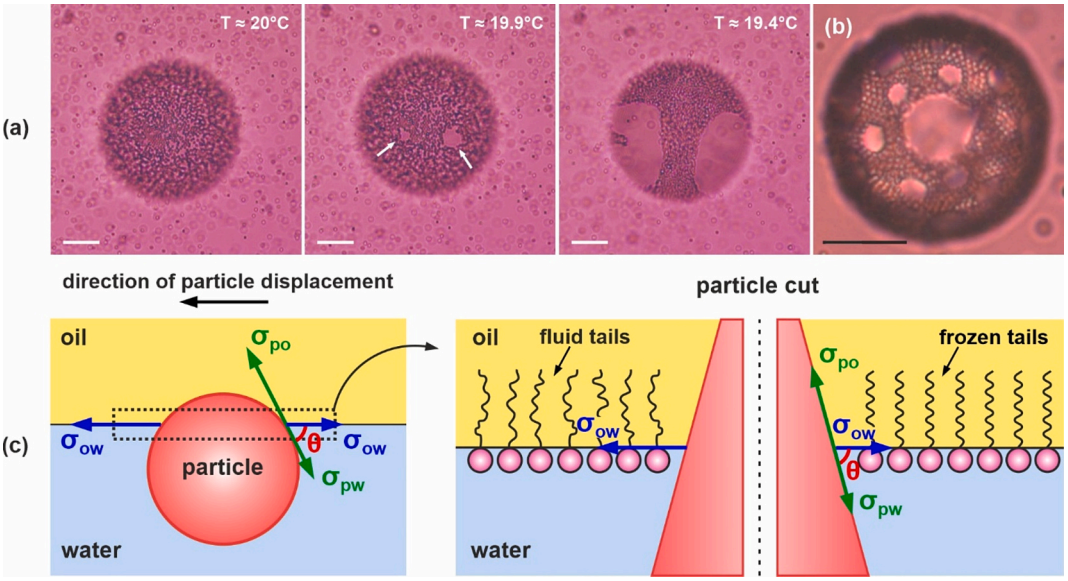

Fig. 16. Ordering of the adsorbed latex particle observed upon freezing of the surfactant adsorption layer. (a,b) Microscopy pictures obtained upon cooling of hexadecane drop with adsorbed chloromethyl latex particles (1 μm diameter), dispersed in: (a) 3 mM Tween 40 surfactant solution +100 mM NaCl. At high temperature, the particles are distributed evenly over the drop surface. When a certain temperature is reached, the particles begin to rearrange and pack into hexagonal lattice. (b) 1 mM $C_{18}EO_{20}$ + 7.8 mM $CaCl_2$. Scale bars = 20 μm. (c) The observed particle rearrangement is related to the local freezing of the surfactant adsorption layer and occurrence of interfacial tension gradient over the drop surface. See text for more details. The figure is adapted from Ref. [53].

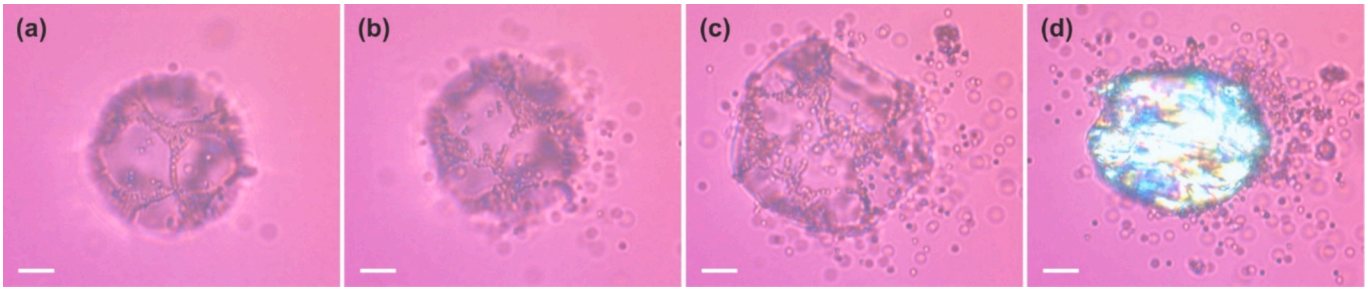

Fig. 17. Particle detachment observed upon emulsion drop cooling. (a) The particles have arranged into stripped-like shapes surrounding regions free of particles, where the initial surfactant adsorption layer freezing had occurred. (b) Upon cooling, the rotator phase starts to form and detachment of individual particles is observed. (c) Drop shape deformations occur although part of the latex particles remain adsorbed on the drop surface. (d) Frozen particle. The experiment is performed with hexadecane drop decorated with chloromethyl latex particles (1 μm in diameter), dispersed in 3 mM Brij S20 + 100 mM NaCl solution. Scale bars = 10 μm.

particles into different patterns. In another study, the defects in the arrangement of liquid crystal molecules confined in emulsion droplets has been shown to also lead to spontaneous formation of ordered structures of adsorbed particles [142].

3.2. *Particle detachment upon rotator phase formation*

After the particles rearrangement occurs, further cooling of the Pickering alkane droplets lead to the rotator phase formation, which enables the drop self-shaping. At almost the same temperatures at which the usual drop deformations begin, another unexpected phenomenon is observed in some systems – particle detachment from the drop surface, see Figs. 15b,c and 17 [53]. The presence of the particles interfered with the shape transformation process, causing some of the particles to desorb first, after which the drop deformations proceeded as usual. This is quite unexpected observation, as particle adsorption onto the liquid-liquid interface is typically considered an irreversible process due to the very high energy required for desorption:

$$E_{des} = \pi\sigma R^2(1 - |\cos\theta|)^2, \quad (4)$$

where σ is the interfacial tension between the two immiscible liquids, R is the adsorbed particle radius, and θ is the three-phase contact angle between the fluid and particle surfaces [136]. For 1 μm particles, this energy is on the order of 10^7 k_BT. However, during rotator phase formation, particle detachment was observed in part of the systems when it was energetically favorable, as discussed below.

To understand the conditions for particle detachment, we analyzed the surface energies using the classical Young-Laplace equation, relating the interfacial tensions at the particle-drop (σ_{po}), drop-solution (σ_{ow}), and particle-solution (σ_{pw}) interfaces with the three-phase contact angle at the particle surface (θ_i), see Figs. 16c and 18 for schematic illustration of the different parameters involved [53]:

$$\cos\theta_i = \frac{\sigma_{po} - \sigma_{pw}}{\sigma_{ow}}. \quad (5)$$

To observe particle detachment from the drop surface, the three-phase contact angle should decrease (when measured through the aqueous phase). According to the equation, this decrease should be accompanied by a significant increase in σ_{ow} or alternatively, to an increase in the difference σ_{po} - σ_{pw}. Indeed, for one of the systems in which the most intensive particle detachment was observed, hexadecane drops

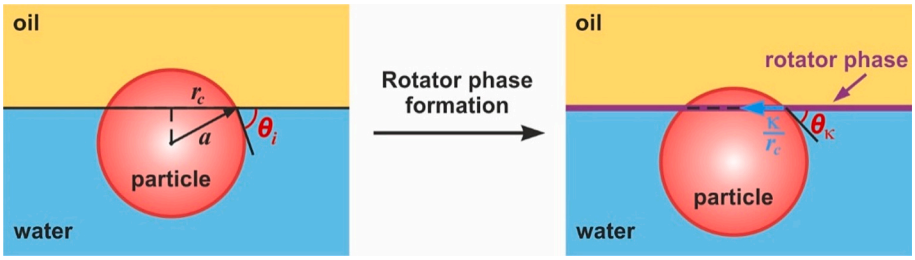

Fig. 18. Schematic representation of the three-phase contact angles, θ_i and θ_κ formed at the oil-water-particle interface in absence and presence of rotator phase respectively. At sufficiently high positive values of the line tension, κ, there is no equilibrium contact angle and the particle is ejected from the oil-water interface. The schematics is adapted from Ref. [53].

dispersed in Brij S20 ($C_{18}EO_{20}$) surfactant solution with NaCl or $CaCl_2$ salts, and adsorbed chloromethyl latex particles, a decrease in σ_{ow} was experimentally observed when measuring the IFT as a function of the temperature [53,80]. However, such a significant decrease in the oil-water interfacial tension was not observed in many other systems where particle detachment still occurred (for example, C_{16} drops in Tween 40 solution with NaCl and chloromethyl latex particles adsorbed on the drop surface) [53].

The simplest analysis, however, disregards the unfavorable interaction between the newly formed rotator phase and the adsorbed particle. It arises as particle disturbs the regular molecular ordering of the rotator phase and can be accounted for by introducing an additional term in the Young-Laplace equation:

$$\cos\theta_i = \frac{\sigma_{po} - \sigma_{pw}}{\sigma_{ow} - \kappa/r_c}, \tag{6}$$

where κ is the line tension, defined as the excess energy per unit length of the contact line, and r_c is the radius of the contact line. The derivation of this equation is shown in the Appendix of Ref. [53]. Line tension usually has small values, therefore it is only significant for very small objects with micrometer and sub-micrometer sizes as shown previously for particles adsorbed liquid-liquid and air-liquid interfaces [143–146]. However, given the small size of the studied particles (≈ 1 μm in diameter), this effect was found to be important for the currently discussed systems.

In the present case, it is expected that $\kappa \geq 0$, because the adsorbed particle disturbs the molecular ordering of the rotator phase, thus increasing the energy of the system. The magnitude of the line tension can be estimated by multiplying the excess energy in the contact zone with the width of the contact zone, i.e. if the rotator phase is formed with thickness h_{PL}: $\kappa \approx h_{PL}(\sigma_{pr} - \sigma_{po})$, where σ_{pr} is the interfacial energy at the particle-rotator phase interface. When no rotator phase exists, $h_{PL} = 0$, so the line tension contribution is negligible, and the classical Young-Laplace equation can be used. In the presence of rotator phase, however, the contact angle of the adsorbed particles changes with the rotator phase thickness [53].

The theoretical analysis of $\theta(h_{PL})$ indicates that for realistic values of the parameters included in the equation, there exists a value of h_{PL} above which there is no energy minimum for the particle to remain adsorbed on the drop surface. In other words, the equation predicts that the magnitude of the unfavorable particle-rotator phase interaction is so high, that the system reduces its energy by spontaneously desorbing the particle, as experimentally observed. The magnitude of the critical line tension above which the particle desorption is predicted is [53]:

$$\kappa_{cr} = R\sigma_{ow}\left(1 - \left(\frac{\sigma_{po} - \sigma_{pw}}{\sigma_{ow}}\right)^{2/3}\right)^{3/2}, \tag{7}$$

where R is the particle radius. Therefore, the critical line tension will decrease with the decrease of the particle size, oil-water interfacial tension, or the initial contact angle of the adsorbed particle.

Realistic values which could be substituted in eq. 7 are: $R \approx 1$ μm, $\theta_i \approx 30°$, $\sigma_{ow} \approx 1$ mN/m, $h_{PL} \approx 10$ nm and $(\sigma_{pr} - \sigma_{po}) \approx 10$ mN/m. Line tension, $\kappa \approx 1.0 \times 10^{-10}$ N/m, is calculated for these values of the parameters. The critical line tension, above which particle desorption is predicted is $\kappa \approx 0.28 \times 10^{-10}$ N/m. Therefore, the particles will spontaneously desorb from the interface [53]. In contrast, if just one frozen layer forms, (i.e. upon adsorption layer freezing), $h_{PL} \approx 2$ nm and the line tension become smaller than the critical value, $\kappa \approx 0.2 \times 10^{-10}$ N/m. In this case, the particles will remain attached to the interface, adopting an equilibrium contact angle.

The discussed mechanism explains all main experimental trends: the particle detachment was observed for chloromethyl latex particles, but was not observed for latex particles with sulfate or with carboxyl surface groups for the same oil-surfactant system. This is most probably because the line tension of the systems is different and only for chloromethyl latex particles, its value exceeds the critical one. Another observation explained by the line tension mechanism is that the particle detachment is more intensive for higher surfactant concentrations, whereas at lower concentrations the number of particles detaching from the interface decreases (for example 3 mM vs 0.1 mM Brij S20). This is related to the oil-water interfacial tension which will be higher at lower surfactant concentrations [53].

In the present analysis, particles which do not interact with one another are assumed. However, if the particles are jammed together, another type of ejection mechanism was observed [53]. In these systems, the whole raft of particles slides over the drop surface, most of the particles move outside of the drop, and only limited number of particles remain attached to the drop, see Fig. 15c. This detachment mechanism is most probably another version of the single particle detachment with only difference that the particles attract each other and are ejected together. Another type of collective particle detachment was observed at later stage when the particles deform and returned to spherical shape due to the action of capillary pressure. Upon this return part of the particles were ejected from the drop surface. Both mechanism of collective detachment were observed at high electrolyte concentrations or if $CaCl_2$ is present in the system because in these cases the electrostatic repulsion is suppressed [53].

The phenomenon of particles detachment upon surface freezing of the surfactant adsorption layer at alkane-water interface was found to have important consequences over the stability of Pickering stabilized oil-in-water emulsions in presence of low molecular weight surfactant. In Ref. [147], the authors demonstrated that the cetyltrimethylammonium chloride (CTAC) freezing at the tetradecane-water interface decorated with silica particles led to desorption of these particles, thus leading to destabilization of the studied bulk emulsion samples through coalescence.

3.3. *Complex shapes formation - Gorgon drops*

In the standard self-shaping process without adsorbed particles, various shapes extruding 1, 2 or 3 fibers were observed, see **Figs. 2h, 3** and **7**a,c. In presence of high surface coverage with strongly interacting

particles which cannot detach from the drop surface, another type of complex shape formation is observed. These shapes resemble the Gorgon Medusa head from the Greek mythology, as they have tens of fibers extruded from the spherical mother drop, see Fig. 15d [53]. These fibers emerge from the spots in-between the adsorbed latex particles, as the rotator phase formation still occurs in these systems. The diameter of the fibers is controlled by the alkane chain length in the oily droplets. Similarly to the case without adsorbed particles, thinner fibers are formed from tetradecane drops, whereas much thicker fibers are extruded from hexadecane drops for the same type of adsorbed latex particles (with sulfate surface groups) and the same surfactant stabilizing the emulsions (1 mM Brij S20 + 0.5 mM $CaCl_2$).

The studies of self-shaping Pickering drops present an alternative method for production of complex hybrid structures. Furthermore, the spontaneous particle detachment mechanism offers a new route for control over the emulsions stability, as well as for recovery of the adsorbed particles, which is especially important for particles used as catalysts, for example. The main factors which should be considered for optimization of the system are: oil and surfactant type, type of latex particles and electrolyte type and concentration.

4. Swimmers – active particles powered from temperature fluctuations

Another interesting part of the story about active emulsion droplets is their behavior in the final stages of evolution, when they begin to extrude thin fibers, see schematics in Fig. 1a. In this stage, soft-micro swimmers are formed. These swimmers can move for many minutes and can be recharged from temperature fluctuations. In this section, we highlight the main characteristics of these swimming drops [34].

Active particles are usually defined as self-driven units able to move autonomously and possibly able to perform specific tasks [1]. The search for active nano-, micro- and millimeter-sized active particles exploded in the last several years due to the rapid advance in several related research areas – soft robotics [6,148–153], nanomedicine [154–157], and artificial life [158–160]. Since 2020, more than 1100 papers including the phrase “active particle” in their titles have been published [161]. However, large part of these particle are metallic or rigid and cannot deform which limits significantly their applicability for study of the motion of live microorganisms. Furthermore, the ability for movement of these active particles is usually determined by the presence of external field (magnetic, electric or electro-magnetic) or by the pre-loaded amount of fuel (for example particles propelled by Marangoni effect due to the release of surfactant molecules) which also (partly) restricts their usage [3,162–176].

4.1. Formation and control parameters

The last stages of the drop shape evolution present an opportunity for a conceptually new type of soft active microswimmers that extrude, long thin elastic filaments, see Fig. 19 [34]. These particles offer several advantages over previously studied swimmers. They are micrometer in size, which can be controllably varied between ca. 1 and 50 μm. Furthermore, their propulsion is completely autonomous, it is driven by small temperature fluctuations rather than external fields or a chemical reaction. An additional benefit of these microswimmers is that they are able to sustain movement for over an hour. They can be easily recharged, and their shape resembles that of living microorganisms, such as the unicellular green algae *Chlamydomonas* [177].

The swimming motion of the self-shaping droplets is driven by the viscous friction between the ejected fibers and the surrounding fluid. The extruded fibers have an elastic nature, and are stabilized by the plastic rotator phase formed on their surface. As the fibers are ejected, the main swimmer “body” is pushed in the opposite direction and swimming motion is induced as shown in Fig. 19a, Supplementary Movie 3 and in Supplementary movies in Ref. [34]. Depending on the numbers of extruded fibers, three types of swimmers can be observed – with one, two or three fibers, see **Figs. 2h, 19** and **20**. The extrusion from triangular particles is symmetrical, thus resulting only in oscillatory displacement around the triangle's center. In contrast, particles extruding one or two fibers are capable of self-propulsion in the viscous medium [34].

The formation of microswimmers is preferred when the surfactants stabilizing the emulsion droplets have longer tail lengths compared to the chain length of the dispersed alkane. This is related to the onset temperature for drop deformations and subsequent evolution into the final stages of the evolutionary sequence [31]. As explained in Sections 2.2–2.4 above, the surfactant adsorption layer freezing induces ordering of the oily molecules near the drop surface, which enable the shape deformations. This process is facilitated when the surfactant tail is longer and the drops are with smaller sizes. Systematic experiments have been performed primarily with tetradecane and pentadecane swimmers, but similar behavior is expected for other systems capable of deformations upon cooling [34].

Several experimental parameters can be adjusted to control these artificial swimmers. For example, depending on the specific oil-surfactant combination, the thickness of the extruded fibers can be finely tuned. Thinner fibers form when the chain length difference between the alkane and the hydrophobic tail of the surfactant is larger, as demonstrated by the comparison between the fibers extruded from C_{14} ($d \approx 0.5$ μm) and C_{15} ($d \approx 2$ μm) alkane droplets in Fig. 20. The fiber

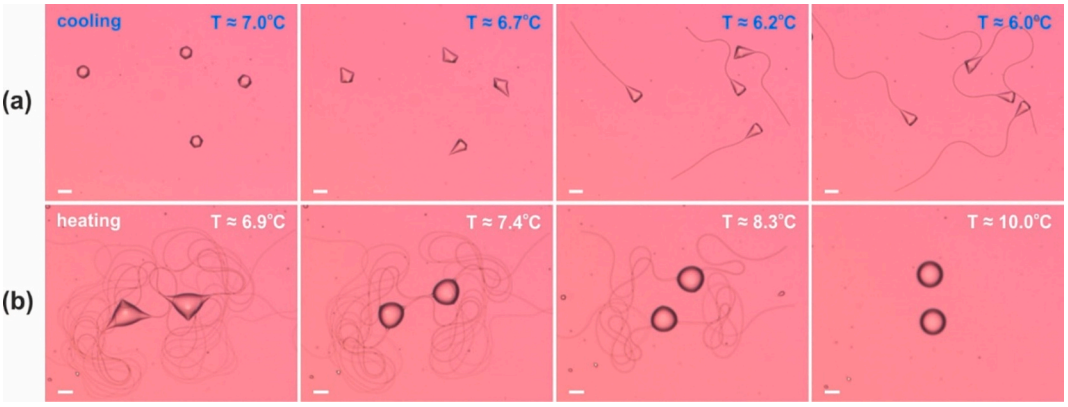

Fig. 19. Soft active microswimmers formed upon cooling and recharged upon heating of the emulsion samples. (a) Microscopy image sequence obtained upon cooling (T are indicated on the pictures). Initially, the drops evolve into polyhedrons, but afterwards instead of significant flattening, more irregular deformations are observed which leads to formation of single-tailed swimmers. (b) Drops extruding two tails observed upon sample heating. The extruded fibers have elastic properties because of the rotator phase covering their surface and are completely sucked into the mother droplet upon heating, therefore recharging it. The emulsion system shown on the pictures is pentadecane drops dispersed in 1.5 wt% Brij 58 solution. Scale bars = 20 μm.

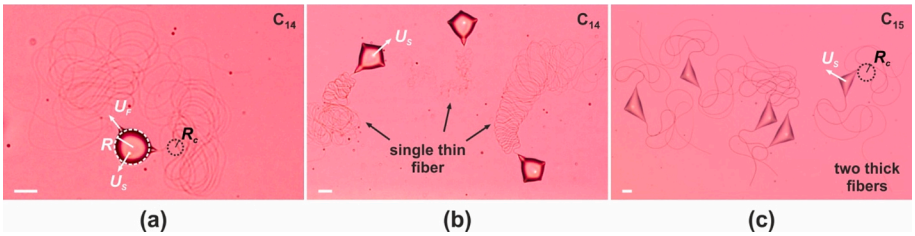

Fig. 20. Microswimmers with thin and thick fibers and schematic representation of the parameters included in the theoretical model. (a) Tetradecane swimmer extruding two thin fibers with diameter ≈ 0.5 μm. Several different quantities which are extracted from the experiment are schematically shown on the picture. (b) Tetradecane swimmers extruding single tails. (c) Pentadecane swimmers extruding two thick tails of diameter ≈ 2 μm. All drops are dispersed in 1.5 wt% Brij 58 surfactant solution. Scale bars = 20 μm. For more detailed explanations see the main text.

diameter is also related to the shape of the swimming body. Thinner fibers are extruded from emulsion drops with a shape closer to the spherical, which have several conical spikes on their surface (for example from C_{14} drops in Brij 58 solution), whereas thicker fibers are extruded from C_{15} drops in Brij 58, where the main body has a pyramidal shape with a tetragonal base for single-fiber and a triangular base for the two-fiber extruding droplets. Thus, the shape of the swimmers can also be controlled by selecting the appropriate oil-surfactant combination [34].

The specific oil-surfactant combination selected for preparing swimming droplets also determines the temperature range in which the droplets can self-propel through the solution. For example, tetradecane drops stabilized by Brij 58 surfactant were found to swim within a narrow 2 °C temperature interval before the bulk alkane began to freeze. In contrast, the temperature interval for pentadecane drops, stabilized by the same surfactant was much wider, approximately 4–8 °C [34]. This difference is probably related to the distinct ordered structures formed by the two alkanes upon "freezing". While tetradecane crystallizes directly into the highly ordered triclinic phase, pentadecane forms a thermodynamically stable rotator phase, which remains present in a wide temperature interval (between ca. -2 and 10 °C) before transitioning into the fully ordered orthorhombic crystalline phase [58]. This would make the pentadecane arrangement slower compared to that of tetradecane molecules, thus extending the temperature interval for swimming.

Furthermore, the swimming duration is also strongly affected by the applied cooling rate, which determines how fast the temperature interval for swimming will be passed through, thus leading to drop freezing. Typically, the swimming motion was observed in the course of 1 to 20 min, but longer periods are also possible provided that the applied cooling rate is sufficiently low or if the swimmer become recharged, see below.

The number of extruded filaments can be controlled to some extent by varying the cooling rate. Usually, lower cooling rates (e.g. < 0.2 °C/min) lead to a higher probability for formation of swimmers with a single tail, whereas higher cooling rates (ca. 0.5 to 1 °C/min) result preferentially in the formation of swimmers with two tails [34].

Swimming motion is observed upon cooling due to the extrusion of fibers covered with plastic rotator phase. However, if cooling is stopped at a fixed temperature, fiber extrusion continues with a very slow rate, making the swimming motion negligible. If the cooling is resumed, extrusion continues. Conversely, heating the sample causes the rotator phase to re-melt, leading to fiber retraction as the extruded material is drawn back into the mother droplet, see Figs. 19b. Notably, such retraction has been observed even for fibers longer than 2500 μm, as demonstrated in Supplementary Video 6 in Ref. [34]. In this way the swimmer become recharged as the extruded oil reverts back to the initial single droplet. By applying consecutive cooling-heating cycles, the same drops can be used for multiple experiments [19].

It should be noted that the swimming motion is powered by the material transfer from the main body into the extruding fiber. Therefore, if the whole oil become transferred from the mother droplet into the thin fibers, then the swimming will no longer continue. In this case a capillary instability process is observed, leading to the formation of several liquid droplets in which the main part of the liquid oil become compressed, connected to one another with thin fibers, see Fig. 21 and Supplementary Movie 3. No actual breakage occurs at this point as the thin fibers filled with a liquid oil are stabilized by the thin layers of plastic rotator phase covering their surface. If the system is gently reheated, the material can revert back to a single droplet. However, once a liquid-to-solid phase transition occurs for the whole material, the process becomes irreversible. Although the frozen fibers retain their shape in the solid state, they disintegrate into hundreds of smaller droplets upon melting, see Section 5.1 below.

In summary, the swimming motion is induced upon small temperature fluctuations related to the rotator phase formation, it may continue for many minutes and the swimmers can be recharged if the temperature is increased before the final liquid-to-solid phase transition occurs.

4.2. *Theoretical description of the swimming motion*

Several experimental parameters can be used to describe quantitatively the system behavior – extrusion speed, U_F, swimming speed, U_S, fiber radius, r, and effective swimmer radius, a, see Fig. 20a. As expected, at higher cooling rates the extrusion and swimming speeds are higher because the surface rotator phase formation is faster. For the same reason, bigger in size swimmers were found to swim faster. Similarly, the extrusion speed is higher in the case of single fiber extrusion and lower if two or three fibers are extruded. Furthermore, the extrusion is much faster for smaller in diameter fibers (0.5 μm) than for the thicker fibers. The swimming speed was found to vary between ca. 0.1 and several μm/s depending on the system, and the extrusion speed varied between ca. 0.5 and 20 μm/s [34]. For the swimmers, extruding thick fibers the swimming velocity magnitude was about 10–50 %, from the fiber extrusion velocity, $U_S/U_F \approx$ 0.1–0.5, whereas for the swimmers with thin fibers $U_S/U_F \approx$ 0.03–0.05.

We developed a theoretical model describing the observed droplets swimming. The model makes a balance between the two opposing forces: the hydrodynamic Stokes drag on the extruding fiber with the drag created by the friction of the swimming mother droplet [34]. The extruded filaments were treated as a uniform in length materials with a characteristic buckling length, which determined their bending stiffness, A. The fiber elastic stiffness was estimated from the measured periodicity of the fiber buckling, characterized by a wavelength l. A direct relationship was derived between the swimming and extrusion speed, fiber bending stiffness and the radius of the extruding droplet [34]:

$$U_S = cU_F l/R, \tag{8}$$

where c is a dimensionless constant which value depends on the number of the extruded fibers and their phases (in-phase or out-of-phase extrusion). Furthermore, the buckling wavelength l can be related to the fiber extrusion speed, bending stiffness, and the filament resistance to the flow in the direction parallel to its axis per unit length, $\xi_{||}$, by the

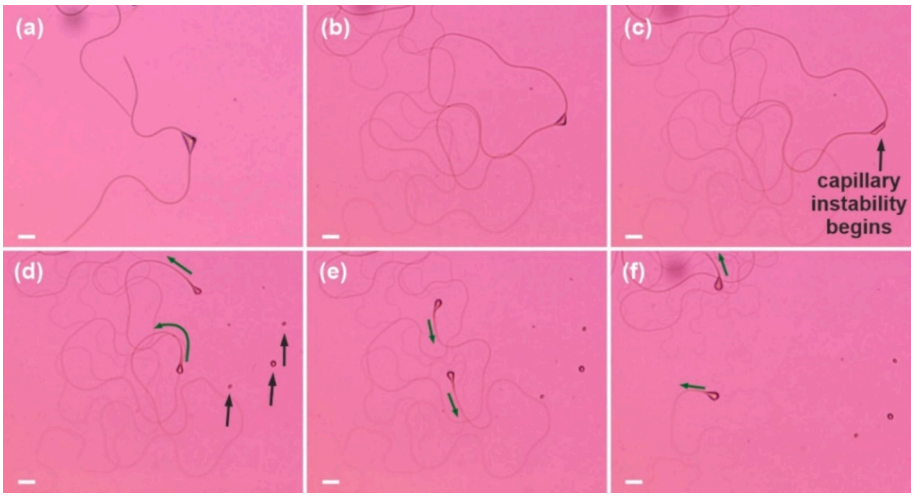

Fig. 21. Capillary instability observed when the microswimmers "run out of fuel". (a) Microswimmer in the beginning of the extrusion process. (b) The main part of the oil transfers into the long filaments which continue to grow upon slow cooling. (c) When the material remaining in the initial "mother droplet" become insufficient, a capillary instability begins. (d-f) The capillary instability leads to formation of several droplets in which the main part of the liquid oil become compressed connected to one another with thin fibers. No real breakage occurs at this point. The green arrows show the direction in which the liquid drops move along the elastic filaments, whereas the black arrows in (d) show the several liquid droplets already formed along the thin fiber. The dynamic process is shown in Supplementary Movie 3. Scale bars = 20 μm. (For interpretation of the references to colour in this figure legend, the reader is referred to the web version of this article.)

following equation:

$$l = \left(\frac{A}{\xi_{\parallel} U_F}\right)^{1/3} \tag{9}$$

A combined relationship relating the fiber extrusion speed with the swimming velocity, swimmer radius and the other constants describing the material characteristics of the system can be obtained by combining eqs. 8 and 9:

$$U_S = \frac{c}{a}\left(\frac{A}{\xi_{\parallel}}\right)^{1/3} U_F^{2/3}. \tag{10}$$

To estimate l we used that: $l \approx 1.2R_c$ where R_c is the radius of the first buckle, which can be measured from the experiment data, $l \approx 25 \pm 5$ μm for the thick fibers, and $l \approx 7 \pm 2$ μm for the thin fibers. The buckling length depends on the bending stiffness of the fiber, A. It was estimated to be 210 ± 60 Nm^2 for the thick fibers, and $A \approx 25 \pm 8$ Nm^2 for the thin fibers [34]. Using these values, we successfully described the swimming motion of both single- and double-tail swimmers, see Fig. 22. The only difference was the value of the constant c which was used, $c \approx 0.142 \pm 0.035$ for the single-tail swimmers and $c \approx 0.093 \pm 0.031$ for the double-tail swimmer. This difference is probably related to the fact that the propulsion forces exerted by the two fibers in the second case do not act in the same direction.

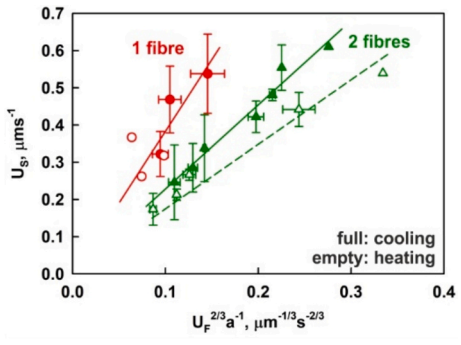

Fig. 22. Plot showing the swimming velocity as a function of the fiber extrusion velocity to the power of 2/3 divided by the swimmer radius. An excellent description of the experimental results is obtained using the derived theoretical model, see eq. 10. Adapted from Ref. [34].

In conclusion, a novel model system exhibiting a complex behavior typically found in living microorganisms was developed [34]. Its chemical composition is extremely simple consisting solely of oily droplets dispersed in aqueous medium with a minimal concentration of surfactant added to it. The propulsion of these synthetic microswimmers is governed by the formation of the rotator phase on the drop surface upon cooling and can be efficiently controlled by changing the oil-surfactant combination or the cooling rate. Furthermore, the swimmers can be recharged allowing for multiple usage of the same emulsion samples in several experiments. The shape of the developed microswimmers resemble this of some real microorganisms, such as *Chlamydomonas applanata* and *Chlamydomonas reinhardtii*. Further experiments with the swimming drops may explore their behavior in crowded environments or the hydrodynamic interactions of systems comprising artificial and biological microswimmers.

5. Self-emulsification, self-dispersion and spontaneous double emulsion formation

The size of entities in disperse systems, such as drops, bubbles, micelles, particles, and crystallites, determine important part of the dispersion properties, including stability, appearance, texture, mouthfeel, viscosity, creaminess, bioavailability and many others [178–184]. The formation of small droplets is typically related either to the use of high surfactant concentrations (as in the spontaneous emulsification techniques) or the relatively inefficient high mechanical energy input (e.g., in the high shear mixers or high-pressure homogenizers) [185]. Comprehensive reviews of various emulsification techniques, along with their advantages and limitations, can be found in Refs [178, 185–190] and will not be presented here. Instead, we focus on two phenomena discovered during self-shaping studies, both closely related to phase transitions within emulsion systems.

Thermal cycling studies of emulsions have revealed two non-trivial phenomena: drop self-dispersion (*SD*) and drop self-emulsification (*SE*). Both processes involve a spontaneous decrease of emulsion drop size upon cooling and/or heating, without the application of mechanical energy. Starting from coarse emulsions with initial droplet sizes of 10–100 μm, *SD* can reduce droplets to approximately 20–100 nm

[35,37], while *SE* typically achieves a minimum size of about 600–800 nm [36,82]. Despite that both *SE* and *SD* results in spontaneous drop size decrease, their underlying mechanisms differ significantly and are discussed in the following subsections.

5.1. *Self-emulsification upon cooling/heating cycling*

The self-emulsification process is closely linked to the self-shaping process, and its efficiency primarily depends on the drop shape deformations that occur during cooling. Four distinct mechanisms for self-emulsification have been identified. One of them realizes upon cooling, one at the moment of freezing, and two during sample heating. These mechanisms will be briefly outlined here, as they are described in details in Refs. [36, 82].

Drop size decrease upon cooling (*SE Mechanism 1*) involves puncturing and bursting of the platelets, as illustrated in **Figs. 23**a and **24**. As discussed in Section 2.1, emulsion drops undergoing spontaneous shape changes upon cooling can transform into hexagonal, tetragonal, or triangular platelets with a cylindrical frame and a thin central part. As the temperature decreases, the central part of the platelet expands, and more molecules from the liquid interior are "pulled" into the cylindrical frame. As a result, the platelet center becomes thinner and may eventually break [36].

Two different breakage mechanisms have been observed. When the central part of the platelet become very thin, a water-oil-water film forms in the center. This film is unstable and ruptures, *SE Mechanism 1a*. This leads to the formation of capillary-unstable, toroidal in shape particles, which typically breaks almost instantaneously into two or more smaller droplets, as shown in Fig. 24a,b. We note that in some systems, where the rotator phase layers are thicker, the toroidal shapes may remain stable for several minutes, thus allowing formation of punctured fluid droplets, as shown for example in Fig. 2c.

Experimental results indicate that the oil film ruptures much more quickly than theoretically predicted if only the negative capillary pressure which drives the molecule transfer from the liquid interior into the meniscus region is accounted for (in which case the film thickness should decrease at a rate proportional to the third power of film thickness, h^3, as predicted by the Reynolds equation) [36,191–193]. The film ruptures once the van der Waals forces acting between the two film surfaces become strong enough to overcome the excessive interfacial energy created by the local surface deformation (at a film thickness $h_{cr} \approx 10$ nm) [36]. Note that no repulsive forces are present within the thin water-oil-water film, as the surfactant tails have the same chemical nature as the oily molecules inside the film, making such films extremely difficult to stabilize by low molecular weight surfactants [194,195].

SE Mechanism 1a is relatively efficient for decrease of the size of big droplets, characterized by d_{32} and d_{v95} diameters, whereas it does not decrease significantly the size of the smallest drops, as limited number of small drops are generated after this type of breakage [82].

Another variation of the drop size reduction mechanism upon cooling, *SE Mechanism 1b*, is also driven by platelet puncturing. In this case, the puncturing is triggered by the mechanical breakage of one or more rods from the expanding frame at the drop periphery, see Fig. 24c and Supplementary Movie 4. This breakage causes local thinning near the broken rod, which leads to puncturing in the adjacent area. Such breakage appears when the plastic rotator phase in the frame does not possess a sufficient mechanical strength to withstand the internal capillary pressure exerted by the liquid oil inside the particle. The resulting asymmetric rupture leads to the formation of a higher number of droplets compared to *SE Mechanism 1a*. However, most of the oil remains in one or two larger drops, while the satellite droplets formed are much smaller and usually higher in number. Therefore, this mechanism decreases the drop diameter when measured by number, but it has smaller effect on the average drop size measured by volume [82]. Note that the inward bending of the rods toward the center of the platelets serves as additional indirect evidence for the presence of positive interfacial tension in these systems.

SE Mechanisms 2 and *3* proceed when an already frozen sample is heated. As shown in **Figs. 1**a, **3, 9, 19** and **20**, various shapes extruding fluid fibers or rods are observed upon drop cooling. These fibers remain stable in the fluid state because they are covered with thin layers of plastic rotator phase. However, once frozen, the molecules rearrange into a crystalline lattice, and the visco-elasto-plastic properties of the rotator phase are lost. Upon heating, the extruded fibers remain stable until they reach the melting temperature, at which point thousands of separate small droplets form due to Rayleigh−Plateau type capillary instability [196–198].

This breakage mechanism has been denoted in our studies as *SE Mechanism 2* and it is schematically shown in Fig. 23 [36,82]. The diameter of the newly formed droplets is about twice the diameter of the frozen fibers. Usually, the extruded fibers are much longer than 100 μm and have diameter around 0.5 to 2 μm. Therefore, from a single fiber, hundreds to thousands of separate drops form after its melting. This mechanism is highly efficient for producing small droplets with diameters between 0.6 and 2 μm, significantly reducing the d_{N95} diameter. However, because the volume of the drops is proportional to the third power of their radius, these small drops contain relatively small amount of the oil and therefore do not significantly reduce the d_{32} and d_{v95},

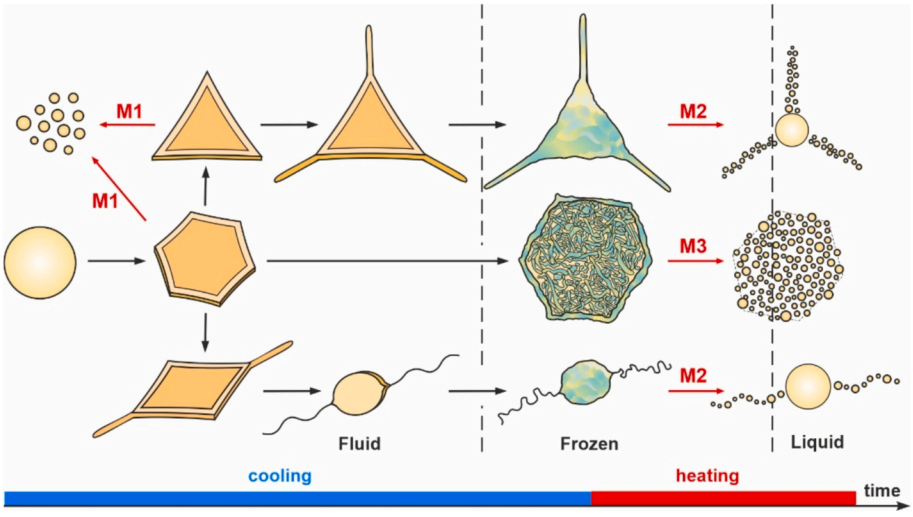

Fig. 23. Schematics of the self-emulsification mechanisms. Adapted from Ref. [36].

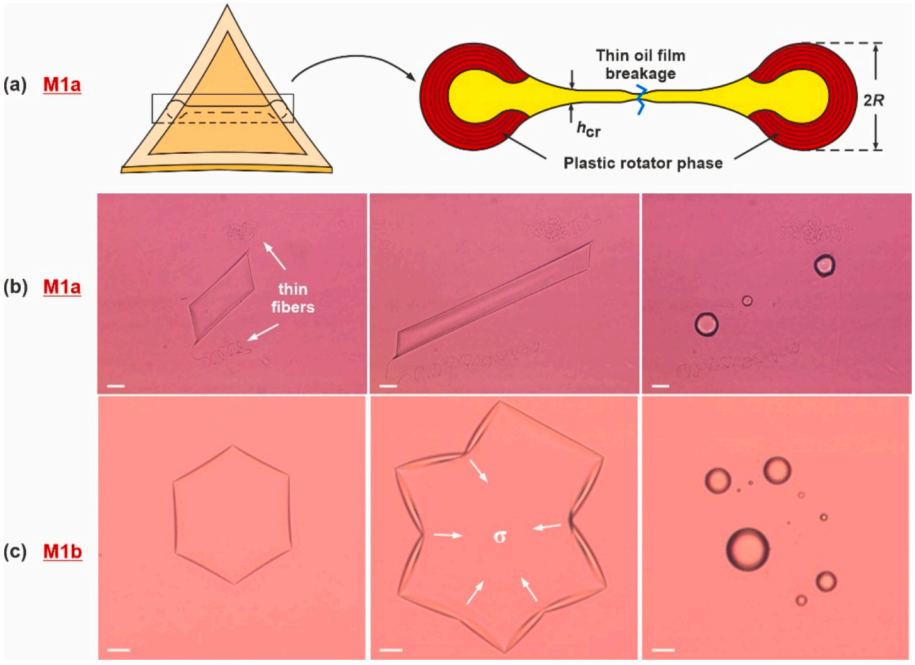

Fig. 24. SE Mechanism 1. (a) Schematics of the thin water-oil-water film breakage driven by the molecule transfer from the liquid particle interior into the thicker frame. Note that surfactant molecules are present at the deformed drop surface, but they have been omitted for visual simplicity. (b) Optical microscopy pictures showing the breakage process. Scale bars = 50 μm. (c) Spontaneous drop bursting induced by the frame breakage due the action of capillary pressure. Scale bars = 20 μm. See also Supplementary Movie 4.

which are much more sensitive to the size of the largest drops in the sample [82].

SE Mechanism 3 (melt-crystal fragmentation) also occurs upon heating and is the most efficient of the self-emulsification mechanisms described so far in reducing drop size. This process involves the bursting (fragmentation) of frozen platelets at the moment of their melting into hundreds of separate droplets, see Figs. 23 and 25. The efficiency of *SE Mechanism 3* primarily depends on the oil-surfactant combination and the shape of the frozen particles. It is independent of the heating rate, as the melting of single-component particles occurs within seconds once the melting temperature is reached, regardless of the temperature ramp. This mechanism is operative only for frozen platelet particles and is driven by the dewetting of still-frozen alkane domains from the just-melted liquid alkane, therefore it is referred to as a melt-crystal fragmentation [36,82].

For dewetting to occur in these systems, the three-phase contact angle between the melted oil, frozen oil substrate, and the aqueous phase, θ_w, measured through the aqueous phase, must decrease below 90°, see schematics in Fig. 25a. The relationship between θ_w and the three relevant interfacial energies is given by the Young-Laplace equation:

$$\cos\theta_w = \frac{\sigma_{so} - \sigma_{sw}}{\sigma_{ow}}, \tag{11}$$

where subscripts *w*, *o* and *s* denote the water, melted oil, and the still-frozen oil phases, respectively. Therefore, the melt-crystal fragmentation occurs only if $\sigma_{so} > \sigma_{sw}$. This condition is rarely met because the melted oil and the solid substrate have identical chemical nature, resulting in low interfacial energy, $\sigma_{so} \approx 3$–8 mN/m [199]. However, the addition of appropriate surfactants, which can form a dense adsorption

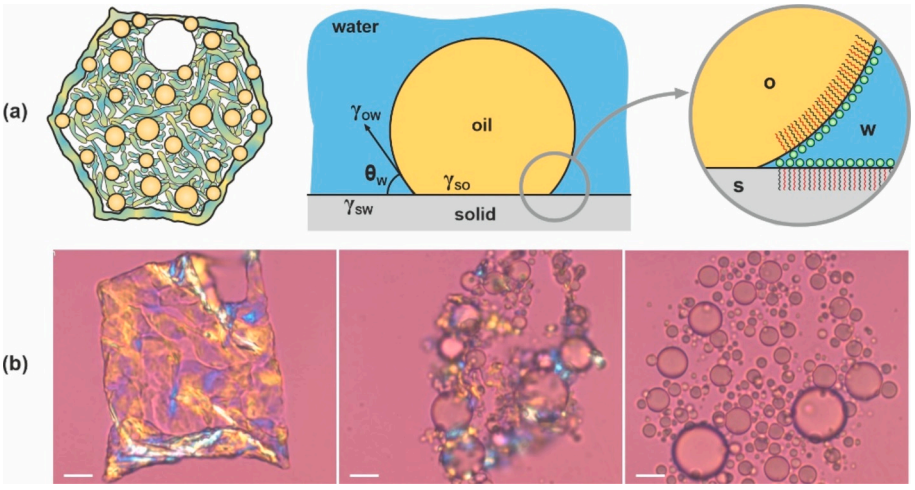

Fig. 25. Melt-crystal fragmentation (*SE Mechanism 3*). (a) Schematics showing liquid oil dewetting from the still solid lipid substrate leading to spontaneous drop size decrease. (b) Optical microscopy pictures illustrating the process. Scale bars = 10 μm.

layer at the frozen oil-water interface and significantly decreasing the σ_{sw} can induce the dewetting process [36].

Analysis of various physicochemical parameters showed that *SE Mechanism 3* primarily occurs in systems where a decrease in interfacial tension upon cooling is detected [82]. As explained above, this decrease is related to formation of dense frozen adsorption monolayer on the oil-water interface which decreases the solid-water interfacial energy, σ_{sw}, facilitating the dewetting process. Systematic experiments revealed that the most efficient melt-crystal fragmentation process occurs when surfactants stabilizing the emulsions have hydrophobic tails that are either comparable in length to the alkane chain or slightly longer. These systems usually fall in *Group A* as classified in Section 2.4, see Fig. 9 and the drop shape deformations begin at $T_d > T_m$. For systems in which the oil-water interfacial tension does not decrease upon cooling, the *SE Mechanism 3* is not observed and even when platelet particles are formed, they melt back into a single drop (with possible formation of few smaller satellite droplets) [82]. If present, *SE Mechanism 3* leads to the most efficient drop size decrease, see Fig. 26a.

SE Mechanisms 1, *2* and *3* are observed with both single- and multi-component emulsion drops. For multicomponent drops, an additional fourth mechanism, *SE Mechanism 4*, contributes to drop size reduction [56]. This mechanism occurs in non-spherical particles formed from mixtures of compounds with significantly different melting temperatures. In these systems, the non-spherical particles formed during drop shape evolution do not remain intact upon freezing. Instead, when the higher-melting component reaches its crystallization point, it solidifies. This disrupts the plastic phase stabilizing the non-spherical shape and as a result the platelet particles, as well as the thin fibers and rods, usually disintegrate into several separate particles which have significantly smaller drop diameters [56].

The main features of the described *SE* process are summarized in Table 1. Its efficiency depends mostly on the oil-surfactant system and the applied temperature protocol. Generally, the most efficient drop size decrease is observed for systems in *Group A*, particularly when cooled slowly. The minimal achievable drop size using these self-emulsification mechanisms is ca. 600 nm by number and 800 nm by volume. The initial drop size can range from 1 to ca. 50 μm. It has been shown that the described self-emulsification mechanisms are efficient not only in model experiments performed in capillaries, but also for bulk samples with higher oil volume fractions, see Fig. 26b [36,82].

5.2. *Self-dispersion and double emulsion formation processes for single-component droplets*

Another, much more powerful method for reducing drop size upon cooling and heating, was found while studying the behavior of triglyceride-in-water emulsion droplets, see Table 1 [35]. This method, referred to as self-dispersion (*SD*) or cold-bursting, does not rely on the

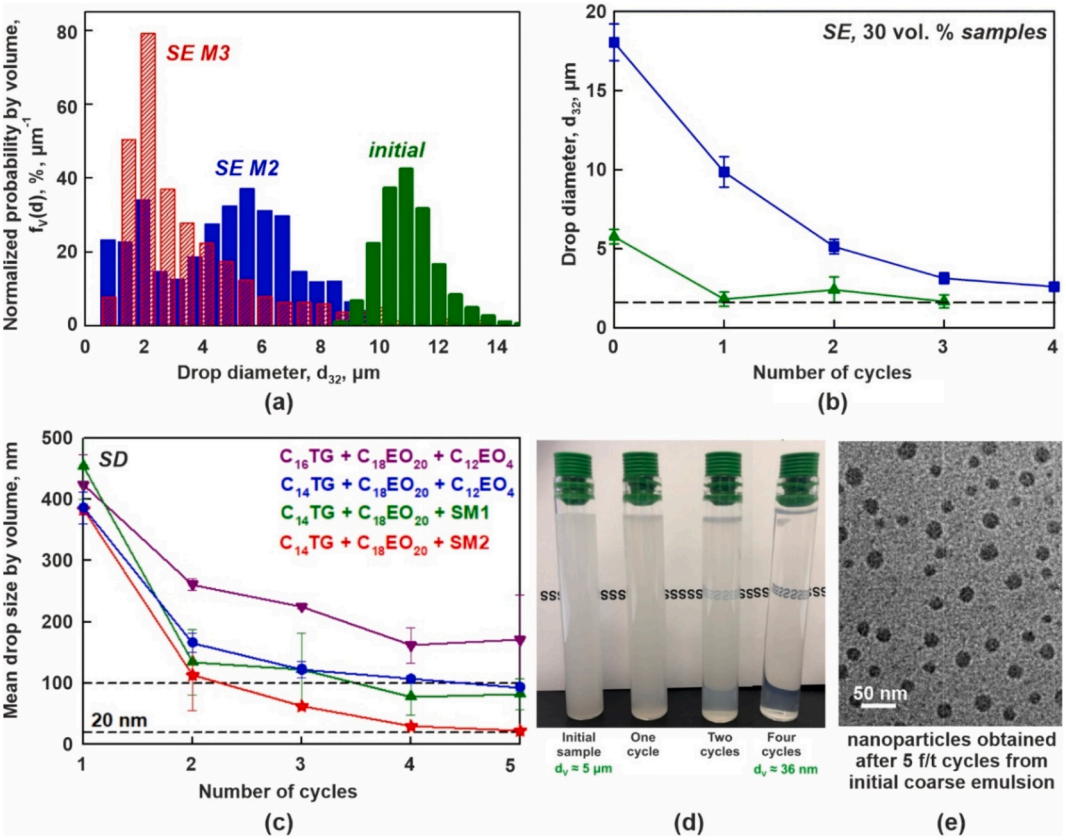

Fig. 26. Quantitative results showing the drop size decrease observed via: (a,b) Self-emulsification upon cooling/heating cycles. (c) Self-dispersion. (a) Drop size distribution after one cycle. The efficiency of *SE Mechanism 2* (blue) and *SE Mechanism 3* (red) is compared. The green bars show the initial drop size distribution. Adapted from Ref. [82]. (b) Drop size decrease as a function of the consecutive cooling-heating cycles applied to the bulk emulsion samples. The experiments have been performed with 30 vol% samples. Adapted from Ref. [36]. Data in (a,b) have been obtained with hexadecane droplets dispersed in 1.5 wt% Brij S20 surfactant solutions. (c) Mean drop size, measured by volume, as a function of the number of cooling and heating cycles applied to the samples with triglyceride droplets, stabilized by various surfactant combinations (as denoted on the graph). The initial drop size is $d_{32} \approx 33$ μm. Adapted from Ref. [35]. (d,e) Macroscopic (d) and cryo-TEM picture (e) demonstrating the drop size decrease in bulk samples via the self-dispersion method. (d) Drop size decrease from ca. 5 μm down to 36 nm is observed after four consecutive cooling-heating cycles applied to sample with Precirol ATO5 oily drops dispersed in 1.5 wt% Brij S20 + 0.5 wt% Brij 30 solution. Adapted from Ref. [54]. (e) Nanoparticles obtained via the self-dispersion method. Nanoparticles are composed of a 6-component triglyceride mixture. Adapted from Ref. [37]. (For interpretation of the references to colour in this figure legend, the reader is referred to the web version of this article.)

Table 1
Comparison between the self-emulsification (*SE*) and self-dispersion (*SD*) processes, observed upon cooling/heating cycling and leading to significant spontaneous drop size decrease.

	Self-emulsification	Self-dispersion
Biggest initial drop size studied	≈ 40–50 μm	≈ 100 μm
Average drop size after 1 cycle	> 1 μm polydisperse	≈ 400 nm ≈ monodisperse
Minimal achievable drop size	≈ 600 nm	≈ 20 nm
Cooling rate	< 2 °C/min	higher – beneficial, up to 15 °C/s studied
Complete freezing is required	No (but the efficiency would be low)	Yes
Re-melting required	Yes (significantly enhanced efficiency)	No
Heating rate	Independent (single-component particles)	Slower – beneficial (< 2 °C/min)
Self-shaping upon cooling required	Yes	No
Demonstrated to be applicable to	Pure alkanes Mixtures of alkanes	Monoacid triglycerides (pure and mixtures) Natural triglycerides (coconut oil, cocoa butter…) Diglycerides Triglyceride-diglycerides-monoglycerides mixtures (e.g. Precirol ATO 5) Phospholipids Alkanes

drop self-shaping process and its efficiency is independent from the shape of the drops obtained upon their freezing. Instead, the self-dispersion is governed by solid-to-solid polymorphic phase transitions, which are commonly observed in many lipids (oils) [58,59,73].

Microscopy images demonstrating the self-dispersion process with trimyristin (C_{14}TAG) droplets are shown in Fig. 27c and Supplementary Movie 5, while results illustrating the drop size decrease after several consecutive cooling-heating cycles are presented in Fig. 26c,d. The most intensive drop disintegration was observed with lipids able to form multiple polymorphic solid phases, such as triglycerides (TAG) [35]. This observation was related to the crystalline structures in which TAG molecules are known to arrange upon cooling.

Pure triglycerides crystallize into three main phases – α, β' and β, ordered from the least thermodynamically stable to the most stable [73]. The α polymorph is the most disordered, with the lowest melting temperature, and its molecules arrange in a hexagonal lattice. The β' polymorph has intermediate properties, whereas the β phase is the most thermodynamically stable, with the highest melting temperature and the molecules are arranged in a triclinic lattice [73].

Upon cooling, the disordered triglyceride molecules in the liquid state usually first arrange into the α phase, as nucleation into this most disordered phase is the easiest [73]. Prolonged storage at low temperatures or heating to temperatures exceeding the melting points of the less stable α and β' polymorphs induces polymorphic phase transitions, leading to the formation of the most stable β phase. These transitions are classified as solid-state or melt-mediated, respectively. However, the β polymorph has a higher mass density than the α phase, and several studies have shown that nanovoids form upon α-to-β phase transition, accompanied by a negative pressure effect [200–202].

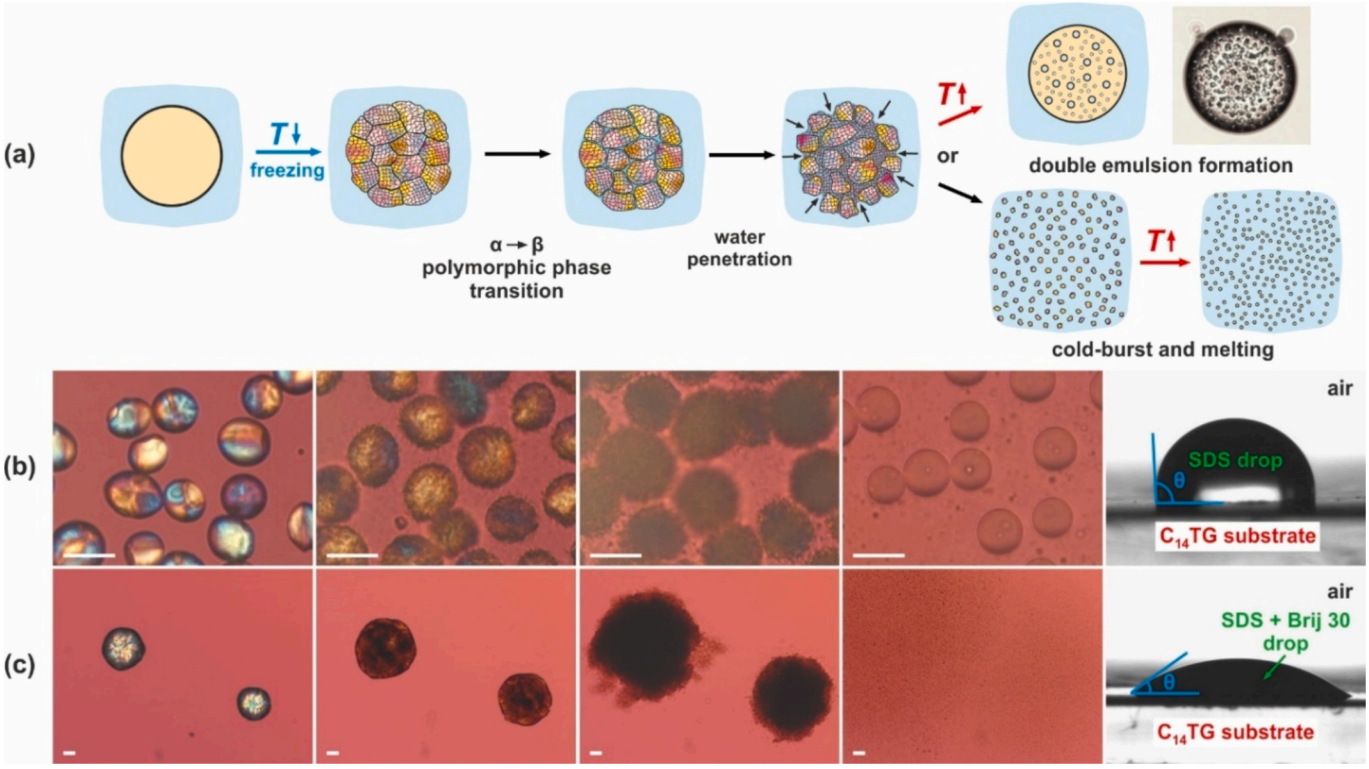

Fig. 27. Cold-bursting mechanism and examples. (a) Schematic representation of the cold-bursting mechanism. Adapted from Ref. [35]. (b,c) Microscopy pictures obtained upon heating of trimyristin emulsion drops dispersed in 0.5 wt% sodium dodecyl sulfate (SDS) surfactant solution (b) and 0.5 wt% SDS + 0.5 wt% Brij 30 (c). The process of water penetration is observed with both systems. However, upon melting the drops dispersed in SDS solution, do not disintegrate, whereas those dispersed in SDS + Brij 30 solution burst into millions of nanometer- sized droplets. The observed difference is related to the wetting ability of the surfactant solution. As seen from the three-phase contact angle measurements (last pictures in b and c), the contact angle at the air-surfactant solution-frozen triglyceride is quite different for these two systems. The solution containing oil-soluble surfactant wets very well the frozen substrate and successfully separates the individual crystalline domains, whereas much higher contact angle is observed in absence of Brij 30. In this case, the water which have penetrated inside the particle remain entrapped in it in the moment of oil melting. Scale bars = 20 μm.

The α-to-β transition has been found to be responsible for the spectacular drop self-dispersion process. The mechanism of this process is schematically illustrated in Fig. 27a and can be described as follows: Upon cooling, the dispersed drops crystallize usually into a polycrystalline structure in α phase. This α phase then transforms into the most stable β phase upon storage or heating above the melting temperature of the α phase. The polymorphic phase transition leads to the formation of frozen particles with a higher mass density, causing the initially formed crystalline domains to shrink. As a result, a nanoporous inner structure is created. This structure cause a negative pressure effect, and upon prolonged storage or heating, the aqueous phase in which the particles are dispersed begins to penetrate into their interior (see the middle images shown in Fig. 27b,c). This leads to a significant increase in particle volume, which is also accompanied by the disappearance of colors when the process is observed in polarized light. Afterwards, two alternative outcomes are possible – the individual crystalline domains may either disintegrate, forming millions of small nanoparticles, or, if the penetrated water remains trapped within the melting particle interior, the formation of water-in-oil-in-water (w/o/w) double emulsion droplets is observed, Fig. 27 [35].

Systematic experiments with various oil-surfactant combinations showed that, for single-component droplets, the outcome of the cold-bursting process is governed by the wetting properties of the aqueous phase over the frozen lipid substrate [35]. The most intensive self-dispersion process is observed in systems where the three-phase contact angle, measured at the frozen lipid-aqueous solution-air contact line, is smaller than 50°. In contrast, double emulsion formation is observed in systems with higher contact angles, $> 100°$, see last images in Fig. 27b,c.

In contrast to the *SE* mechanisms described above for spontaneous self-shaping droplets, the self-dispersion process can be very efficient not only when the system is heated above the melting point of the dispersed oil, but also when the sample is stored for a prolonged period at temperatures well below the melting point [35]. This is governed by the fact that the polymorphic phase transition can proceed at low temperatures, enabling the aqueous phase penetration and subsequent disintegration even in the solid state. As a result, complete cold-bursting has been observed even after storing trilaurin particles at 5 °C, despite their melting temperature being 46 °C [35]. However, the storage temperature significantly influences the kinetics of the process and the complete disintegration occurs much more rapidly as the sample temperature approaches the melting temperature of the oil.

Another notable difference between the *SE* and *SD* processes is related to their dependence on the cooling rate, Table 1. While relatively slow cooling rates (e.g. < 2 °C/min) are required for the *SE* process to occur, as the development of non-spherical shapes upon cooling is essential, the *SD* process becomes more efficient at higher cooling rates. This difference is related to the number of individual crystalline domains that form during liquid-to-solid phase transition. It is well known that higher cooling rates result in the formation of a higher number of smaller crystallites, compared to those formed when the sample is slowly frozen [203,204].

In addition, the efficiency of the *SD* method is significantly enhanced compared to that of the *SE* method, both regarding the smallest achievable drop size and the average drop sizes obtained after a single cooling-heating cycle. While the *SE* method requires several consecutive cycles to achieve submicrometer-size droplets, particularly for drops larger than ca. 10 μm, the *SD* method is able to disintegrate drops as big as 100 μm into 400 nm entities after just one cycle of cooling and heating. By applying several consecutive freeze-thaw cycles, the minimal achievable drop diameter is between 20 and 200 nm depending on the specific oil-surfactant combination, see Fig. 26c-e. This method is effective for a variety of substance, including diglycerides, triglycerides, alkanes, and particles loaded with active substances at concentrations of up to 30–40 wt% [35,205]. Furthermore, it has been successfully applied to synthetic mixtures of monoacid triglycerides, as well as complex natural triglyceride oils (e.g. coconut oil, cocoa butter), see **Figs. 26**d,e and **28**d,e [35,37,54]. The peculiarities of the *SD* process for multicomponent particles are explained in the next section.

We note that the cold-bursting described above differs significantly from the well-known phase inversion temperature (PIT) process, which is also capable of producing nanometer-sized droplets. More specifically, PIT is a low-energy method whose mechanism relies on temperature-induced changes in the properties of surfactant [185,206]. Typically, nonionic polyoxyethylene surfactants are employed, whose solubility significantly decreases upon heating due to the disruption of H-bonds and progressive dehydration of their hydrophilic moieties. This dehydration alters the spontaneous curvature of the surfactant molecules, leading to formation of structures with zero spontaneous curvature around the PIT. When the temperature is rapidly changed afterwards, the system becomes quenched in a metastable state, resulting in the formation of kinetically stable nanodroplets. It has been also demonstrated that the PIT process can occur at temperatures a few degrees below the actual PIT when a bicontinuous emulsion coexists with an excess of oil phase [207,208].

In contrast, the cold-bursting method operates under fundamentally different principles [35,37,82]. It realizes when the initially dispersed droplets undergo crystallization (i.e. the oil phase is in a solid state, a condition incompatible with the PIT process). Furthermore, no bicontinuous phase is formed, and the cold-bursting mechanism does not depend on changes in surfactant curvature. It can be realized with both nonionic and ionic surfactants [35]. In addition, although the heating increases the kinetics of the disintegration, in fact – it is not needed, the cold-bursting can proceed even at a constant low temperature over prolonged storage. Moreover, the size of the resulting nanoparticles/nanodroplets is determined by the size of the crystalline domains formed during the liquid-to-solid phase transition, whereas in the PIT method, the droplet size is determined by the spontaneous curvature of the surfactant molecules.

5.3. *Self-dispersion for mixed droplets*

One major difference between highly pure and mixed oils is that introducing molecules with various structures within the same mixture leads to a significant expansion of the melting region, compared to the one observed in pure substances [73]. However, this results in the coexistence between solid lipid domains and molten domains within the same particle in a wide temperature interval, which complicates the disintegration process. Experiments with various model triglyceride mixture (composed of highly pure monoacid TAGs), as well as with natural triglyceride oils, revealed that the *SD* process is possible for them and can be highly efficient [37,54,209]. Several additional requirements, alongside the good wetting ability of the surfactant solution over the solid lipid substrate, were found to be essential, see Fig. 28:

(1) Along with the low values of the three-phase contact angle at the air-surfactant solution-frozen lipid interface (measured through the aqueous droplet), it was found that the equilibrium surface tension of the aqueous solution should be low, e.g. 30 mN/m or lower, and it should decrease quickly, see Fig. 28a. This condition facilitates the quick wetting of the pores and is crucial for the occurrence of the self-dispersion process [54].

Only one of the following two conditions needs to be met to enable bursting in complex TAG mixtures. However, if both conditions are met for a given system, the *SD* efficiency will be maximized.

(2) To allow a phase separation between the freshly melted oil and the still frozen domains, the three-phase contact angle at the melted oil-frozen oil-aqueous solution interface should be high, Fig. 28b. In this case, the already molten oil can be emulsified into small droplets within the continuous aqueous phase, even before the longer components become melted, see Fig. 28e for illustration [54]. This *SD* mechanism is somewhat analogous to the *SE Mechanism 3*.

(3) A very efficient boosting effect was observed for lipid particles

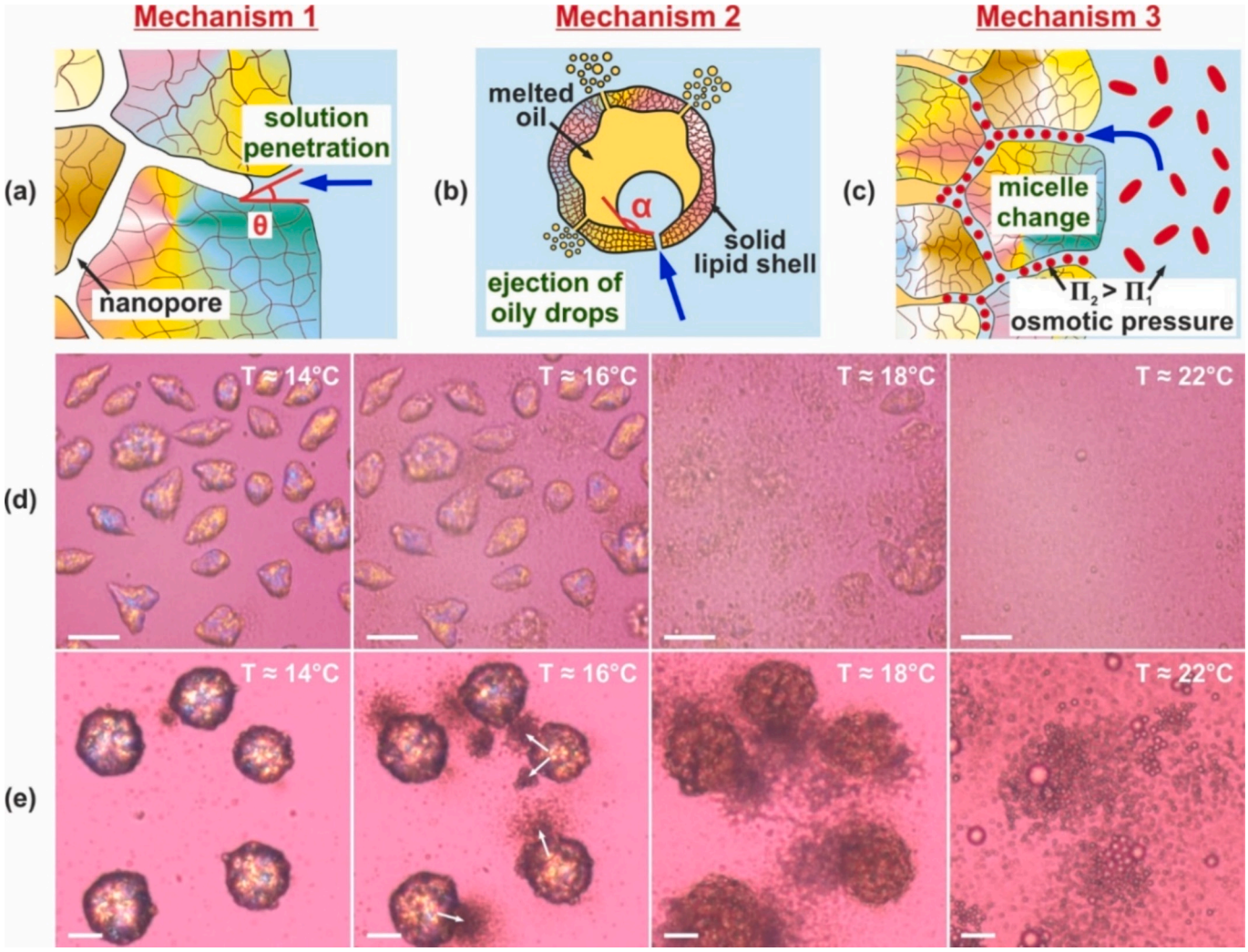

Fig. 28. Cold-bursting with natural triglyceride oils – mechanisms and examples. (a) Analogous to the pure TAGs, one of the most important conditions for intensive cold-bursting process with natural TAG oils is that the three-phase contact angle at the air-solution-frozen TAG interface should be low (b-c) For mixed TAG oils, one of the two additional mechanisms should also be operative for intensive cold-bursting. The two options are: (b) high values of the three-phase contact angle measured through the aqueous phase at the frozen oil-liquid oil-surfactant contact line, which causes ejection of liquid oily drops before the complete melting of the solid lipid shell, or (c) changes in the micelles shape and size, causing osmotic pressure gradient between the surfactant micelles that have penetrated inside the particle and those in the bulk medium. The osmotic pressure causes further penetration of the surfactant solution and subsequent disintegration of the frozen particle into numerous small droplets. (d-e) Microscopy pictures of coconut oil drops dispersed in 1.5 wt% Tween 20 + 0.5 wt% monoolein solution. The drops are quickly frozen (≈ 2.5 °C/s cooling rate) and then heated at a rate of 0.5 °C/min. The images obtained upon heating are present. For smaller in size drops shown in (d), mostly *SD Mechanisms 1* and *3* are operative, while for larger particles shown in (e), all three mechanisms are operative. The white arrows show the direction in which the melted oily drops are ejected from the still-frozen lipid shell at temperatures << T_m. Scale bars = 20 μm. Adapted from Ref. [54].

dispersed in solutions containing supramolecular aggregates which are able to change their shape when the aqueous solution penetrates the inner nanoporous structure [54], see Fig. 28c. This shape change creates an osmotic pressure gradient due to the difference in composition between the aqueous phase penetrated inside the nanopores and the external aqueous phase. The osmotic pressure gradient drives further penetration of the aqueous phase into the nanopores, thereby enhancing the *SD* efficiency.

The osmotic pressure effect can be realized in several ways. For example, when an oil-soluble surfactant is solubilized within micelles formed by a water-soluble surfactant, the micelles size increases and their shape changes. However, once an oily phase become available, it is thermodynamically preferable for the oil-soluble surfactant molecules to escape the mixed micelles and either adsorb or dissolve into the oily phase. Therefore, higher in number and smaller in size spherical micelles form. It should be noted that results from experiments with various oil-soluble surfactants indicated that much more efficient disintegration is observed when the oil-soluble surfactant do not co-crystallize with the melted oil. For example, such *co*-crystallization was observed for polyoxyethylene (2) oleoyl ether surfactant, whereas the monoolein surfactant phase separated from the TAG mixture, thus leading to significantly enhanced bursting efficiency, although both surfactants fulfilled both conditions (1) and (3) [37].

A similar boosting effect due to the creation of osmotic pressure gradient was observed when electrolytes are present in the aqueous phase [209]. Additionally, combining two or more water-soluble surfactants, along with co-surfactants able to form non-spherical micelles, has also been shown to significantly enhance the bursting process [54].

Under optimized conditions, the smallest particle sizes that were achieved starting from coarse emulsions, ranged from ca. 20 nm for synthetic TAG mixtures [37], Fig. 26e, to ca. 30–40 nm for mixtures of mono-, di- and triglycerides used in pharmacy [54], Fig. 26d and about 150–200 nm for drops composed of natural triglyceride oils, such as coconut oil, palm kernel oil and cocoa butter [54,209]. Further

experiments are needed to establish how active substances dissolved in the initial coarse emulsion droplets will affect the self-dispersion efficiency. Initial results suggest that dissolving model drugs at concentrations up to ca. 30 wt% in the oil before emulsification does not significantly disrupt the efficiency of the cold-bursting process [35].

5.4. Double emulsion formation for mixed droplets

Spontaneous formation of double emulsion droplets upon cooling-heating cycles was also observed for mixed TAG drops [37,54]. However, besides for solutions which had poor wetting properties over the solid lipid substrate, Fig. 27a,b, such double w/o/w drops formation was also observed even for solutions able to induce complete cold-bursting [37]. An illustration is presented in Fig. 29 where for the same oily droplets, a solution of Tween 20 + monopalmitin and monostearin oil-soluble surfactants has been shown to induce either complete disintegration (Fig. 29a) or double w/o/w emulsion formation (Fig. 29d) [37].

The observed variations in drops behavior were governed by the phase behavior of mixed drops combined with different cooling/heating rates. Rapid cooling allowed formation of numerous small crystallites, which can be efficiently disintegrated during slow heating as aqueous phase penetrates the structure; otherwise, an inefficient bursting is observed, Fig. 29b. When slow cooling is applied, smaller in number and bigger in size domains are formed, limiting the number of nanopores. When slow heating is applied afterwards, it leads to bursting, but some bigger droplets remain in the sample, Fig. 29c. If a slowly cooled sample is quickly re-melted, the penetrated water does not have sufficient time to disintegrate the domains, nor to escape the lipid globule, thus it remains trapped inside the droplet, forming a double water-in-oil-in-water drop, Fig. 29d [37].

Studies of self-emulsification and self-dispersion processes showed that by utilizing the phase behavior of dispersed oils in combination with suitable surfactants, one can achieve spontaneous drop size decrease without specific equipment, mechanical energy input or excessive heating.

6. Applications

The studies of self-shaping, self-emulsification and self-dispersion phenomena governed by the phase transitions in emulsion systems are interested not only from a scientific viewpoint, but also present various possibilities for technological advancement in several industrial fields, see Fig. 30. For that reason, the described processes were protected by two international patents [205,210]. In this section some of the possible applications are outlined.

6.1. Preparation of anisotropic micrometer- and sub-micrometer-sized particles

Anisotropic in shape particles are of high interest for several research areas including drug delivery, medical imaging, and composite materials [10–14,211–217]. Usually anisotropic particles are prepared with specific methods with low productivity which also require special equipment, for example microfluidic or lithography techniques [21,121,122,218–220]. However, these methods have limited applicability for production of soft lipid particles with desired shape and size.

As explained in Section 2, the self-shaping process produces particles with various non-spherical shapes in a very simple manner. It does not require any specific apparatus and can be scaled up to large volumes and continuous mode of operation if an appropriate reactor is constructed [209]. The applicability of the process to various classes of organic molecules, including alkanes, alkenes, alcohols and triglycerides, makes it widely versatile allowing an easy selection of the most appropriate material depending on the required application. However, the long preservation of the non-spherical shape can be only provided for selected fluid shapes, see Fig. 10 and the discussion related to it, or if the oily drops are crystallized in a given shape and then stored at temperatures lower than the oil melting point.

Another possibility to overcome this limitation is to polymerize the obtained non-spherical soft particles, thus preserving their non-spherical shape indefinitely in time. This concept has been realized with hexadecyl acrylate and stearyl methacrylate in two independent studies [51,52]. Both monomers have long saturated alkyl chains enabling the self-shaping phenomenon when appropriate long chain surfactants are used. After self-shaping proceeded at low temperatures, the deformed particles were polymerized using an UV light and polymeric anisotropic particles were prepared. To enable the UV polymerization of the deformed droplets, a photo initiator was included in the initial droplets (α-ketoglytaric acid or diphenyl 2,4,6-trimethylbenzoyl phosphine oxide). Depending on the initial emulsion drop size, the size of polymeric particles may vary between ca. 50 nm up to ca. 1 mm. The obtained polymeric particles remained stable below the glass transition temperature of the prepared polymer, for example for poly(stearyl methacrylate) $T_g \approx 311$ K [51]. Furthermore, the non-spherical polymer particles may be modified by inclusion of magnetic particles in them, making them responsible to an external magnetic field [51].

Additionally, the possibility to easily prepare synthetic swimmers which are solely driven by the internal phase transitions rather than externally applied fields presents a new opportunity for studying the swimmers hydrodynamics and to compare them with the one observed in real biological swimmers. For example, the beating patterns in *Chlamydomonas*, unicellular green algae, which swims with two flagellates show a possible change in the relative phase between the two flagella. In contrast, the swimming drops did not show such synchronization – the drops which extruded fibers out-of-phase remained to do so until freezing, as well as those which initially began to extrude two fibers which were in phase. This observation shows that the hydrodynamic interactions are not responsible for the fiber synchronization, therefore the observed phase shift in the *Chlamydomonas* likely arises from an internal coupling inside the microorganism [34].

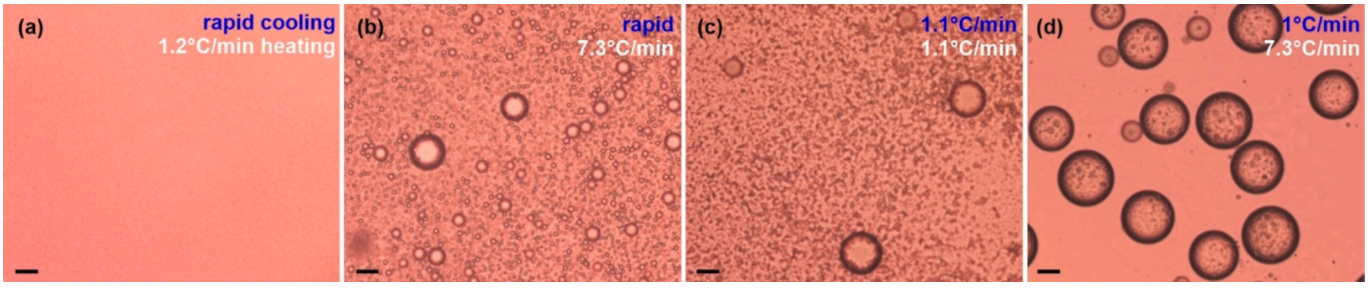

Fig. 29. Cooling-heating protocol influence over the self-dispersion and double w/o/w emulsion formation for mixed TAG drops (trilaurin + trimyristin = 1:1), dispersed in Tween 20 solution containing monopalmitin and monostearin oil-soluble surfactants. The freezing/melting kinetics (as denoted on the pictures) affects the outcome of the cooling-heating cycle. Reproduced with permission from Ref. [37]. Initial drop size in the studied monodisperse samples was about 45 μm. Scale bars = 20 μm.

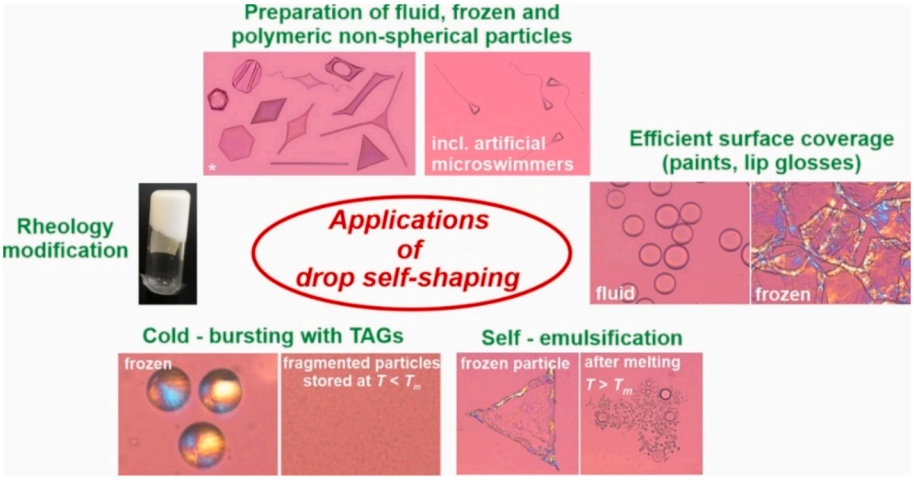

Fig. 30. Examples illustrating possible applications of the studied phenomena. These include – preparation of particles with non-spherical shapes, including artificial microswimmers; spontaneous drop size decrease without mechanical energy input via the cold-bursting and self-emulsification processes; emulsion rheology modification while the continuous phase is still in liquid state, etc. *Note that this is not a directly obtained microscopy image, but is a collage with real deformed particles, combined together (all other images included in the paper are as directly observed in the experiments).

6.2. Rheology modification

It has been well established that the shape of the dispersed colloids can greatly affect the rheological properties of the disperse systems [221–223]. Therefore, producing non-spherical lipid particles in the dispersions could serve as an alternative structuring route for rheology modification. This idea was demonstrated and explored in Refs [26, 55, 224].

Detailed studies of hexadecane-in-water emulsions stabilized by appropriate surfactants, which enable the self-shaping process, showed that the minimal oil volume fraction required to produce non-flowing, gel-like dispersions containing non-spherical lipid particles, without any additives, was ca. 11 vol% (≈ 8.7 wt%) [55]. This was achieved for emulsions with initial droplets sizes ranging from 4 to 13 μm. In contrast, emulsions prepared with shorter chain surfactants, which did not induce spontaneous shaping, required much higher oil volume fractions to reach similar viscosities: ca. 60 vol% to obtain similar rheological profile as the sample containing 11 vol% hexadecane and non-spherical particles, and about 70 vol% to form non-flowing gel-like samples with spherical frozen particles [55].

Fig. 31 illustrates the differences between emulsions containing spherical and non-spherical particles alongside their rheological properties. The effects of initial drop size and surfactant type were also revealed in Ref. [55]. Interestingly, although smaller drops are generally more prone to deformations than bigger in size droplets, dispersions with thin, long fibers exhibited lower viscosities compared to those with the same oil concentration enclosed into larger particles, Fig. 31d. This was explained with the mechanical properties of the different particles. Thin fibers were fragile and easily break into smaller pieces with lower aspect ratios, whereas larger non-spherical particles had higher

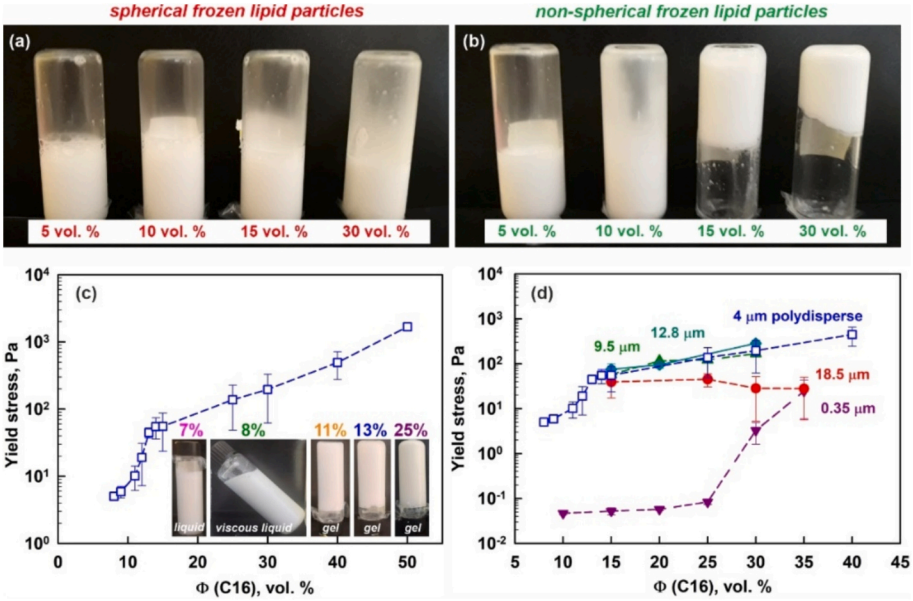

Fig. 31. Rheological behavior of hexadecane dispersions with solid particles, stabilized by different surfactants. (a) Dispersions with particles, stabilized by Tween 20 surfactant. These particles do not self-shape upon cooling and freeze in spherical shapes. (b) Dispersions with particles, stabilized by Tween 40 surfactant ($C_{16}SorbEO_{20}$). Drops in these emulsions change their shape upon freezing which significantly change the rheological properties of the sample once the drops freeze. (c,d) Yield stresses as a function of the hexadecane volume fraction for samples stabilized by Brij 58 and Brij 52 surfactants. (c) The threshold concentration beyond which the samples appear as non-flowing gels is 11 vol%. (d) Yield stresses for samples with different initial sizes. (c,d) Adapted from Ref. [55].

mechanical strength, enabling them to better sustain the weight of the dispersion [55].

This proof-of-concept study demonstrated the high impact of frozen lipid particle shape on rheological properties. Such rheological modifications are highly desirable in various food and cosmetic products such as mousses, yogurts, ice creams, cosmetic creams, as well as for the sustained release of active ingredients in pharmaceuticals [225–229]. In contrast, gelation is undesirable in applications where fluid flow is essential, such as in heat-exchange systems. In these cases, surfactant which prevent the formation of non-spherical shapes upon cooling should be selected [26].

6.3. Spontaneous formation of nanoemulsions from initial coarse emulsions

The self-emulsification and spontaneous self-dispersion (cold-bursting) phenomena can be used for decrease of the emulsion drop size without the need for mechanical energy input or excessive heating, see the detailed description in Section 5 above. Self-emulsification associated with spontaneous self-shaping of oily droplets typically reduces drop sizes to around 600 nm by number and 800 nm by volume [36,82]. The cold-bursting mechanism is much more efficient for the drop size decrease. In this case, the size decreases from tens of micrometers to about 400 nm after only one cooling and heating cycle. With multiple consecutive cycles (usually 3 are sufficient), drop sizes can further decrease to 100–200 nm, and in the most efficient systems, even as low as 20 nm. Emulsions with 100 nm drops are translucent and those with 20 nm are completely transparent [35]. These findings apply to various triglycerides, triglyceride mixtures and natural triglyceride oils [35,37,82]. Triglyceride nanoemulsions and solid lipid nanoparticles (SLNs) are widely utilized in pharmaceutics, cosmetics and food applications [230–234]. Usually such small particles can be prepared only with several cycles of emulsification through high-pressure homogenizers or ultrasonication. In contrast, the cold-bursting process achieves this under much milder conditions without specialized equipment. Furthermore, it has been shown that it is applicable to droplets containing pre-dissolved active ingredients [35]. Cold-bursting has been successfully demonstrated both in bulk batch samples [35,37,82] and in specifically designed flow cell, allowing continuous production of dispersions with nanometer-sized particles [209].

6.4. Particle recovery and colloidosomes production

The unique features seen from the studies of self-shaping drops in presence of adsorbed particles can also be utilized [49,50,53]. As explained in details in Section 3 above, the rotator phase formation cause reorganization of the latex particles adsorbed on the drops surface and in some cases detachment of the adsorbed particles from the drop surface. Therefore, the self-shaping phenomenon can be used to control the stability of the Pickering stabilization and to induce a detachment of the adsorbed particles from the drop surface. Destruction of Pickering emulsions is very important in petroleum extraction from oil sands [235–237] or as an alternative road for targeted delivery of active compounds [238–240]. Particle recovery is also desired for nanoparticle catalyst systems [241]. Furthermore, the spontaneous arrangement of particles adsorbed on the drop surface can be potentially used as a template for production of complex colloidosomes [18,242,243].

6.5. Active emulsion droplets as model systems for study the appearance of life on earth

The fundamental question of how life first emerged on Earth remains one of the biggest unsolved challenges in science [244]. One of the theories, independently developed by A. Oparin and J. Haldane in the early 20th century has recently regained significant attention [245,246]. This theory suggests that small droplets (called coacervates), formed through liquid-liquid phase separation in complex chemical mixtures, may have served as primitive compartments that concentrated molecules and facilitated chemical reactions [247]. Such compartmentalization is considered a crucial step for the transition from non-living to living matter [248].

Building on this idea, researchers investigating active droplets have suggested them as promising model systems for studying protocells with primitive life-like functionalities, including division and growth, metabolism, self-propulsion, and environmental responses [249]. All these key characteristics are typically used to explain what the definition for a living organism is. Variety of experimental approaches have been explored to replicate these functionalities. Many of these strategies rely on generating and maintaining chemical gradients, often through chemical reaction or the application of external fields [249–256].

The processes described in this review present a novel opportunity for the development of systems with life-like functionalities. In particular, small emulsion drops, driven by surface or polymorphic phase transition, can undergo spontaneous shape changes upon cooling (morphogenesis) via the drop self-shaping process, discussed in Section 2. Furthermore, part of the generated shapes exhibits autonomous motion (Section 4), which is another fundamental characteristic of living systems. These same droplets are also capable of division through the self-emulsification and cold-bursting mechanisms (Section 5), thus demonstrating another key functionality typical for the living organisms.

Although these behaviors are currently studied separately, they are realized in systems with very similar compositions. Therefore, they can potentially be integrated into a unified platform for the study of protocell-like systems. Importantly, rather than relying on chemical gradients as the currently developed model systems, the systems discussed here are driven by physical phase transitions. These transitions are robust, as they occur without altering the chemical composition of the material. Moreover, they are plausibly relevant to the prebiotic conditions, since the small temperature fluctuations required to trigger them would have naturally occurred during the planet's day-night cycles.

7. Outlook and perspectives

Surface and polymorphic phase transitions have long been recognized for their crucial role in determining the stability, functionality, and dynamic behavior of materials. By combining this knowledge with the unique characteristics of emulsions, we have opened a new avenue for research in the domain of active soft matter. Our investigations revealed several unexpected phenomena in this field including spontaneous drop shaping and splitting upon cooling, engulfing of continuous phase or drop bursting like spores upon heating. By exploring the governing factors of these processes, we uncovered their underlying mechanisms. These findings can now be applied to a range of systems and may help guide the design of new functional materials. They also provide a solid foundation for studying the remaining open questions.

Most of our experiments were performed using diluted samples in thin rectangular glass capillaries to simplify the observations. However, bulk rheology experiments [55], as well as the experiments performed in the flow-cell prototype reactor [209] have demonstrated that similar deformations occur even in more concentrated systems. Studying how droplets behave in crowded environments, or how they interact with interfaces and even living cells, remains an exciting area for future work.

Another area requiring further research involves the structure of the deformed droplets, and especially the distribution of ordered phases on their surfaces. Currently, only indirect observations are available and it is unclear whether the ordered phase covers uniformly the entire droplet surface or it is (mainly) localized at particle periphery. Furthermore, it is unknown how this distribution evolves with temperature and upon shape changes. Moreover, while experimental observations suggest that there is a preferred radius of curvature for the formation of the rotator

phase, the exact underlying reasons for this preference are still unknown.

Another related question is how many different rotator phases can form in a single droplet during cooling. X-ray results suggest that at least two distinct rotator phases form in hexadecane droplets [81]. However, it is not clear whether they occur together within the same droplet or not, what their exact structure is and if they can be observed in other confined geometries. The mechanical properties of these non-spherical fluid particles have not been explored and deserve a further investigation (for example via atomic force microscopy methods).

Significant progress in addressing these questions is expected through advanced molecular modeling. Initial steps in this direction have already been made [97,257–259]. While simulating a full atomistic model of a droplet even as small as 50 nm is currently beyond reach, simplified models are expected to yield valuable information about the effect of surfactants and curvature over the observed phase behavior.

Coupling structural data with molecular dynamic simulations will also enable the development of a robust thermodynamic model. Such model should be capable of predicting the observed shape transformation sequence and the energy landscape of these transitions. Performing similar experiments in microgravity conditions would also help clarify how buoyancy affects the shape evolution, which the current models suggest might play an important role [86].

Interestingly, an impressive similarity was noted between the shapes seen in the self-shaping oily droplets and those found in diatoms – unicellular algae that form intricate, silica-based shells [260]. These organisms, which contribute to around 20–25 % of the oxygen produced on the planet annually [261–263], have a very different chemistry, yet many of their shapes bear a strong resemblance to the oil-based droplets we study. Understanding how such similar forms emerge from very different materials could reveal deeper morphogenesis principles and shed new light to the related question about the origin of LUCA (Last Universal Common Ancestor) [264].

Another non-trivial connection between the phase transitions studies and biological organisms is the biological temperature limits. Studies have shown that the chromatin and myelin in rat brain cells undergo a rotator-to-liquid phase transition at about 44 °C, which aligns with the upper temperature at which rats can function as living organisms [265]. Further investigations in this direction will allow us better understanding on the role of lipids phase transitions and properties in living organisms.

Answering these and related questions will deepen our understanding of phase transitions and self-organization in soft matter systems, therefore allowing a further precision in designing materials with tailored properties and responsive behavior. These insights are particularly important in fields such as drug delivery, soft robotics, cosmetics, artificial cells, and others. As this research area continues to evolve, it will offer an exciting intersection of fundamental science and real-world applications.

Notation

Capital latin letters

A	area per molecule, Fig. 4; curved surface area in eq. 2; bending stiffness (Section 4.2)
E	droplet energy, eq. 2
E_{des}	energy for particle desorption, eq. 4
$\mathscr{E}$	dimensionless energy, eq. 3
G	Gibbs free energy
H	enthalpy
K_B	bending elasticity constant in presence of several ordered layers
$K_{B,mono}$	bending elasticity constant when just one ordered layer is present
P	drop perimeter (Section 2.6)
$\mathscr{P}$	dimensionless perimeter, eq. 3
R	latex particles radius (Section 3)
R_c	radius of the first buckle (Section 4.2)
S	entropy
$\mathscr{S}$	dimensionless entropy, eq. 3
T	temperature
T_d	temperature at which drop shape deformations begin
T_g	glass transition temperature
T_m	melting temperature
T_r	temperature for rotator phase formation
T_f	drop freezing temperature
U_S	swimming speed
U_F	fiber extrusion speed
V	volume

Small Latin letters

a	swimmer radius
c	constant in eq. 8
d	fiber/rods diameter; drop diameter (Section 2.4)
h_{mono}	thickness of a single ordered layer
h_{PL}	plastic phase thickness
k_B	Boltzmann constant
l	buckling wavelength, eq. 8
p_c	capillary pressure
r	radius of curvature (Section 2.3); fiber radius (Section 4.2)
r_c	contact line radius, eq. 6

Greek letters

α	TAG polymorphic phase (Section 5)
α	dimensionless parameter in eq. 3
β	TAG polymorphic phase (Section 5)
β'	TAG polymorphic phase (Section 5)
Δ	change in a given quantity
Δn	chain length difference
ε	perturbation amplitude (Section 4.2)
θ	three-phase contact angle
θ_i	initial three-phase contact angle (Section 3)
θ_w	melted oil-solid oil-aqueous phase (Section 5)
κ	line tension
κ_{cr}	critical line tension beyond which spontaneous particle desorption occurs
μ	chemical potential
$\xi_{\|\|}$	filament resistance to flow in direction parallel to its axis per unit length, eq. 9
σ	oil-water interfacial tension
σ_{po}	particle-oil interfacial tension (Section 3)
σ_{pr}	particle-rotator phase interfacial tension (Section 3)
σ_{pw}	particle-surfactant solution interfacial tension (Section 3)
σ_{ow}	oil-water interfacial tension
σ_{so}	solid oil-liquid oil interfacial tension (Section 5)
σ_{sw}	solid oil-surfactant solution interfacial tension (Section 5)
Φ	oil volume fraction

Abbreviations

C_n	n-alkane with n C-atoms in the alkyl chain
C_nTAG	monoacid triglyceride with n C-atoms in each fatty acid residue
CMC	critical micelle concentration
DSC	differential scanning calorimetry
EO	ethylene oxide group (-O-CH_2-CH_2-)
IFT	interfacial tension
PEG	polyethylene glycol
SAXD	small angle X-ray diffraction

SAXS	small angle X-ray scattering
SD	self-dispersion
SE	self-emulsification
SLN	solid lipid nanoparticles
SM	surfactant mixture (Fig. 26)
TAG	triacylglycerol
UV	ultraviolet
WAXS	wide angle X-ray scattering

Surfactants

Brij 52 or $C_{16}EO_2$ polyoxyethylene (2) hexadecyl ether
Brij 58 or $C_{16}EO_{20}$ polyoxyethylene (20) hexadecyl ether
Brij S20 or $C_{18}EO_{20}$ polyoxyethylene (20) octadecyl ether
C_nEO_m polyoxyethylene with *m* ethylene oxide units and *n* C-atoms in the alkyl chain
CTAB cetyltrimethylammonium bromide
C_{18}TAB octadecyltrimethylammonium bromide
Lutensol AT50 polyoxyethylene (50) hexadecyl-octadecyl ether
SDS sodium dodecyl sulfate
Tween 20 or $C_{12}SorbEO_{20}$ polyoxyethylene (20) sorbitan monolaurate
Tween 40 or $C_{16}SorbEO_{20}$ polyoxyethylene (20) sorbitan monopalmitate
Tween 60 or $C_{18}SorbEO_{20}$ polyoxyethylene (20) sorbitan monostearate
Tween 80 or $C_{18:1}SorbEO_{20}$ polyoxyethylene (20) sorbitan monooleate

Supplementary data to this article can be found online at https://doi.org/10.1016/j.cis.2025.103624.

CRediT authorship contribution statement

Diana Cholakova: Writing – review & editing, Writing – original draft, Visualization, Validation, Supervision, Project administration, Methodology, Investigation, Formal analysis, Data curation, Conceptualization.

Declaration of competing interest

The authors declare that they have no known competing financial interests or personal relationships that could have appeared to influence the work reported in this paper.

Acknowledgements

The study was funded by Bulgarian Ministry of Education and Science, under the National Research Program "VIHREN", project ROTA-Active (no. KP-06-DV-4/16.12.2019). The author is grateful to Prof. S. Tcholakova and Prof. N. Denkov (Sofia University) for the critical reading and useful discussions.

Data availability

Data will be made available on request.

References

[1] Wyatt Shields IV C, Velev O. The evolution of active particles: toward externally powered self-propelling and self-reconfiguring particle systems. Chem 2017;3:539–59. https://doi.org/10.1016/j.chempr.2017.09.006.
[2] Pishvar M, Harne RL. Foundations for soft, smart matter by active mechanical metamaterials. Adv Sci 2020;7:2001384. https://doi.org/10.1002/advs.202001384.
[3] Ignes-Mullol J, Sagues F. Active, self-motile, and driven emulsions. Curr Opin Colloid Interface Sci 2020;49:16–26. https://doi.org/10.1016/j.cocis.2020.04.007.
[4] van der Gucht J. Grand challenges in soft matter physics. Front Physiol 2018;6:87. https://doi.org/10.3389/fphy.2018.00087.
[5] Mulla Y, Aufderhorst-Roberts A, Koenderink GH. Shaping up synthetic cells. Phys Biol 2018;15:041001. https://doi.org/10.1088/1478-3975/aab923.
[6] Palagi S, Fischer P. Bioinspired microbots. Nat Rev Mater 2018;3:113–24. https://doi.org/10.1038/s41578-018-0016-9.
[7] Soussan E, Cassel S, Blanzat M, Rico-Lattes I. Drug delivery by soft matter: matrix and vesicular carriers. Angew Chem Int Ed 2009;48:274–88. https://doi.org/10.1002/anie.200802453.
[8] Merindol R, Walther A. Materials learning from life: concepts for active, adaptive and autonomous molecular systems. Chem Soc Rev 2017;46:5588–619. https://doi.org/10.1039/cs6cs00738d.
[9] Lum GZ, Ye Z, Dong X, Marvi H, Erin O, Hu W, et al. Shape-programmable magnetic soft matter. Proc Natl Acad Sci U S A 2016;113:E6007–15. https://doi.org/10.1073/pnas.1608193113.
[10] Kapate N, Clegg J, Mitragotri S. Non-spherical micro- and nanoparticles for drug delivery: progress over 15 years. Adv Drug Deliv Rev 2021;177:113807. https://doi.org/10.1016/j.addr.2021.05.017.
[11] Moore T, Cook A, Bellotti E, Palomba R, Manghnani P, Spano R, et al. Shape-specific microfabricated particles for biomedical applications: a review. Drug Deliv Transl Res 2022;12:2019–37. https://doi.org/10.1007/s13346-022-01143-4.
[12] Nejati S, Vadeghani E, Khorshidi S, Karkhaneh A. Role of particle shape on efficient and organ-based drug delivery. Eur Polym J 2020;122:109353. https://doi.org/10.1016/j.eurpolymj.2019.109353.
[13] He S, Pascucci D, Caggioni M, Lindberg S, Schultz K. Rheological properties of phase transitions in polydisperse and monodisperse colloidal rod systems. AIChE J 2021;67:e17401. https://doi.org/10.1002/aic.17401.
[14] Studart A, Shum HC, Weitz D. Arrested coalescence of particle-coated droplets into nonspherical supracolloidal structures. J Phys Chem B 2009;113(12):3914–9. https://doi.org/10.1021/jp806795c.
[15] Bromley K, MacPhee C. BslA-stabilized emulsion droplets with designed microstructure. Interface Focus 2017;7:20160124. https://doi.org/10.1098/rsfs.2016.0124.
[16] Tsibranska S, Tcholakova S, Golemanov K, Denkov N, Pelan E, Stoyanov S. Role of interfacial elasticity for the rheological properties of saponin-stabilized emulsions. J Colloid Interface Sci 2020;564:264–75. https://doi.org/10.1016/j.jcis.2019.12.108.
[17] Pawar A, Caggioni M, Ergun R, Hartel R, Spicer P. Arrested coalescence in Pickering emulsions. Soft Matter 2011;7:7710–6. https://doi.org/10.1039/C1SM05457K.
[18] Shum H, Abate A, Lee D, Studart A, Wang B, Chen C-H, et al. Droplet microfluidics for fabrication of non-spherical particles. Macromol Rapid Commun 2010;31(2):108–18. https://doi.org/10.1002/marc.200900590.
[19] Dahiya P, Caggioni M, Spicer P. Arrested coalescence of viscoelastic droplets: polydisperse doublets. Philosoph Trans Royal Soc A: Math, Phys Eng Sci 2016;374:20150132. https://doi.org/10.1098/rsta.2015.0132.
[20] Pawar A, Caggioni M, Hartel R, Spicer P. Arrested coalescence of viscoelastic droplets with internal microstructure. Faraday Discuss 2012;158:341–50. https://doi.org/10.1039/c2fd20029e.
[21] Caggioni M, Traini D, Young P, Spicer P. Microfluidic production of endoskeleton droplets with controlled size and shape. Powder Technol 2018;329:129–36. https://doi.org/10.1016/j.powtec.2018.01.050.
[22] Bon S, Mookhoek S, Colver P, Fischer H, van der Zwaag S. Route to stable non-spherical emulsion droplets. Eur Polym J 2007;43(11):4839–42. https://doi.org/10.1016/j.eurpolymj.2007.09.001.
[23] Spicer P, Hartel R. Crystal comets: dewetting during emulsion droplet crystallization. Aust J Chem 2005;58:655–9. https://doi.org/10.1071/CH05119.
[24] Giso M, Zhao P, Spicer P, Atherton T. Crystal comets: a geometric model for sculpting anisotropic particles from emulsions. Langmuir 2020;36:13853–9. https://doi.org/10.1021/acs.langmuir.0c02249.
[25] Giso M, Zhao P, Spicer P, Atherton T. A phase diagram of morphologies for anisotropic particles sculpted from emulsions. J Colloid Interface Sci 2022;605:138–45. https://doi.org/10.1016/j.jcis.2021.07.045.
[26] Golemanov K, Tcholakova S, Denkov ND, Gurkov T. Selection of surfactants for stable paraffin-in-water dispersions, undergoing solid-liquid transition of the dispersed particles. Langmuir 2006;22:3560–9. https://doi.org/10.1021/la053059y.
[27] Pictures B. C shown on p. 363 in General discussion, Faraday Discuss129; 2005. p. 353–66. https://doi.org/10.1039/b416303f.
[28] Shinohara Y, Kawasaki N, Ueno S, Kobayashi I, Nakajima M, Amemiya Y. Observation of the transient rotator phase of *n*-hexadecane in emulsified droplets with time-resolved two-dimensional small- and wide-angle X-ray scattering. Phys Rev Lett 2005;94:097801. https://doi.org/10.1103/PhysRevLett.94.097801.
[29] Shinohara Y, Takamizawa T, Ueno S, Sato K, Kobayashi I, Nakajima M, et al. Microbeam X-ray diffraction analysis of interfacial heterogeneous nucleation of *n*-hexadecane inside oil-in-water emulsion droplets. Cryst Growth Des 2008;8:3123–6. https://doi.org/10.1021/cg701018x.
[30] Denkov N, Tcholakova S, Lesov I, Cholakova D, Smoukov SK. Self-shaping of oil droplets via the formation of intermediate rotator phases upon cooling. Nature 2015;528:392–5. https://doi.org/10.1038/nature16189.
[31] Cholakova D, Denkov N, Tcholakova S, Lesov I, Smoukov SK. Control of drop shape transformations in cooled emulsions. Adv Colloid Interface Sci 2016;235:90–107. https://doi.org/10.1016/j.cis.2016.06.002.
[32] Haas PA, Goldstein R, Smoukov SK, Cholakova D, Denkov N. Theory of shape-shifting droplets. Phys Rev Lett 2017;118:088001. https://doi.org/10.1103/PhysRevLett.118.088001.
[33] Guttman S, Sapir Z, Schultz M, Butenko A, Ocko B, Deutsch M, et al. How faceted liquid droplets grow tails. Proc Natl Acad Sci U S A 2016;113:493–6. https://doi.org/10.1073/pnas.1515614113.

[34] Cholakova D, Lisicki M, Smoukov SK, Tcholakova S, Lin EE, Chen J, et al. Rechargeable self-assembled droplet microswimmers driven by surface phase transitions. Nat Phys 2021;17:1050–5. https://doi.org/10.1038/s41567-021-01291-3.
[35] Cholakova D, Glushkova D, Tcholakova S, Denkov N. Nanopore and nanoparticles formation with lipids undergoing polymorphic phase transitions. ACS Nano 2020;14:8594–604. https://doi.org/10.1021/acsnano.0c02946.
[36] Tcholakova S, Valkova Z, Cholakova D, Vinarov Z, Lesov I, Denkov N, et al. Efficient self-emulsification via cooling-heating cycles. Nature Comm 2017;8:15012. https://doi.org/10.1038/ncomms15012.
[37] Cholakova D, Glushkova D, Pantov M, Tcholakova S, Denkov N. Triglyceride mixtures: cold-bursting and double emulsion formation. Colloids Surf A 2023;668:131439. https://doi.org/10.1016/j.colsurfa.2023.131439.
[38] Cholakova D, Denkov N, Tcholakova S, Valkova Z, Smoukov SK. Multilayer formation in self-shaping emulsion droplets. Langmuir 2019;35(16):5484–95. https://doi.org/10.1021/acs.langmuir.8b02771.
[39] Glushkova D, Cholakova D, Biserova A, Tsvetkova K, Tcholakova S, Denkov N. Drop shape stability vs shape shifting: role of surfactant adsorption layer. Coll Surf A: Physicochem Eng Aspects 2023;656:130374. https://doi.org/10.1016/j.colsurfa.2022.130374.
[40] Cholakova D, Biserova A, Tcholakova S, Denkov N. Self-shaping of triglyceride and alkane drops: similarities and differences. Coll Surf A: Physicochem Eng Aspects 2024;692:134037. https://doi.org/10.1016/j.colsurfa.2024.134037.
[41] Guttman S, Ocko B, Deutsch M, Sloutskin E. From faceted vesicles to liquid icoshedra: where topology and crystallography meet. Curr Opin Colloid Interface Sci 2016;22:35–40. https://doi.org/10.1016/j.cocis.2016.02.002.
[42] Guttman S, Sapir Z, Ocko B, Deutsch M, Sloutskin E. Temperature-tuned faceting and shape changes in liquid alkane droplets. Langmuir 2017;33:1305–14. https://doi.org/10.1021/acs.langmuir.6b02926.
[43] Butenko AV, Hsu E, Matoz-Fernandez DA, Shool L, Schofield AB, Lee D, et al. Sphere-to-icosahedron droplet shape transformations in interfacially frozen Pickering emulsions. ACS Nano 2025;19:7793–803. https://doi.org/10.1021/acsnano.4c13476.
[44] Hacmon S, Liber SR, Shool L, Butenko AV, Atkins A, Sloutskin E. "Magic numbers" in self-faceting of alcohol-doped emulsion droplets. Small 2023;19:2301637. https://doi.org/10.1002/smll.202301637.
[45] Hsu E, Lee D, Sloutskin E. Non-classical Euler buckling and brazier instability in cylindrical liquid droplets. Nano Lett 2024;24:8717–22. https://doi.org/10.1021/acs.nanolett.4c02075.
[46] Marin O, Tkachev M, Sloutskin E, Deutsch M. Polyhedral liquid droplets: recent advances in elucidation and application. Curr Opin Colloid Interface Sci 2020;49:107–17. https://doi.org/10.1016/j.cocis.2020.05.006.
[47] Reiner J, Martin D, Ott F, Harnisch L, Gaukel V, Karbstein HP. Influence of the triglyceride composition, surfactant concentration and time-temperature conditions on the particle morphology in dispersions. Colloids Interfaces 2023;7:22. https://doi.org/10.3390/colloids7010022.
[48] Reiner J, Walter EM, Karbstein HP. Assessment of droplet self-shaping and crystallization during temperature fluctuations exceeding the melting temperature of the dispersed phase. Colloids Surf A 2023;656B:130498. https://doi.org/10.1016/j.colsurfa.2022.130498.
[49] Marin O, Deutsch M, Zitoun D, Sloutskin E. Nanoparticle positioning on liquid and polymerized faceted droplets. Phys Chem C 2019;123(46):28192–200. https://doi.org/10.1021/acs.jpcc.9b07809.
[50] Liber S, Butenko A, Caspi M, Guttman S, Schultz M, Schofield A, et al. Precise self-positioning of colloidal particles on liquid emulsion droplets. Langmuir 2019;35(40):13053–61. https://doi.org/10.1021/acs.langmuir.9b01833.
[51] Lesov I, Valkova Z, Vassileva E, Georgiev GS, Ruseva K, Simeonov M, et al. Bottom-up synthesis of polymeric micro- and nanoparticles with regular anisotropic shapes. Macromolecules 2018;51:7456–62. https://doi.org/10.1021/acs.macromol.8b00529.
[52] Marin O, Alesker M, Guttman S, Gershinsky G, Edri E, Shpaisman H, et al. Self-faceting of emulsion droplets as a route to solid icosahedra and other polyhedra. J Colloid Interface Sci 2019;538:541–5. https://doi.org/10.1016/j.jcis.2018.11.111.
[53] Cholakova D, Valkova Zh, Tcholakova S, Denkov N, Binks B. Spontaneous particle desorption and "Gorgon" drop formation from particle-armored oil drops upon cooling. Soft Matter 2020;16:2480–96. https://doi.org/10.1039/c9sm02354b.
[54] Cholakova D, Glushkova D, Tcholakova S, Denkov N. Cold-burst method for nanoparticles formation with natural triglyceride oils. Langmuir 2021;37:7875–89. https://doi.org/10.1021/acs.langmuir.0c02967.
[55] Valkova Z, Rusanova K, Tcholakova S, Cholakova D, Denkov N. Rheology of dispersions containing non-spherical lipid particles. Colloids Surf A 2025;710:136284. https://doi.org/10.1016/j.colsurfa.2025.136284.
[56] Cholakova D, Valkova Zh, Tcholakova S, Denkov N, Smoukov SK. "Self-shaping" of multicomponent drops. Langmuir 2017;33(23):5696–706. https://doi.org/10.1021/acs.langmuir.7b01153.
[57] Feng J, Valkova Zh, Lin E, Nourafkan E, Wang T, Tcholakova S, et al. Minimum surfactant concentration required for inducing self-shaping of oil droplets and competitive adsorption effects. Soft Matter 2022;18:6729–38. https://doi.org/10.1039/d1sm01326b.
[58] Cholakova D, Denkov N. Rotator phases in alkane systems: in bulk, surface layers and micro/nano-confinements. Adv Colloid Interface Sci 2019;269:7–42. https://doi.org/10.1016/j.cis.2019.04.001.
[59] Small DM. The physical chemistry of lipids: From alkanes to phospholipids. New York: Plenum; 1986.
[60] Sirota EB, King HE, Singer DM, Shao HH. Rotator phases of normal alkanes: an X-ray scattering study. J Chem Phys 1993;98:5809–24. https://doi.org/10.1063/1.464874.
[61] Sirota EB, Singer DM. Phase transitions among the rotator phases of the normal alkanes. J Chem Phys 1994;101:10873–82. https://doi.org/10.1063/1.467837.
[62] Sirota EB, Herhold AB. Transient phase-induced nucleation. Science 1999;283:529–32. https://doi.org/10.1126/science.283.5401.529.
[63] Gang H, Gang O, Shao H, Wu X, Patel J, Hsu C, et al. Rotator phases and surface crystallization in α-eicosene. J Phys Chem B 1998;102(15):2754–8. https://doi.org/10.1021/jp980603l.
[64] Gang O, Wu X, Ocko B, Sirota E, Deutsch M. Surface freezing in chain molecules. II. Neat and hydrated alcohols. Phys Rev E 1998;58:6086. https://doi.org/10.1103/PhysRevE.58.6086.
[65] Ocko B, Braslau A, Pershan P, Als-Nielson J, Deutsch M. Quantized layer growth at liquid-crystal surfaces. Phys Rev Lett 1986;57:94–7. https://doi.org/10.1103/PhysRevLett.57.94.
[66] Doerr A, Wu X, Ocko B, Sirota E, Gang O, Deutsch M. Surface freezing in mixtures of molten alkanes and alcohols. Coll Surf A: Physicochem Eng Aspects 1997;128:63–74. https://doi.org/10.1016/S0927-7757(96)03907-6.
[67] Tsuura M, Shuto A, Hiraki S, Imai Y, Sakamoto H, Matsubara H, et al. Surface freezing and molecular miscibility of binary fluoroalkanol-alkanol liquid mixture. Coll Surf A: Physicochem Eng Aspects 2017;525:31–7. https://doi.org/10.1016/j.colsurfa.2017.04.047.
[68] Leyva-Gutierrez F, Wang T. Rotator phases of aliphatic aldehydes and implications for wax crystal growth in plants. Cryst Growth Des 2023;23(4):2351–60. https://doi.org/10.1021/acs.cgd.2c01350.
[69] Zhang H, Maguire S, Nie C, Priestley R, Chirik P, Register R, et al. Rotator phases in chemically recyclable oligocyclobutanes. Chem Mater 2024;36(23):11596–605. https://doi.org/10.1021/acs.chemmater.4c02576.
[70] Kenn RM, Boehm C, Bibo AM, Peterson IR. Moehwald, Als-Nielsen J, Kjaer K, Mesophases and crystalline phases in fatty acid monolayers. J Phys Chem 1991;95:2092–7. https://doi.org/10.1021/j100158a034.
[71] Small DM. Lateral chain packing in lipids and membranes. J Lipid Res 1984;25:1490–500. https://doi.org/10.1016/S0022-2275(20)34422-9.
[72] Chapman D. The polymorphism of glycerides. Chem Rev 1962;62(5):433–56. https://doi.org/10.1021/cr60219a003.
[73] Cholakova D, Denkov N. Polymorphic phase transitions in triglycerides and their mixtures studied by SAXS/WAXS techniques: in bulk and in emulsions. Adv Colloid Interface Sci 2024;323:103071. https://doi.org/10.1016/j.cis.2023.103071.
[74] Clarkson C, Malkin T. Alternation in long-chain compounds. Part II. An X-ray and thermal investigation of the triglycerides. J Chem Soc 1934:666–71. https://doi.org/10.1039/JR9340000666.
[75] Koynova R, Caffrey M. Phases and phase transitions of the phosphatidylcholines. Biochim Biophys Acta, Rev Biomembr 1998;1376:91–145. https://doi.org/10.1016/S0304-4157(98)00006-9.
[76] Cullis P, De Kruijff B. Lipid polymorphism and the functional roles of lipids in biological membranes. Biochim et Biophys Acta (BBA) - Reviews on Biomembranes 1979;559(4):399–420. https://doi.org/10.1016/0304-4157(79)90012-1.
[77] Xu L, Zuo Y. Reversible phase transitions in the phospholipid monolayer. Langmuir 2018;34(29):8694–700. https://doi.org/10.1021/acs.langmuir.8b01544.
[78] Sirota E, Herhold A, Varma-Nair M. Structure, thermodynamics, and transition kinetics of nonadecylcyclohexane. J Chem Phys 2000;113:8225–36. https://doi.org/10.1063/1.1314859.
[79] Sedev R. Limiting area per molecule of nonionic surfactants at the water/air interface. Langmuir 2001;17(2):562–4. https://doi.org/10.1021/la000572x.
[80] Denkov N, Cholakova D, Tcholakova S, Smoukov SK. On the mechanism of drop self-shaping in cooled emulsions. Langmuir 2016;32(31):7985–99. https://doi.org/10.1021/acs.langmuir.6b01626.
[81] Cholakova D, Glushkova D, Valkova Zh, Tsibranska-Gyoreva S, Tsvetkova K, Tcholakova S, et al. Rotator phases in hexadecane emulsion drops revealed by X-ray synchrotron techniques. J Colloid Interface Sci 2021;604:260–71. https://doi.org/10.1016/j.jcis.2021.06.122.
[82] Valkova Z, Cholakova D, Tcholakova S, Denkov N, Smoukov SK. Mechanisms and control of self-emulsification upon freezing and melting of dispersed alkane drops. Langmuir 2017;33:12155–70. https://doi.org/10.1021/acs.langmuir.7b02048.
[83] Wu XZ, Ocko BM, Sirota EB. Sinha Sk, Deutsch M, Cao BH, Kim MW, surface tension measurements of surface freezing in liquid normal alkanes. Science 1993;261:1018–21. https://doi.org/10.1126/science.261.5124.1018.
[84] Ocko BM, Wu XZ, Sirota EB, Sinha SK, Gang O, Deutsch M. Surface freezing in chain molecules: Normal alkanes. Phys Rev E 1997;55:3164. https://doi.org/10.1103/PhysRevE.55.3164.
[85] Sharker K. Islam Md, Das S, Counterion effect on Krafft temperature and related properties of octadecyltrimethylammonium bromide. J Surfactant Deterg 2017;20:923–32. https://doi.org/10.1007/s11743-017-1957-5.
[86] Haas P, Cholakova D, Denkov N, Goldstein RE, Smoukov SK. Shape-shifting polyhedral droplets. Phys Rev Res 2019;1:023017. https://doi.org/10.1103/PhysRevResearch.1.023017.
[87] Cholakova D, Tsvetkova K, Tcholakova S, Denkov N. Rheological properties of rotator and crystalline phases of alkanes. Coll Surf A: Physicochem Eng Aspects 2022;634:127926. https://doi.org/10.1016/j.colsurfa.2021.127926.

[88] Tkachenko AV, Rabin Y. Fluctuation-stabilized surface freezing of chain molecules. Phys Rev Lett 1996;76:2527. https://doi.org/10.1103/PhysRevLett.76.2527.
[89] Sirota EB. Remarks concerning the relation between rotator phases of bulk n-alkanes and those of Langmuir monolayers of alkyl-chain surfactants on water. Langmuir 1997;13:3849–59. https://doi.org/10.1021/la9702291.
[90] Xie B, Liu G, Jiang S, Zhao Y, Wang D. Crystallization behavior of n-octadecane in confined space: crossover to rotator phase from transient to metastable induced by surface freezing. J Phys Chem B 2008;112:13310–5. https://doi.org/10.1021/jp712160k.
[91] Fu D, Liu Y, Liu G, Su Y, Wang D. Confined crystallization of binary n-alkane mixtures: stabilization of a new rotator phase by enhanced surface freezing and weakened intermolecular interactions. Phys Chem Chem Phys 2011;13:15031–6. https://doi.org/10.1039/c1cp21281h.
[92] Su Y, Liu G, Xie B, Fu D, Wang D. Crystallization features of normal alkanes in confined geometry. Acc Chem Res 2014;47:192–201. https://doi.org/10.1021/ar400116c.
[93] Wang LP, Sui J, Zhai M, Tian F, Lan XZ. Physical control of phase behavior of hexadecane in nanopores. J Phys Chem C 2015;119:18697–706. https://doi.org/10.1021/acs.jpcc.5b03728.
[94] Evans E, Skalak R. Mechanics and thermodynamics of biomembranes. CRC; 1980.
[95] Israelachvili JN. Intermolecular and surface forces. Academic; 2011.
[96] Ueno S, Hamada Y, Sato K. Controlling polymorphic crystallization of *n*-alkane crystals in emulsion droplets through interfacial heterogeneous nucleation. Cryst Growth Des 2003;3:935–9. https://doi.org/10.1021/cg0300230.
[97] Burrows SA, Lin EE, Cholakova D, Richardson S, Smoukov SK. Structure of the hexadecane rotator phase: combination of X-ray spectra and molecular dynamics simulations. J Phys Chem B 2023;127:7772–84. https://doi.org/10.1021/acs.jpcb.3c02027.
[98] Evans E. Bending resistance and chemically induced moments in membrane bilayers. Biophys J 1974;14:923–31. https://doi.org/10.1016/S0006-3495(74)85959-X.
[99] Love AEH. The small free vibrations and deformation of a thin elastic shell. Philosoph Trans Royal Soc A: Math, Phys Eng Sci 1888;179:491–546. https://doi.org/10.1098/rsta.1888.0016.
[100] Sandra K, Sandra P, Vanhoenacker G, Steenbeke M. Profiling nonionic surfactants applied in pharmaceutical formulations by using comprehensive two-dimensional LC with ELSD and MS detection. LCGC North Am 2018;36:385–93.
[101] Trathnigg B, Kollroser M, Rapper C. Liquid exclusion adsorption chromatography, a new technique for isocratic separation of nonionic surfactants. III. Two-dimensional separation of fatty alcohol ethoxylates. J Chromatogr A 2001;922:193–205. https://doi.org/10.1016/s0021-9673(01)00938-4.
[102] Haas PA, Goldstein RE, Cholakova D, Denkov N, Smoukov SK. Comment on "faceting and flattening of emulsion droplets: a mechanical model". Phys Rev Lett 2021;126:259801. https://doi.org/10.1103/PhysRevLett.126.259801.
[103] Garcia-Aguilar I, Fonda P, Sloutskin E, Giomi L. Faceting and flattening of emulsion droplets: a mechanical model. Phys Rev Lett 2021;126:038001. https://doi.org/10.1103/PhysRevLett.126.038001.
[104] Cholakova D, Pantov M, Tcholakova S, Denkov N. Structure of rotator phases formed in C_{13}-C_{21} alkanes and their mixtures: in bulk and in emulsion drops. Crystal Growth Des 2024;24:362–77. https://doi.org/10.1021/acs.cgd.3c01088.
[105] Tanjeem N, Minnis M, Hayward R, Shields IV C. Shape-changing particles: from materials design and mechanisms to implementation. Adv Mater 2022;34(3):2105758. https://doi.org/10.1002/adma.202105758.
[106] Martin N, Sharma K, Harniman R, Richardson R, Hutchings R, Alibhai D, et al. Light-induced dynamic shaping and self-division of multipodal polyelectrolyte-surfactant microarchitectures via azobenzene photomechanics. Sci Rep 2017;7:41327. https://doi.org/10.1038/srep41327.
[107] Wang X, Bukusoglu E, Miller D, Pantoja M, Xiang J, Lavrentovich O, et al. Synthesis of optically complex, porous, and anisometric polymeric microparticles by templating from liquid crystalline droplets. Adv Funct Mater 2016;26(40):7343–51. https://doi.org/10.1002/adfm.201602262.
[108] Mondiot F, Wang X, de Pablo J, Abbott N. Liquid crystal-based emulsions for synthesis of spherical and non-spherical particles with chemical patches. J Am Chem Soc 2013;135(27):9972–5. https://doi.org/10.1021/ja4022182.
[109] Wang X, Bukusoglu E, Abbott N. A practical guide to the preparation of liquid crystal-templated microparticles. Chem Mater 2017;29(1):53–61. https://doi.org/10.1021/acs.chemmater.6b02668.
[110] Liu M, Jin L, Yang S, Wang Y, Murray C, Yang S. Shape morphing directed by spatially encoded, dually responsive liquid crystalline elastomer micro-actuators. Adv Mater 2023;35(5):2208613. https://doi.org/10.1002/adma.202208613.
[111] Liu M, Fu J, Yang S. Synthesis of microparticles with diverse thermally responsive shapes originated from the same janus liquid crystalline microdroplets. Small 2023;19(47):2303106. https://doi.org/10.1002/smll.202303106.
[112] Wei W-S, Xia Y, Ettinger S, Yang S, Yodh A, Molecular heterogeneity drives reconfigurable nematic liquid crystal drops. Nature 209;576:433–436. doi:https://doi.org/10.1038/s41586-019-1809-8.
[113] Peddireddy K, Čopar S, Le KV, Jampani V. Self-shaping liquid crystal droplets by balancing bulk elasticity and interfacial tension. PNAS 2021;118(14):e2011174118. https://doi.org/10.1073/pnas.2011174118.
[114] Čejková J, Hanczyc M, Štěpánek F. Multi-armed droplets as shape-changing protocells. Artif Life 2018;14(1):71–9. https://doi.org/10.1162/ARTL_a_00255.
[115] Li Y, Pahlavan A, Chen Y, Granick S. Oil-on-water droplets faceted and stabilized by vortex halos in the subphase. PNAS 2023;120(4):e2214657120. https://doi.org/10.1073/pnas.2214657120.
[116] Tsibranska S, Tcholakova S, Golemanov K, Denkov N, Arnaudov L, Pelan E, et al. Origin of the extremely high elasticity of bulk emulsions, stabilized by yucca Schidigera saponins. Food Chem 2020;316:126365. https://doi.org/10.1016/j.foodchem.2020.126365.
[117] Hobley L, Ostrowski A, Rao F, Stanley-Wall N. BslA is a self-assembling bacterial hydrophobin that coats the Bacillus subtilis biofilm. PNAS 2013;110:13600–5. https://doi.org/10.1073/pnas.1306390110.
[118] Bromley K, Morris R, Hobley L, MacPhee C. Interfacial self-assembly of a bacterial hydrophobin. PNAS 2015;112:5419–24. https://doi.org/10.1073/pnas.1419016112.
[119] Dimitrova L, Boneva M, Danov K, Kralchevsky P, Basheva E, Marinova K, et al. Limited coalescence and Ostwald ripening in emulsions stabilized by hydrophobin HFBII and milk proteins. Coll Surf A: Physicochem Eng Aspects 2016;509:521–38. https://doi.org/10.1016/j.colsurfa.2016.09.066.
[120] Basheva E, Kralchevsky P, Christov N, Danov K, Stoyanov S, Blijdenstein T, et al. Unique properties of bubbles and foam films stabilized by HFBII hydrophobin. Langmuir 2011;27:2382–92. https://doi.org/10.1021/la104726w.
[121] Wacker J, Louis G, Razaname C, Parashar V, Gijs M. Exotic droplets formed in microfluidic chips with uniform wettability. Microelectronic Eng 2011;88(8):1891–3. https://doi.org/10.1016/j.mee.2010.12.034.
[122] Gao Y, Zhao C-X, Sainsbury F. Droplet shape control using microfluidics and designer biosurfactants. J Colloid Interface Sci 2021;584:528–38. https://doi.org/10.1016/j.jcis.2020.09.126.
[123] Lobel B, Baiocco D, Al-Sharabi M, Routh A, Zhang Z, Cayre O. Nonspherical particle stabilized emulsions formed through destabilization and arrested coalescence. Langmuir 2025;41(1):550–62. https://doi.org/10.1021/acs.langmuir.4c03812.
[124] Wu L, Liao Z, Liu M, Yin X, Li X, Wang M, et al. Fabrication of non-spherical Pickering emulsion droplets by cyclodextrins mediated molecular self-assembly. Coll Surf A: Physicochem Eng Aspects 2016;490:163–72. https://doi.org/10.1016/j.colsurfa.2015.11.036.
[125] Li H, Liu W, Zhang W, Yin G, Wang H, Wang Z. Formation of particle coated fusiform droplets via lowering interface tension with polyaluminum sulfate. J Dispers Sci Technol 2013;34(10):1316–23. https://doi.org/10.1080/01932691.2012.744680.
[126] Datta S, Shum H, Weitz D. Controlled buckling and crumpling of nanoparticle-coated droplets. Langmuir 2010;26(24):18612–6. https://doi.org/10.1021/la103874z.
[127] Merkel T, Gräf V, Walz E, Schuchmann H. Production of particle-stabilized nonspherical emulsion drops in simple shear flow. Chem Eng Technol 2015;38(8):1490–3. https://doi.org/10.1002/ceat.201500068.
[128] Zarzar LD, Sresht V, Sletten EM, Kalow JA, Blankschtein D, Swager TM. Dynamically reconfigurable complex emulsions via tunable interfacial tensions. Nature 2015;518:520–4. https://doi.org/10.1038/nature14168.
[129] Djalali S, Frank BD, Zeininger L. Responsive drop method: quantitative *in situ* determination of surfactant effectiveness using reconfigurable Janus emulsions. Soft Matter 2020;16:10419–24. https://doi.org/10.1039/d0sm01724h.
[130] Marques PS, Krajewska M, Frank BD, Prochaska K, Zeininger L. Morphology-dependent aggregation-induced emission of Janus emulsion systems. Chem A Eur J 2023;29:e202203790. https://doi.org/10.1002/chem.202203790.
[131] Frank BD, Djalali S, Baryzewska AW, Giusto P, Seeberger PH, Zeininger L. Reversible morphology-resolved chemotactic actuation and motion of Janus emulsion droplets. Nature Comm 2022;13:2562. https://doi.org/10.1038/s41467-022-30229-3.
[132] Frank BD, Romero P, Concellon A, Zeininger L. Reversible phase transitions of anionic and cationic surfactant mixtures drive shape morphing droplets. Adv Mater 2025:2506100. https://doi.org/10.1002/adma.202506100.
[133] Zeininger L, Nagelberg S, Harvey KS, Savagatrup S, Herbert MB, Yoshinaga K, et al. Rapid detection of *salmonella enterica* via directional emission from carbohydrate-functionalized dynamic double emulsions. ACS Cent Sci 2019;5:789–95. https://doi.org/10.1021/acscentrsci.9b00059.
[134] Chevalier Y, Bolzinger M-A. Emulsions stabilized with solid nanoparticles: Pickering emulsions. Coll Surf A: Physicochem Eng Aspects 2013;439:23–34. https://doi.org/10.1016/j.colsurfa.2013.02.054.
[135] Binks B, Lumsdon S. Pickering emulsions stabilized by monodisperse latex particles: effects of particle size. Langmuir 2001;17(15):4540–7. https://doi.org/10.1021/la0103822.
[136] Binks B. Particles as surfactants – similarities and differences. Curr Opin Colloid Interface Sci 2002;7:21–41. https://doi.org/10.1016/S1359-0294(02)00008-0.
[137] Golemanov K, Tcholakova S, Kralchevsky P, Ananthapadmanabhan K, Lips A. Latex-particle-stabilized emulsions of anti-Bancroft type. Langmuir 2006;22(11):4968–77. https://doi.org/10.1021/la0603875.
[138] Dickinson E. Food emulsions and foams: stabilization by particles. Curr Opin Colloid Interface Sci 2010;15(1–2):40–9. https://doi.org/10.1016/j.cocis.2009.11.001.
[139] Xiao J, Li Y, Huang Q. Recent advances on food-grade particles stabilized Pickering emulsions: fabrication, characterization and research trends. Trends Food Sci Technol 2016;55:48–60. https://doi.org/10.1016/j.tifs.2016.05.010.
[140] Ortiz D, Pochat-Bohatier C, Cambedouzou J, Bechelany M, Miele P. Current trends in Pickering emulsions: particle morphology and applications. Engineering 2020;6(4):468–82. https://doi.org/10.1016/j.eng.2019.08.017.
[141] Tran L, Kim H-N, Li N, Yang S, Stebe K, Kamien R, et al. Shaping nanoparticle fingerprints at the interface of cholesteric droplets. Sci Adv 2018;4:eaat8597. https://doi.org/10.1126/sciadv.aat8597.

[142] Rahimi M, Roberts T, Armas-Pérez J, de Pablo J. Nanoparticle self-assembly at the interface of liquid crystal droplets. PNAS 2015;112:5297–302. https://doi.org/10.1073/pnas.1422785112.
[143] Kralchevsky PA, Nikolov AD, Ivanov IB. Film and line tension effects on the attachment of particles to an interface: IV. Experimental studies with bubbles in solutions of dodecyl sodium sulfate. J Colloid Interface Sci 1986;112:132–43. https://doi.org/10.1016/0021-9797(86)90075-5.
[144] Matsubara H, Chiguchi K, Law BM. Pickering emulsion transition in 2,6-Lutidine plus water critical liquid mixtures. Langmuir 2020;36:12601–6. https://doi.org/10.1021/acs.langmuir.0c02161.
[145] Matsubara H, Otsuka J, Law BM. Finite-size and solvent dependent line tension effects for nanoparticles at the air-liquid surface. Langmuir 2018;34:331–40. https://doi.org/10.1021/acs.langmuir.7b03700.
[146] Matsubara H. Spontaneous demulsification of Pickering emulsion by controlling interfacial tensions. J Oleo Sci 2025;74:559–65. https://doi.org/10.5650/jos.ess24346.
[147] Shishida K, Matsubara H. Demulsification of silica stabilized Pickering emulsions using surface freezing transition of CTAC adsorbed films at the tetradecane-water interface. J Oleo Sci 2023;72:1083–9. https://doi.org/10.5650/jos.ess23102.
[148] Rus D, Tolley M, Design, fabrication and control of soft robots. Nature 201;521:467–475. doi:https://doi.org/10.1038/nature14543.
[149] Trivedi D, Rahn C, Kier W, Walker I. Soft robotics: biological inspiration, state of the art, and future research. Appl Bionics Biomech 2008;5:99–117. https://doi.org/10.1080/11762320802557865.
[150] Xiao Z, Voigtmann M, Simmchen J. Biomimetic chemotactic motion of self-assembling doublet microrobots. Adv Intell Syst 2025:2400839. https://doi.org/10.1002/aisy.202400839.
[151] Parmar J, Ma X, Katuri J, Simmchen J, Stanton M, Trichet-Paredes C. Nano and micro architectures for self-propelled motors. Sci Techn Adv Mat 2015;16:014802. https://doi.org/10.1088/1468-6996/16/1/014802.
[152] Wang W, Duan W, Ahmed S, Mallouk T, Sen A. Small power: autonomous nano- and micromotors propelled by self-generated gradients. Nanotoday 2013;8(5):531–54. https://doi.org/10.1016/j.nantod.2013.08.009.
[153] Elgeti J, Winkler R, Gompper G. Physics of microswimmers – single particle motion and collective behavior: a review. Rep Prog Phys 2015;78:056601. https://doi.org/10.1088/0034-4885/78/5/056601.
[154] Yan G, Solovev A, Huang G, Cui J, Mei Y. Soft microswimmers: material capabilities and biomedical applications. Curr Opin Colloid Interface Sci 2022;61:101609. https://doi.org/10.1016/j.cocis.2022.101609.
[155] Medina-Sánchez M, Schwarz L, Meyer A, Hebenstreit F, Schmidt O. Cellular cargo delivery: toward assisted fertilization by sperm-carrying micromotors. Nano Lett 2016;16:555–61. https://doi.org/10.1021/acs.nanolett.5b04221.
[156] Bunea A-I, Taboryski R. Recent advances in microswimmers for biomedical applications. Micromachines 2020;11:1048. https://doi.org/10.3390/mi11121048.
[157] Singh AV, Ansari MHD, Mahajan M, Srivastava S, Kashyap S, Dwivedi P, et al. Sperm cell driven microrobots – emerging opportunities and challenges for biologically inspired robotic design. Micromachines 2020;11:448. https://doi.org/10.1080/17425247.2019.1676228.
[158] Deamer D. A giant step towards artificial life? Trends Biotechnol 2005;23:336–8. https://doi.org/10.1016/j.tibtech.2005.05.008.
[159] Aguilar W, Santamaria-Bonfil G, Froese T, Gershenson C. The past, present, and future of artificial life. Front Robot AI 2014;1:1–15. https://doi.org/10.3389/frobt.2014.00008.
[160] Menzel AM. Tuned, driven, and active soft matter. Phys Rep 2015;554:1–45. https://doi.org/10.1016/j.physrep.2014.10.001.
[161] Scopus search performed on 20 March 2025. "Active Particle" in the title. 2025.
[162] Dreyfus R, Baudry J, Roper M, Fermigier M, Stone H, Bibette J. Microscopic artificial swimmers. Nature 2005;437:862–5. https://doi.org/10.1038/nature04090.
[163] Mandal P, Patil G, Kakoty H, Ghosh A. Magnetic active matter based on helical propulsion Acc. Chem Res 2018;51:2689–98. https://doi.org/10.1021/acs.accounts.8b00315.
[164] Ahmed D, Baasch T, Blondel N, Läubli N, Dual J, Nelson B. Neutrophil-inspired propulsion in a combined acoustic and magnetic field. Nat Commun 2017;8:770. https://doi.org/10.1038/s41467-017-00845-5.
[165] Dey K, Wong F, Altemose A, Sen A. Catalytic motors—Quo Vadimus? Curr Opin Colloid Interface Sci 2016;21:4–13. https://doi.org/10.1016/j.cocis.2015.12.001.
[166] Tierno P, Güell O, Sagués F, Golestanian R, Pagonabarraga I. Controlled propulsion in viscous fluids of magnetically actuated colloidal doublets. Phys Rev E 2010;81:011402. https://doi.org/10.1103/PhysRevE.81.011402.
[167] Aubret A, Ramananarivo S, Palacci J. Eppur si muove, and yet it moves: patchy (phoretic) swimmers. Curr Opin Colloid Interface Sci 2017;30:81–9. https://doi.org/10.1016/j.cocis.2017.05.007.
[168] Moran J, Posner J. Microswimmers with no moving parts. Phys Today 2019;72:44–50. https://doi.org/10.1063/PT.3.4203.
[169] Wang D, Gao C, Wang W, Sun M, Guo B, Xie H, et al. Shape-transformable, fusible rodlike swimming liquid metal nanomachine. ACS Nano 2018;12(10):10212–20. https://doi.org/10.1021/acsnano.8b05203.
[170] Still T, Yunker P, Yodh A. Surfactant-induced Marangoni effect alter the coffee-rings of evaporating colloidal drops. Langmuir 2012;28:4984–8. https://doi.org/10.1021/la204928m.
[171] Das S, Steager E, Ani Hsieh M, Stebe K, Kumar V. Experiments and open-loop control of multiple catalytic microrobots. J Micro-Bio Robot 2018;14:25–34. https://doi.org/10.1007/s12213-018-0106-1.
[172] Boniface D, Cottin-Bizonne C, Kervil R, Ybert C, Detcheverry F. Self-propulsion of symmetric chemically active particles: point-source model and experiments on camphor disks. Phys Rev E 2019;99:062605. https://doi.org/10.1103/PhysRevE.99.062605.
[173] Čejková J, Schwarzenberger K, Eckert K, Tanaka S. Dancing performance of organic droplets in aqueous surfactant solutions. Colloids Surf A 2019;566:141–7. https://doi.org/10.1016/j.colsurfa.2019.01.027.
[174] Berli C, Bellino M. Toward droplets displaying life-like interaction behaviors. Biomicrofluidics 2023;17:021302. https://doi.org/10.1063/5.0142115.
[175] Harris H. *Chlamydomonas* as a model organism. Annu Rev Plant Biol 2001;52:363–406. https://doi.org/10.1146/annurev.arplant.52.1.363.
[176] Petteson AE, Gopinath A, Arratia PE. Active colloids in complex fluids. Curr Opin Colloid Interface Sci 2016;21:86–96. https://doi.org/10.1016/j.cocis.2016.01.001.
[177] Zhu K, Huang Y, Yang L, Xuan M, Zhou T, He Q. Motion control of chemically powered colloidal motors. Adv Colloid Interface Sci 2025;341:103475. https://doi.org/10.1016/j.cis.2025.103475.
[178] Gupta A, Burak Eral H, Alan Hattona T, Doyle P. Nanoemulsions: formation, properties and applications. Soft Matter 2016;12:2826–41. https://doi.org/10.1039/C5SM02958A.
[179] McClements D, Jafari S. Chapter 1 - General aspects of nanoemulsions and their formulation. In: Nanoemulsions. Formulation, Applications, and Characterization; 2018. p. 3–20. https://doi.org/10.1016/B978-0-12-811838-2.00001-1.
[180] Mason T, Wilking J, Meleson K, Chang C, Graves S. Nanoemulsions: formation, structure, and physical properties. J Phys Condens Matter 2006;18:R635. https://doi.org/10.1088/0953-8984/18/41/R01.
[181] Parthasarathi S, Muthukumarc C, Anandharamakrishnan C. The influence of droplet size on the stability, *in vivo* digestion, and oral bioavailability of vitamin E emulsions. Food Funct 2016;7:2294–302. https://doi.org/10.1039/C5FO01517K.
[182] Jiang T, Charcosset C. Encapsulation of curcumin within oil-in-water emulsions prepared by premix membrane emulsification: impact of droplet size and carrier oil on the chemical stability of curcumin. Food Res Int 2022;157:111475. https://doi.org/10.1016/j.foodres.2022.111475.
[183] Nakaya K, Ushio H, Matsukawa S, Shimizu M, Ohshima T. Effects of droplet size on the oxidative stability of oil-in-water emulsions. Lipids 2005;40:501–7. https://doi.org/10.1007/s11745-005-1410-4.
[184] Gallegos C, Partal P, Franco J. Droplet-size distribution and stability of lipid injectable emulsions. Am J Health-System Pharm 2009;66(2):162–6. https://doi.org/10.2146/ajhp080031.
[185] Cholakova D, Vinarov Z, Tcholakova S, Denkov N. Self-emulsification in chemical and pharmaceutical technologies. Curr Opin Colloid Interface Sci 2022;59:101576. https://doi.org/10.1016/j.cocis.2022.101576.
[186] Taha A, Ahmed E, Ismaiel A, Ashokkumar M, Xu X, Pan S, et al. Ultrasonic emulsification: an overview on the preparation of different emulsifiers-stabilized emulsions. Trends Food Sci Technol 2020;105:363–77. https://doi.org/10.1016/j.tifs.2020.09.024.
[187] Anton N, Vandamme TF. The universality of low-energy nano-emulsification. Int J Pharm 2009;377:142–7. https://doi.org/10.1016/j.ijpharm.2009.05.014.
[188] Solans C, Morales D, Homs M. Spontaneous emulsification. Curr Opin Colloid Interface Sci 2016;22:88–93. https://doi.org/10.1016/j.cocis.2016.03.002.
[189] Mason TG, Bibette J. Emulsification in viscoelastic media. Phys Rev Lett 1996;77:3481. https://doi.org/10.1103/PhysRevLett.77.3481.
[190] Maindarkar S, Dubbelboer A, Meuldijk J, Hoogland H, Henson M. Prediction of emulsion drop size distributions in colloid mills. Chem Eng Sci 2014;118:114–25. https://doi.org/10.1016/j.ces.2014.07.032.
[191] Scheludko A. Thin liquid films. Adv Colloid Interface Sci 1967;1:391–464. https://doi.org/10.1016/0001-8686(67)85001-2.
[192] Ivanov IB, editor. Thin liquid films: Fundamentals and applications. Marcel Dekker; 1988.
[193] Vrij A, Overbeek JTG. Rupture of thin liquid films due to spontaneous fluctuations in thickness. J Am Chem Soc 1968;90:3074–8. https://doi.org/10.1021/ja01014a015.
[194] Politova N, Tcholakova S, Denkov ND. Factors affecting the stability of water-oil-water emulsion films. Colloids Surf A 2017;522:608–20. https://doi.org/10.1016/j.colsurfa.2017.03.055.
[195] Arnaudova T, Mitrinova Z, Denkov N, Growney D, Brenda R, Tcholakova S. Foamability and foam stability of oily mixtures. Colloids Surf A 2022;653:129987. https://doi.org/10.1016/j.colsurfa.2022.129987.
[196] Stone HA. Dynamics of drop deformation and breakup in viscous fluids. Annu Rev Fluid Mech 1994;26:65–102. https://doi.org/10.1146/annurev.fl.26.010194.000433.
[197] Eggers J, Villermaux E. Physics of liquid jets. Rep Prog Phys 2008;71:036601. https://doi.org/10.1088/0034-4885/71/3/036601.
[198] Toor A, Helms BA, Russell TP. Effect of nanoparticle surfactants on the breakup of free-falling water jets during continuous processing of reconfigurable structured liquid droplets. Nano Lett 2017;17:3119–25. https://doi.org/10.1021/acs.nanolett.7b00556.
[199] Kraack H, Deutsch M, Sirota EB. N-alkane homogeneous nucleation: crossover to polymer behaviour. Macromolecules 2000;33:6174–84. https://doi.org/10.1021/ma000312m.
[200] Cebula D, McClements DJ, Povey MJW. Small angle neutron scattering from voids in crystalline trilaurin. J Am Oil Chem Soc 1990;67:76. https://doi.org/10.1007/BF02540630.

[201] Lencki RW, John Craven R. Negative pressure effects during pure triacylglycerol crystallization. Cryst Growth Des 2012;12:4981–6. https://doi.org/10.1021/cg300901v.
[202] Peyronel F, Quinn B, Marangoni AG, Pink DA. Ultra small angle X-ray scattering for pure tristearin and tripalmitin: model predictions and experimental results. Food Biophys 2014;9:304–13. https://doi.org/10.1007/s11483-014-9365-0.
[203] Acevedo NC, Marangoni AG. Characterization of the nanoscale in triacylglycerol crystal networks. Cryst Growth Des 2010;10:3327–33. https://doi.org/10.1021/cg100468e.
[204] Acevedo NC, Marangoni AG. Toward nanoscale engineering of triacylglycerol crystal networks. Cryst Growth Des 2010;10:3334–9. https://doi.org/10.1021/cg100469x.
[205] Smoukov SK, Denkov ND, Tcholakova SS, Lesov II, Cholakova DP, Valkova ZN. A method for the preparation of particles with controlled shape and/or size. WIPO Patent/2017/085508A1; 2017.
[206] Shinoda K, Saito H. The stability of o/w type emulsions as functions of temperature and the HLB of emuldifiers: the emulsification by PIT-method. J Colloid Interface Sci 1969;30:258–63. https://doi.org/10.1016/S0021-9797(69)80012-3.
[207] Friberg SE, Corkery RW, Blute IA. Phase inversion temperature (PIT) emulsification process. J Chem Eng Data 2011;56:4282–90. https://doi.org/10.1021/je101179s.
[208] Roger K. Nanoemulsification in the vicinity of phase inversion: disruption of bicontinuous structures in oil/surfactant/water systems. Curr Opin Colloid Interface Sci 2016;25:120–8. https://doi.org/10.1016/j.cocis.2016.09.015.
[209] Lesov L, Glushkova D, Cholakova D, Georgiev MT, Tcholakova S, Smoukov SK, et al. Flow reactor for preparation of lipid nanoparticles via temperature variations. J Ind Eng Chem 2022;112:37–45. https://doi.org/10.1016/j.jiec.2022.03.043.
[210] Denkov N, Tcholakova S, Glushkova D, Cholakova D, Smoukov S, Oil-in-water emulsion of nano-sized self-emulsified particulates, WIPO Patent WO2020/260577 2020, PCT/EP2020/068018.
[211] Champion JA, Mitragotri S. Role of target geometry in phagocytosis. Biophys Comp Biology 2006;103:4930–4. https://doi.org/10.1073/pnas.0600997103.
[212] Palombra RP, Palange AL, Rizzuti IF, Ferreira M, Cervadoro A, Barbato MG, et al. Modulating phagocytic cell sequestration by tailoring nanoconstruct softness. ACS Nano 2018;12:1433–44. https://doi.org/10.1021/acsnano.7b07797.
[213] Aghmiouni DK, Khoee S. Dual-drug delivery by anisotropic and uniform hybrid nanostructures: a comparative study of the function and substrate-drug interaction properties. Pharmaceutics 2023;15:1214. https://doi.org/10.3390/pharmaceutics15041214.
[214] Altas BO, Kalaycioglu GD, Lifshiz-Simon S, Talmon Y, Aydogan N. Tadpole-like anisotropic polymer/lipid Janus nanoparticles for nose-to-brain drug delivery: importance of geometry, elasticity on mucus-penetration ability. Mol Pharm 2024;21:633–50. https://doi.org/10.1021/acs.molpharmaceut.3c00773.
[215] Besendorfer G, Roosen A. Particle shape and size effects on anisotropic shrinkage in tape-cast ceramic layers. J Am Ceram Soc 2008;91:2514–20. https://doi.org/10.1111/j.1551-2916.2008.02510.x.
[216] Li L, Yan H, Wang Z, Feng X, Tian J. Super-resolution pulsed magnetic particle imaging using shape anisotropic nanoparticles. Int J Magnetic Particle Imaging 2024;10:2403018. https://doi.org/10.18416/IJMPI.2024.2403018.
[217] Gao Y, Yu Y, Sanchez L, Yu Y. Seeing the unseen: imaging rotation in cells with designer anisotropic particles. Micron 2017;101:123–31. https://doi.org/10.1016/j.micron.2017.07.002.
[218] Kersey FR, Merkel TJ, Perry JL, Napier ME, DeSimone JM. Effect of aspect ratio and deformability on nanoparticle extravasation through nanopores. Langmuir 2012;28:8773–81. https://doi.org/10.1021/la301279v.
[219] Manghnani PN, Di Francesco V, La Capria CP, Schlich M, Miali ME, Moore TL, et al. Preparation of anisotropic multiscale micro-hydrogels via two-photon continuous flow lithography. J Colloid Interface Sci 2022;608:622–33. https://doi.org/10.1016/j.jcis.2021.09.094.
[220] Latito V, Zambelli T. Heat: a powerful tool for colloidal particle shaping. Adv Colloid Interface Sci 2024;331:103240. https://doi.org/10.1016/j.cis.2024.103240.
[221] Heine D, Petersen M, Grest G. Effect of particle shape and charge on bulk rheology of nanoparticle suspensions. J Chem Phys 2010;132:184509. https://doi.org/10.1063/1.3419071.
[222] Chinesta F, Ausias G. Rheology of non-spherical particle suspensions. London: Elsevier Ltd; 2015. https://doi.org/10.1016/C2015-0-01208-4.
[223] Mewis J, Wagner NJ. Colloidal suspension rheology. Cambridge University Press; 2011. https://doi.org/10.1017/CBO9780511977978.
[224] Reiner J, Ly TT, Liu L, Karbstein HP. Melt emulsions: influence of the cooling procedure on crystallization and recrystallization of emulsion droplets and their influence on dispersion viscosity upon storage. Chem Ing Tech 2022;94:356–64. https://doi.org/10.1002/cite.202100143.
[225] Gallegos C, Franco JM. Rheology of food, cosmetics and pharmaceuticals. Curr Opin Colloid Interface Sci 1999;4:288–93. https://doi.org/10.1016/S1359-0294(99)00003-5.
[226] Tabilo-Munizaga G. Barbosa-Canovas, rheology for the food industry. J Food Eng 2005;67:147–56. https://doi.org/10.1016/j.jfoodeng.2004.05.062.
[227] Dickinson E. Emulsion gels: the structuring of soft solids with protein-stabilized oil droplets. Food Hydrocoll 2012;28:224–41. https://doi.org/10.1016/j.foodhyd.2011.12.017.
[228] Fajami T, Madadlou A. An overview on preparation of emulsion-filled gels and emulsion particulate gels. Trends Food Sci Technol 2019;86:85–94. https://doi.org/10.1016/j.tifs.2019.02.043.
[229] Shi Z, Shi Z, Wu M, Shen Y, Li G, Ma T. Fabrication of emulsion gel based on polymer sanxan and its potential as a sustained-release delivery system for β-carotene. Int J Biol Macromol 2020;164:597–605. https://doi.org/10.1016/j.ijbiomac.2020.07.177.
[230] Naseri N, Valizadeh H, Zakeri-Milani P. Solid lipid nanoparticles and nanostructured lipid carriers: structure, preparation and application. Adv Pharm Bull 2015;5:305–13. https://doi.org/10.15171/apb.2015.043.
[231] Pardeike J, Hommoss A, Müller RH. Lipid nanoparticles (SLN,NLC) in cosmetic and pharmaceutical dermal products. Int J Pharm 2009;366:170–84. https://doi.org/10.1016/j.ijpharm.2008.10.003.
[232] Weiss J, Decker EA, McClements DJ, Kristbergsson K, Helgason T, Awad T. Solid lipid nanoparticles as delivery systems for bioactive food components. Food Biophys 2008;3:146–54. https://doi.org/10.1007/s11483-008-9065-8.
[233] Fathi M, Mozafari MR, Mohebbi M. Nanoencapsulation of food ingredients using lipid based delivery systems. Trends Food Sci Technol 2012;23:13–27. https://doi.org/10.1016/j.tifs.2011.08.003.
[234] Khadka P, Ro J, Kim H, Kim I, Kim JT, Kim H, et al. Pharmaceutical particle technologies: an approach to improve drug solubility, dissolution and bioavailability. Asian J Pharm Sci 2014;9:304–16. https://doi.org/10.1016/j.ajps.2014.05.005.
[235] He L, Lin F, Li X, Sui H, Xu Z. Interfacial sciences in unconventional petroleum production: from fundamentals to applications. Chem Soc Rev 2015;44:5446–94. https://doi.org/10.1039/c5cs00102a.
[236] Chen Y, Bai Y, Chen S, Ju J, Li Y, Wang T, et al. Stimuli-responsive composite particles as solid-stabilizers for effective oil harvesting. ACS Appl Mater Interfaces 2014;6:13334–8. https://doi.org/10.1021/am504124a.
[237] Tang J, Quinlan PJ, Tam KC. Stimuli-responsive Pickering emulsions: recent advances and potential applications. Soft Matter 2015;11:3512–29. https://doi.org/10.1039/c5sm00247h.
[238] Juarez JA, Whitby CP. Oil-in-water Pickering emulsion destabilisation at low particle concentrations. J Colloid Interface Sci 2012;368:319–25. https://doi.org/10.1016/j.jcis.2011.11.029.
[239] Sy PM, Anton N, Idoux-Gillet Y, Dieng SM, Messaddeq N, Ennahar S, et al. Pickering nano-emulsion as a nanocarrier for pH-triggered drug release. Int J Pharm 2018;549:299–305. https://doi.org/10.1016/j.ijpharm.2018.07.066.
[240] Zhao X, Huang B, El-Aooiti M, Rousseau D. Demulsification to control solute release from Pickering crystal-stabilized water-in-oil emulsions. J Colloid Interface Sci 2018;509:360–8. https://doi.org/10.1016/j.jcis.2017.08.091.
[241] Yang H, Zhou T, Zhang W. A strategy for separating and recycling solid catalysts based on the pH-triggered Pickering-emulsion inversion. Angew Chem Int Ed 2013;52:7455–9. https://doi.org/10.1002/anie.201300534.
[242] Whitby CP, Wanless EJ. Controlling Pickering emulsion destabilisation: a route to fabricating new materials by phase inversion. Materials 2016;9:626. https://doi.org/10.3390/ma9080626.
[243] Cho Y-S, Kim S-H, Yi G-R, Yang S-M, Kim Y-K, Choi C-J. Fabrication of nonspherical or macroporous particles using emulsion droplets as confining geometries. In: 10th IEEE Int. Conference Nanotechn; 2010. https://doi.org/10.1109/NANO.2010.5697773.
[244] Walker SI. Origins of life: a problem for physics, a key issues review. Rep Prog Phys 2017;80:092601. https://doi.org/10.1088/1361-6633/aa7804.
[245] Oparin AI. The origin of life. MacMillan; 1938.
[246] Haldane JBS. The origin of life Ration. Annu 1929;148:3–10.
[247] Hansma HG. Chapter 9: liquid-liquid phase separation at the origins of life in droplets of life. Membrane-less organelles, biomolecular condensates, and biological liquid-liquid phase separation. Editor: Vladimir N. Uversky. Elsevier; 2022. https://doi.org/10.1016/B978-0-12-823967-4.00006-3.
[248] Lin Y, Jing H, Liu Z, Chen J, Liang D. Dynamic behavior of complex coacervates with internal lipid vesicles under nonequilibrium conditions. Langmuir 2020;36:1709–17. https://doi.org/10.1021/acs.langmuir.9b03561.
[249] Zwicker D, Seyboldt R, Weber CA, Hyman AA, Julicher F. Growth and division of active droplets provides a model for protocells. Nat Phys 2017;13:408–13. https://doi.org/10.1038/NPHYS3984.
[250] Yoshinaga N, Nagai KH, Sumino Y, Kitahata H. Drift instability in the motion of a fluid droplet with a chemically reactive surface driven by Marangoni flow. Phys Rev E 2012;86:016108. https://doi.org/10.1103/PhysRevE.86.016108.
[251] Wang L, Lin Y, Zhou Y, Xie H, Song J, Li M, et al. Autonomic behaviors in lipase-active oil droplets. Angew Chem Int Ed 2019;58:1067–71. https://doi.org/10.1002/anie.201812111.
[252] Matsuo M, Kurihara K. Proliferating coacervate droplets as the missing link between chemistry and biology in the origins of life. Nat Commun 2021;12:5487. https://doi.org/10.1038/s41467-021-25530-6.
[253] Banno T, Kuroha R, Toyota T. pH-sensitive self-propelled motion of oil droplets in the presence of cationic surfactants containing hydrolysable ester linkages. Langmuir 2012;28:1190–5. https://doi.org/10.1021/la2045338.
[254] Kim KE, Balaj RV, Zarzar LD. Chemical programming of solubilizaing, nonequilibrium active droplets. Acc Chem Res 2024;57:2372–82. https://doi.org/10.1021/acs.accounts.4c00299.
[255] Yin Y, Niu L, Zhu X, Zhao M, Zhang Z, Mann S, et al. Non-equilibrium behavior in coacervate-based protocells under electric-field-induced excitation. Nat Commun 2016;7:10658. https://doi.org/10.1038/ncomms10658.
[256] Hanczyc MM, Toyota T, Ikegami T, Packard N, Sugawara T. Fatty acid chemistry at the oil-water interface: self-propelled oil droplets. J Am Chem Soc 2007;129:9386–91. https://doi.org/10.1021/ja0706955.
[257] Iliev S, Tsibranska S, Ivanova A, Tcholakova S, Denkov N. Computational assessment of hexadecane freezing by equilibrium atomistic molecular dynamics

simulations. J Colloid Interface Sci 2023;638:743–57. https://doi.org/10.1016/j.jcis.2023.01.126.
[258] Tsibranska S, Iliev S, Ivanova A, Aleksandrov N, Tcholakova S, Denkov N. Types of phases obtained by molecular dynamics simulations upon freezing of hexadecane-containing systems. Colloids Surf A 2024;697:134466. https://doi.org/10.1016/j.colsurfa.2024.134466.
[259] Burrows SA, Shon JW, Peychev B, Slavchov RI, Smoukov SK. Phase transitions of fluorotelomer alcohols at the water|alkane interface studied via molecular dynamics simulation. Soft Matter 2024;20:2243–57. https://doi.org/10.1039/d3sm01444d.
[260] Gordon R, Hanczyc M, Denkov N, Tiffany M, Smoukov S. In: Gordon Sharov, editor. In habitability of the universe before earth. Academic Press; 2018. p. 427–90.
[261] Benoiston A-S, Ibarbalz FM, Bittner L, Guidi L, Jahn O, Dutkiewicz S, et al. The evolution of diatoms and their biogeochemical functions. Philos Trans R Soc Lond B 2017;372:20160397. https://doi.org/10.1098/rstb.2016.0397.
[262] Kale A, Karthick B. The diatoms: big significance of tiny glass houses. Reson 2015; 20:919–30. https://doi.org/10.1007/s12045-015-0256-6.
[263] Kroger N, Poulsen N. Diatoms-from cell wall biogenesis to nanotechnology. Annu Rev Geent 2008;42:83–107. https://doi.org/10.1146/annurev.genet.41.110306.130109.
[264] Gordon R. A call for research on the basis for polygonal pleomorphism in archae. BioSystems 2025;252:105478. https://doi.org/10.1016/j.biosystems.2025.105478.
[265] Kotel'nikova E, Platonova N, Filatov S. Identification of biogenic paraffins and their thermal phase transitions. Geol Ore Deposits 2007;49:697–709. https://doi.org/10.1134/S1075701507080041.